Universität Hamburg
DER FORSCHUNG | DER LEHRE | DER BILDUNG

CHyN
Centre for Hybrid Nanostructures

FACILE METRICS MONITOR EFFECTIVE DEGRADATION OF INORGANIC-ORGANIC NANOHYBRIDS

Dissertation

zur Erlangung des Doktorgrades

der Naturwissenschaften

(Dr.rer.nat)

dem

Fachbereich Chemie

der Universität Hamburg

vorgelegt von

Ziyao Liu

aus

Hunan, China

Hamburg, 2019

The presented work conducted under the supervision of Dr. Neus Feliu and Prof. Wolfgang Parak at Phillips University of Marburg (from October 2016 to December 2017) and at the Center for Hybrid Nanostructure (CHyN) of the University of Hamburg (from January 2018 to June 2019)

First Evaluator: Prof. Dr. Wolfgang Parak

Second Evaluator: Prof. Dr. Michael Fröba

Disputation date: 27092019

Date：

Index

Abstract

Currently, organic-inorganic nanohybrids (NHs) emerge as promising and sophisticated nanoplatforms for the treatment of cancer as well as detection of biomarker with excellent performance. Unfortunately, the further development of its biological application is often hampered by the degradation of NHs in the course of cellular journey. Since the majority of NHs are either degraded in the digestive condition or changed by biological matrix, its low targeting efficiency suggest that it is of necessity to re-evaluate the degradation process with the help of quantitative strategies. Probing into NHs degradation not only provides prerequisite knowledge for designing more tailored nanostructures, but also increases the probability to accomplish their holding promise. Thereafter, we are going to explore the effective degradation of NHs in this study, which overcomes the challenges associated with cell growth and exocytosis. To establish the methods for degradation study, two types of NHs, rare earth NHs and metal-organic frameworks (MOF), have been adopted for following studies: 1) investigation of degradation study for the test at acid buffer and *in vitro* condition, 2) inspection of precise shape change during the degradation process, 3) exploration of the relationship between cell growth and cellular degradation. Conclusively, we come up with facile metrics for tracking the degradation of NHs. As this method verifies the degradation scenarios of the polymeric part and inorganic core in the acid buffer and cellular condition, we believe it is a suitable model for monitoring the biological fate of classic NHs structure.

Zusammenfassung

Derzeit entwickeln sich organisch-inorganische Nanohybride (NHs) zu aussichtsreichen Nanoplattformen für die Krebsbehandlung und Detektion von Biomarkern mit exzellenter Performance. Leider ist die weitere Entwicklung dieser biologischen Anwendungen noch eingeschränkt, vor allem die Zersetzung der NHs bei der Zellaufnahme. Da der Großteil der NHs entweder durch die digestiven Bedingungen zersetzt oder durch die biologische Matrix verändert wird, ist es im Hinblick auf die geringe Effizienz bei der Zielsuche und Aufnahme bei nicht-spezifischen Zellen sinnvoll, den Degradierungsprozess mit Hilfe quantitativer Strategien neu abzuschätzen.

Weil die Erforschung von Nanostrukturen nicht nur die Grundvoraussetzung für die Entwicklung maßgeschneiderter Nanostrukturen darstellt, sondern auch die Wahrscheinlichkeit erhöht, dass sie ihr Versprechen der Haltbarkeit erfüllen, werden wir in dieser Studie den wirksamen Abbau untersuchen, der die mit dem Zellwachstum und der Exozytose verbundenen Herausforderungen bewältigt.

Zur Festlegung der Methoden für die Studie zu den Zersetzungsprozessen wurden zwei Arten von NHs, Seltenerden-NHs und metallorganische Gerüstverbindungen (metal-organic frameworks; MOF) für die folgenden Studien verwendet: 1) Untersuchung der Abbaustudie für den Test in Säurepuffer und in vitro-Bedingungen, 2) Überprüfung der genauen Formänderung während des Abbauprozesses, 3) Untersuchung der Beziehung zwischen Zellwachstum und Zellabbau. Zusammenfassend stellen wir einfache Metriken zur Verfolgung des Abbaus von NHs vor. Da diese Methode die Abbauszenarien des Polymerteils und des anorganischen Kerns im Säurepuffer und im Zellzustand verifiziert, halten wir sie für ein geeignetes Modell zur Überwachung der biologischen Veränderung der klassischen NHs-Struktur.

1. Introduction

The promising prospects of organic/inorganic nanohybrids (NHs)-based nanomedicine have inspired countless scientists to construct the tailor-made nanoplatforms for drug delivery systems, gene transfection vehicles and biomarkers sensing detectors. To our disappointment, numerous well-confined nanostructures fail at their mission to specifically target the intended site[1], since cellular transformation and degradation of NHs bring down their potential to meet the requirements of specific targeting. The understanding of how cells sense and respond to the foreign NHs provides with the basic knowledge to build a bridge between chemistry design and therapeutic efficiency. Along with a better understanding of the cellular behaviors of NHs, the concept of "magic bullet" becomes increasingly realistic. On the other hand, the higher surface energy endows NHs with the ability to absorb multiple proteins, form irreversible aggregation and initiate biochemistry reaction, leading to a complete change of originally designed NHs surface. Therefore, the surface properties of NHs play crucial roles in receptors recognition, cellular internalization as well as cytotoxicity. On account of the above considerations, it is urgent and crucial to conduct a thorough study of the degradation and biotransformation of NHs.

1.1. The degradation of nanohybrids (NHs)

1.1.1. The biological environment changes and degrades the structure of NHs

What happens to NHs once they have been administered in the biological environment? In the beginning, the physiological condition alters the surface of NHs. The high surface energy of NHs gives rise to adsorbed proteins on the surface of NHs, termed as protein corona (PC), which represents the true identity of NHs[2, 3]. The profile of PC depends on many factors, such as physicochemical characteristics[4-6], environmental temperature[7] and incubation period[8]. The acquired new identity gets command of their biological behaviors and fate, such as their pharmacokinetics[9, 10], biodistribution[11], and therapeutic efficacy[12, 13]. The example in Figure 1 demonstrates how PC affects the aggregation status of liposome and response of cells and tissues[14]. As for the inorganic nanoparticles, the effect of PC on their biological behaviors have been extensively studied and comprehensively reviewed by scientists[15-17]. It well accepted the PC can reduce cytotoxicity and optimize the biocompatibility[18]. It had been reported the transferrin-functionalized silica nanoparticles lose their targeting ability when PC formed on their surface[19]. In the next step, the biological condition can gradually degrade NHs or excrete it out. Low pH can be found at stomach and tumors at the organ level, endosomes and lysosomes at the cellular level. The acidity can corrode the inorganic core of NHs, such as silver NHs[20], iron oxide NHs[21] and silica NHs[22]. Furthermore, the biological environment is full of digestive enzymes, which are capable of digesting the organic part[22]. Some studies adopt enzymes to cut the chemical bonds in order to controllably release drugs[23]. In addition, it has been proven

that enzymes are able to digest the PC adsorbed onto the NHs surface[24]. In simulation of the intracellular conditions, the superparamagnetic, iron oxide nanoparticles (SPIOs) with three different surface coatings were demonstrated to exhibit multiple kinetics of dissolution at an acidic buffer with a citrate chelating agent, including magnetic properties, as well as size and shape of the nanocrystals[25]. The ^{51}Cr-labeled SPIOs were further adopted to study their pharmacokinetics parameters in mice after oral gavage, the results showed the degradation of the SPIOs cores in the acidic stomach, tested by the released ionic. It is noteworthy that what we have acknowledged about biodegradation of specific NHs and the reliable techniques is a tip of the iceberg, and that our understanding should be further extended. Characterizing the degradation of NHs can help in the prediction of their biological outcomes and in turn speed up medical applications.

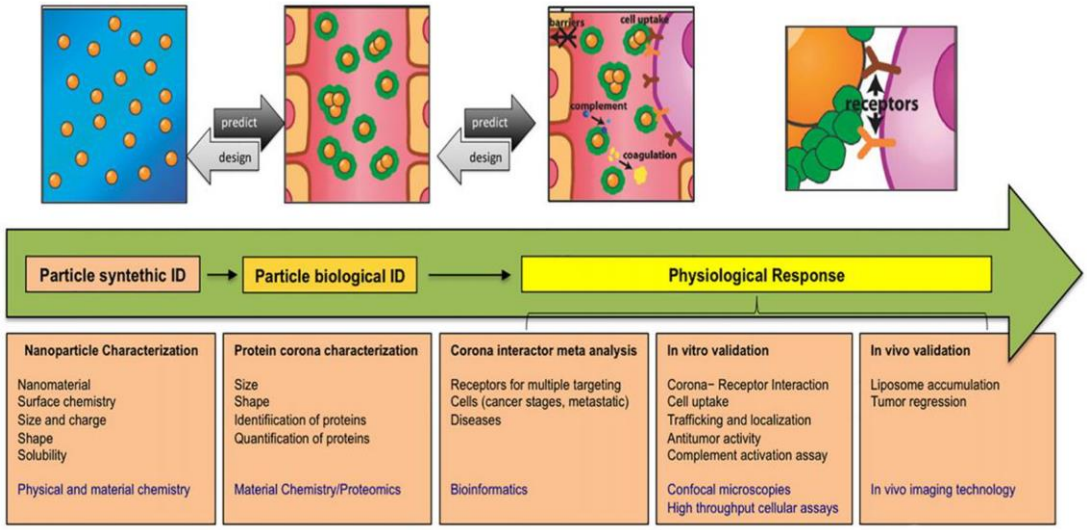

Figure 1-1*. Correlation between the original identity, the biological identity and the physiological response of liposomes in a biological environment. Liposomes are fabricated with the original surface. When attached to proteins in biological environments, a new particle identity emerges that is mainly responsible for the physiological response. Cited from reference 14.*

1.1.2. The degradation of NHs affects their biological behaviors

The hostile environment in the biological medium can eventually degrade or excrete out NHs[26]. It seems that the process of degradation was the major barrier that hindered NHs from fulfilling their holding promise. Hence, a comprehensive understanding of the degradation process of NHs in the body is of vital importance to move forward clinical trials and expand their applications in disease diagnosis. PC, defined as the biological identity of NHs [27], is the outermost entity to react with cells. Numerous studies have shown that PC governs the cellular uptake[28, 29], tumor

targeting efficiency[19] and inflammatory condition[30]. From the administration to the ultimate degradation or exocytosis, the PC on the surface of NHs evolves with surrounding condition[31]. The absorbed proteins constantly change with surrounding ones in the physiological matrix[32]. The previous study suggested lysosome enzymes may digest a part of PC[24]. The degradation of PC will largely affect the various cell-NHs interaction. Diverse researches have investigated PC-mediated NHs internalization with cells[33], pharmacokinetics profile[34] in the blood and accumulation in tissues[35]. However, there are a few studies concentrating on corona degradation after internalization and on the effects of the degraded PC. To fill this research gap, gold nanoparticles (Au NPs) were incubated with dye-labeled three proteins, human serum albumin (HSA),γ-globulin (HGG), and serum fibrinogen (HSF), to reveal the protein degradation under the extracellular and intracellular condition as well as their corresponding impacts on cytotoxicity (Figure1-2)[36]. On the basis of results, HSA exhibited the fastest degradation manners while HSF exhibited the slowest one. Of note, the results also demonstrated Au NPs-HSA reduced cell viability, lowered the content of adenosine triphosphate and mitochondrial membrane potential, and activated reactive oxygen species.

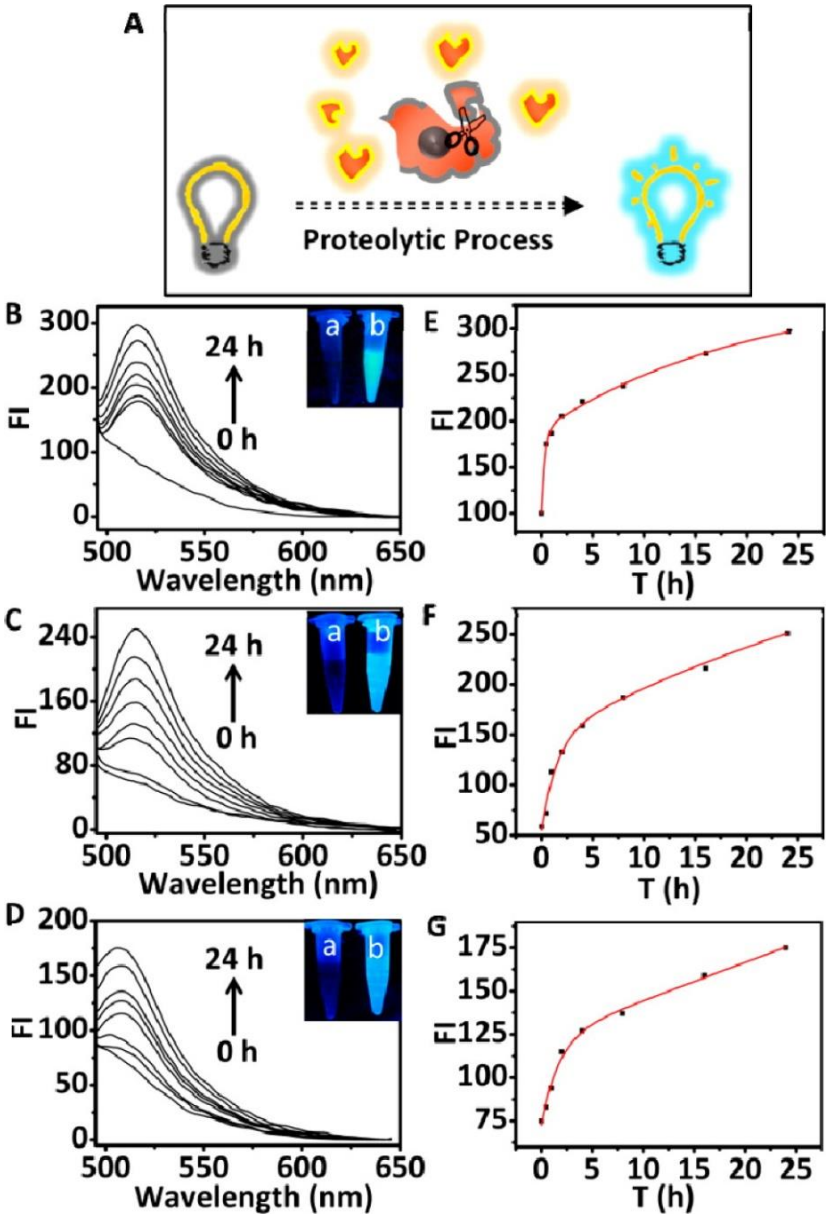

Figure1-2. *Schematic illustration of the fluorescence off/on for the composite between gold nanoparticles and proteins labeled with fluorescein isothiocyanate (Au@Protein-FITC) NPs (A). The fluorescence spectra of the released FITC after enzymatic digestion of the PC for gold nanoparticles were incubated with gold nanoparticles were incubated with FITC-labeled human serum albumin (Au@HSA-FITC NPs) (B), gold nanoparticles were incubated with FITC-labeled γ-globulin (Au@HGG-FITC NPs) (C), and gold nanoparticles were incubated with FITC-labeled serum fibrinogen (Au@HSF-FITC NPs) (D). The peak fluorescence intensity of FITC after being extracted from the original surface of Au@HSA-FITC NPs (E), Au@HGG-FITC NPs (F), and Au@HSF-FITC NPs (G) plotted according to the time (red). Inset: photographs of the composites (a) before and (b) after the digestion procedures under illumination with UV light. The figure was extracted from reference 36.*

For the next part of NHs, it is clear that the engineered organic surface can be cut by specific enzymes. Some special bonds are designed to be cut by enzymes, which can be used to release drugs[37, 38], proteins[39, 40] and guest molecules[41] in a controllable manner. NHs can be modified by enzyme-responsive bonds that increase the targeting efficiency. Intracellular enzymes are considered to cut the tailor-made organic shell containing the ester bond[42]. In this way, it is assumed that the part of organic shell can be degraded during their cellular journey, which brings out some questions about NHs degradation. Can the remaining organic part finish the designed mission? How should we design the NHs so as to resist the degradation of enzymes? It is likely that answers to these questions give us different insights about the chemical design of NHs. Dextran coated SPIOs were widely used for the contrast agent. The lysosome enzyme, α-glucosidase, has the power to digest the carboxydextran shell of SPIOs[43]. This results revealed the iron oxide core induces reactive oxygen species generation, c-Jun N-terminal kinase activation and apoptosis subsequently, and finally the depletion of Kupffer cell *in vivo*. Therefore, the potential toxicity of iron-based contrast agents should be re-evaluated as far as the above factors are concerned, especially in patients with liver diseases.

For their inner part, that is inorganic core, there are two major clearance ways[44]: 1) urinary excretion and 2) hepatobiliary and feces clearance (Figure 1-3). Nanoparticles that are larger than 6 nm or contain heavy metals will be quickly trapped by the reticuloendothelial system while those with small diameter (<5.5 nm) are rapidly wiped out by the urinary system because they can enter the kidney filtration.

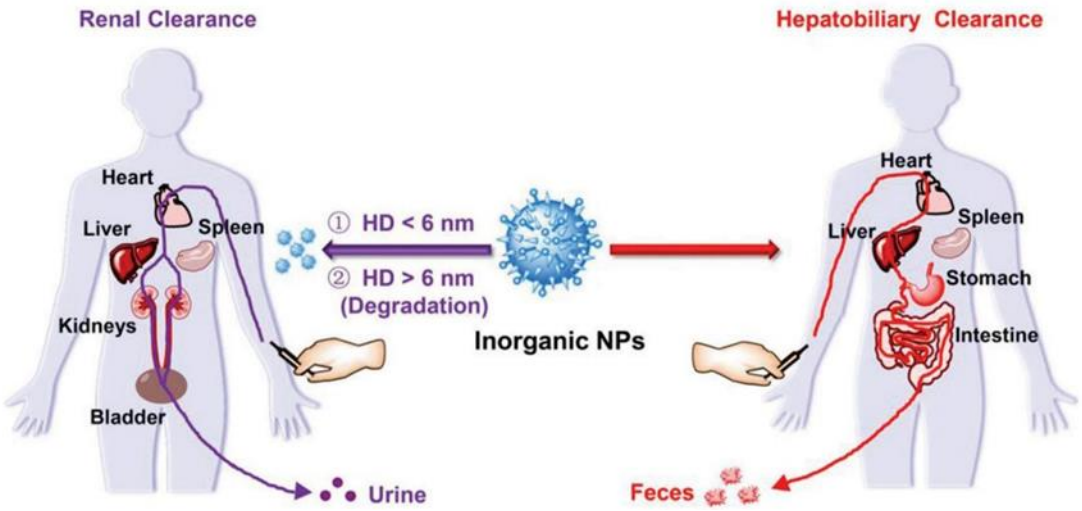

Figure 1-3*. It describes two specific metabolic pathways of some typical inorganic nanoparticles such as quantum dots with different compositions, surface properties, and sizes. Through tuning their sizes and shapes, surface chemistries and doping strategies, the tailor-made inorganic nanoparticles can be quickly degraded under*

specific biological conditions and then easily cleared by different metabolic pathways. Taken from reference 44.

Some inorganic cores are known to be degraded, such as iron oxide nanoparticles, silver nanoparticles and silica nanoparticles. These nanoparticles with larger sizes could be also excreted through the kidneys after their degradation during the long journey *in vivo*. With regard to corroded inorganic core, they can continuously release metal ions, leading to long-term potential risk. Furthermore, the degraded iron oxide NHs affect the iron metabolism, the condition of ferritin and expression of genes involved iron homeostasis[45]. The co-treatment with hypochlorite and reactive radical intermediates of the human neutrophil enzyme myeloperoxidase proved to be the catalysts for the biodegradation of *in vitro* single-walled carbon nanotubes (Figure 1-4)[46]. The results obtained from molecular modeling suggested that interplay between basic amino acids on the enzyme and the carboxyl groups on the carbon nanotubes is near the catalytic site. Of note, the degraded nanotubes substantially brought down the inflammatory reaction when aspirated into lungs by mice.

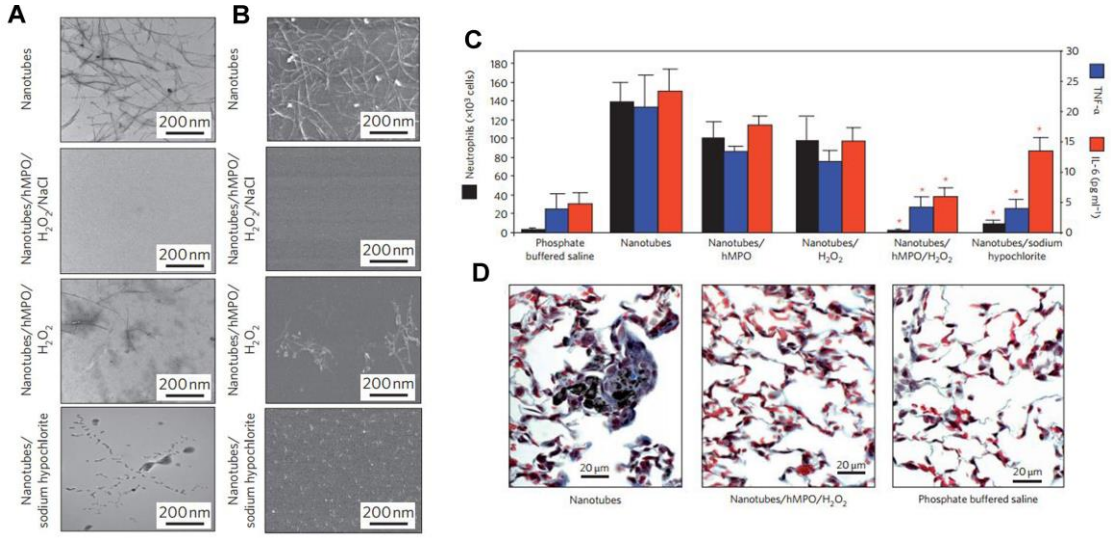

Figure1-4*. Nanotubes treated with different conditions for 24hours which included human myeloperoxidase (hMPO), hydrogen peroxide (H_2O_2), sodium hypochlorite and sodium chloride(NaCl). The shape evolution tracked by Transmission electron microscopy (TEM) (A) and SEM(B) analyses. The neutrophil counts and amount of TNF-a (blue) and IL-6 (red) in bronchoalveolar lavage fluid were tested after exposure to the specific treatments for 24 hours by means of pharyngeal aspiration (C). Representative images of lung extracted from mice exposed to 40 mg/animal nanotubes, demonstrating the formation of granuloma on day 7 after pharyngeal aspiration. However, there is no granuloma formation in the groups of phosphate buffered saline and degraded nanotubes (D).Quoted from reference 46.*

Comparatively, some inorganic cores such as gold NHs[47] are regarded as inert entities. It would raise another issue about “long-lived” biosafety. As a result, understanding NHs degradation is an intricate task that needs adequately studying for biomedical applications, especially for the translation of such materials into clinical trials.

1.1.3. The studies closely related to degradation

Encouraged by the intricate mechanism of biodegradation, some works have been devoted so as to explore the *in vivo* NHs degradation. Since most studies shed light on the biodistribution of inorganic nanoparticles over months[48], the absorbed profile of PC on the surface of iron oxide nanoparticles, *in vitro* degradation and *in vivo* biodistribution were evaluated for four months[49]. The results indicated the nanoparticles types govern the degradation kinetics in both the liver and kidney. Nonetheless, the PC composition may drive the degradation rate in the cellular lysosome. Gold/iron nanoparticles were investigated for one year after intravenous administration[50]. The heterostructures were degraded by a two-stage dissolution including primary degradation of iron oxide crystal and the secondary process of the gold inorganic core degraded into smaller particles. Previously, our group has reported the detachment of the radio-labeled core-shell Au nanoparticles (Figure 1-5)[47]. Then, the monodisperse radioactively labeled Au nanoparticles (^{198}Au) and tailor-made polymer labeled with ^{111}In were constructed for the *in vitro* and *in vivo* degradation study. The quantitative biodistribution study characterized ^{198}Au and ^{111}In independently. The data revealed that partial polymer shell had been cleared *in vivo*, while ^{198}Au accumulated mostly in the liver after intravenous injection. Furthermore, cellular experiments indicated the degradation of the organic shell was attributed to proteolytic enzymes in the liver.

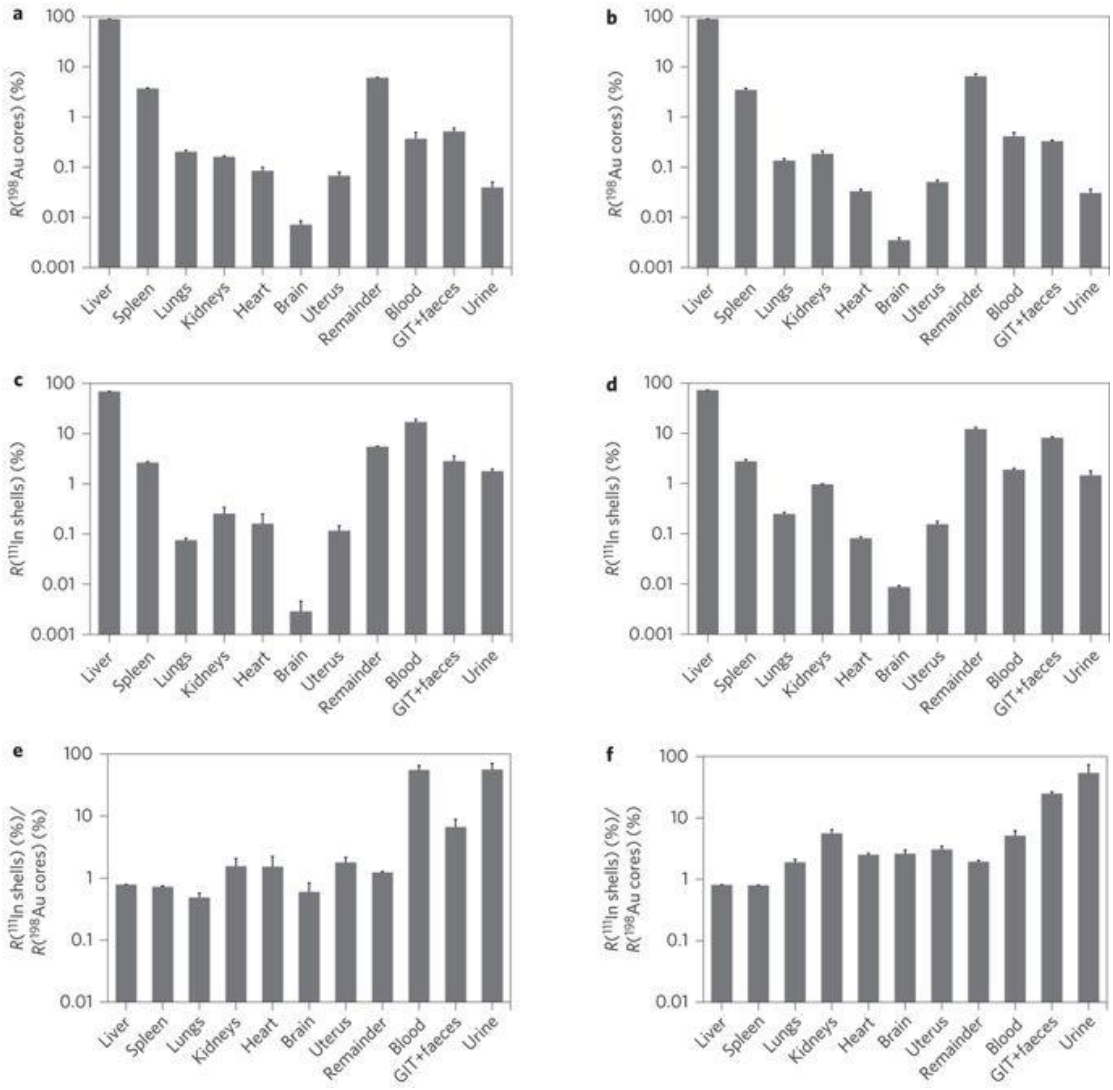

Figure 1-5. *Au nanoparticles with radiolabel of ^{98}Au in the core and ^{111}In in the shell were intravenously injected in to rats and their radio elements were tested in different organs. The graph demonstrated the biodistribution of double-labeled Au nanoparticles after 1 hour and 24 hours. The retentions R were termed as percent of the total radioactivity for the respective radioisotope. Biodistribution of the ^{98}Au nanoparticle core at 1 hour (a) and 24 hours (b). Biodistribution of the ^{111}In nanoparticle surface at 1 hour (c) and 24 hours (d).The ratio of ^{111}In to ^{98}Au in each organ and tissue at 1 hour (e) and 24 hours (f). The figure cited from reference 47.*

However, the extremely complex *in vivo* condition poses an unbridgeable barrier for us to realize the effective biodegradation at the cellular scale, due to the complicated interplay among organs, dynamic motion of blood and multiple biological factors. Furthermore, cellular degradation is the first scenario that allows us to get to know the biotransformation of NHs in depth, which supplied with useful information about chemical design. Fortunately, the stem-cell spheroids model had been established to track the biodegradation of plasmonic nanoparticles by magnetic and thermal characteristics for 27 days (Figure 1-6)[51], which provided straightforward insight into

the intracellular status during long-term tissue maturation, showing that magnetism of global spheroid can screen the degradation process. The model further evidenced a near-complete NHs loss over 27-day tissue maturation, as was confirmed by TEM. Notably, the same degradation profile was found at the endosome level in the cell-free endosomal extract.

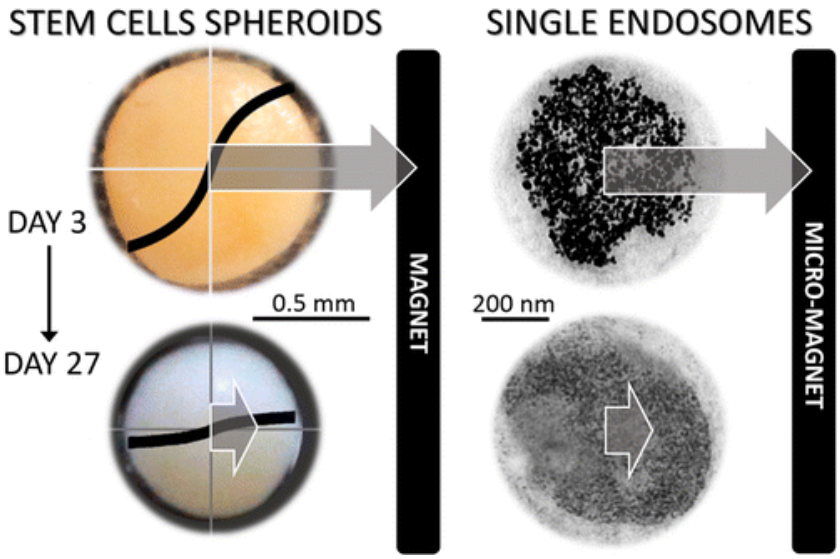

Figure 1-6. *The model has been built by spheroids composed of stem cells having incorporated iron oxide nanoparticles. The change of physicochemical characteristics was used to follow the biological fate of the internalized nanoparticles within their tissue-like condition. A cell-free endosome model was fabricated to track the degradation behaviors at the single-endosome scale. Taken from reference 51.*

This method further illustrated that the inert gold shell can protect the magnetic core and properties from the hostile environment in another study[52]. The magnetic and tissular tools are suitable models to detect nanoparticles degradation in connection with physicochemical characteristics at the cellular scale. Additionally, this method also makes it possible for the screen in biostability and biocompatibility in a long time.

Previously, our group adopted the triple labeling to follow the fate of quantum dots. The quantum dots possess intrinsic fluorescence, the surface polymer and the attached proteins are fluorescent labeled. The final nanoplatform has three fluorescence, the inorganic core, the organic shell and the proteins. On account of the results, the nanoparticles did not stay as a constant entity provided that they enter to the biological environment. Different components have different pharmacokinetics and biodistribution (Figure1-7)[53].

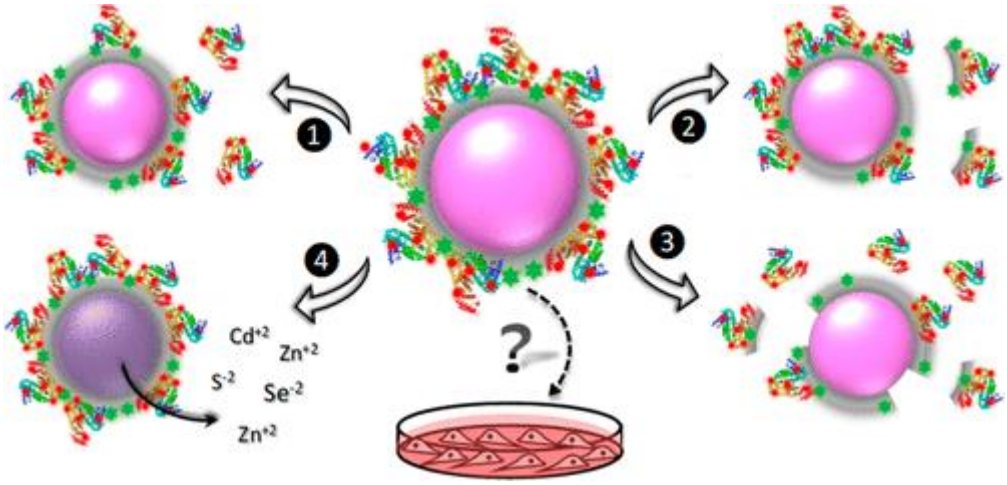

Figure 1-7*. Cells were incubated with these NHs, and after the removal of non-internalized NHs, exocytosis of different parts can be tracked by flow cytometry and confocal microscopy. The results revealed only a part of proteins transported with the surface polymer into cells. Quantum dots with proteins stayed longer inside cells compared to free proteins. Enzymes can degrade part of the polymer shell on the surface of NHs, which is slower than protein desorption. Cited from reference 53.*

Regardless of deeper understandings on the cellular degradation, there still remain some ambiguous questions: 1) once internalized by cells, what is the precise shape change of NHs? 2) How does cell growth dilute the concentration of NHs in an individual cell? 3) How can we distinguish the exocytosis from degradation? In search of answers to the above questions, specific nanoplatforms are thus constructed in order to go deep into cellular degradation

1.2. The biological applications of rare earth (RE) based NHs

The RE elements are composed of the lanthanide series (from lanthanum to lutetium), yttrium, and scandium, which are widely used as catalysts and biotechnology. Extensive efforts have also been made to develop the biological applications of RE-based NHs because of, their unique optical properties and low cytotoxicity[54]. Attractive properties of RE-based NHs include long lifetimes, high photostability, absence of blinking, large Stokes shifts, and narrow emission lines that can be exploited for detecting the biomarker, and visualizing the tumor cells (Figure1-8)[55].

Figure 1-8. *The biological applications of RE-based NHs. The advantages of high photostability and colorimetric purity make them perfect for bioprobe detections. Taken from reference 55.*

The intrinsic nature of the RE-based elements largely determines the fluorescent properties of the material. It can be used for the DNA [56, 57]and protein[58] detection, taking advantage of high photostability and a facile combination between magnetic and luminescent properties. The europium chelates have already been adopted as progress for enzyme-linked immunoabsorbent assay[59]. The remarkable optical properties and high biocompatibility endow RE-based NHs with the ability to label the specific cells and proteins. However, to visualize designed proteins in a living cell is challenging owing to the fast photobleaching of fluorescent proteins or of organic dyes. In this regard, RE-based NHs can provide the improvements thanks to their high photostability and absence of emission intermittency. Besides, it is a requisite to detect intracellular reactive oxygen species in cell biology, which emerges as a signal in a variety of physiological cellular processes and plays a vital role in pathophysiological conditions such as atherosclerosis, inflammatory processes, and neurodegenerative and malignant diseases. Recently, RE-based NHs have been applied to quantitative and dynamic detection of H_2O_2 concentration in living cells [60]. It is worth mentioning that magnetic resonance imaging is applicable to medical imaging, being renowned for its non-invasive properties and high penetrability[61]. Additionally, Gd^{3+} ions have a high magnetic moment with the treatment of the magnetic field originated from their unpaired electrons but are highly toxic. Therefore, the Gd^{3+} chelates have been extensively adopted as MRI contrast agents such as Gd-DPTA and Gd-DOPTA[62, 63]. And thus the natural inorganic surface CaP covered $NaGdF_4$:Ce/Tb NHs has been proposed (Figure1-9)[64]. After being internalized by the specific tumor cells, it was found that the $NaGdF_4$:Ce/Tb@CaP was found to be mostly gathered in the lysosome, which leads

the dissolution of CaP coatings as non-toxic ions to start DOX release and gives rise to cancer cell death. Meanwhile, the element of Gd makes possible for NHs to serve as an effective imaging contrast. In conclusion, the emerging prospects of RE-based NHs in biology lead us to conduct in-depth researches on their biological behaviors.

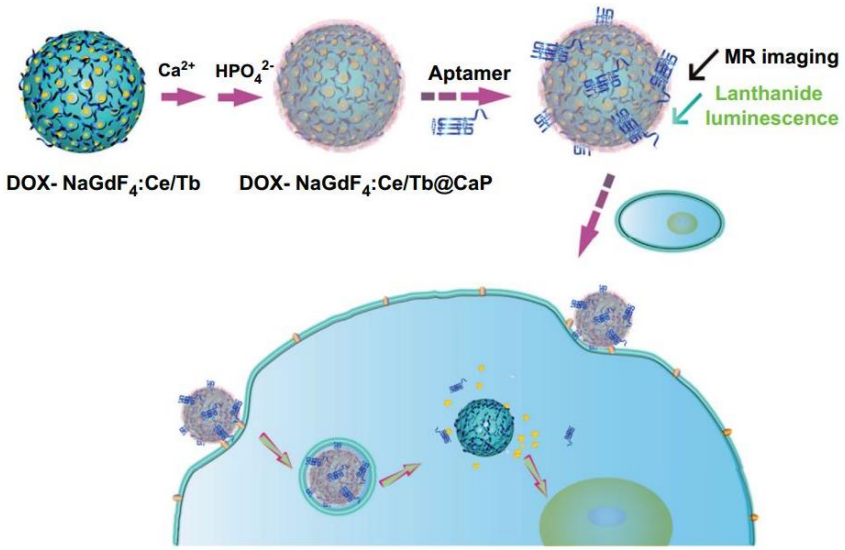

Figure 1-9. *DOX- loaded NaGdF4:Ce/Tb@CaP-Apt NHs were taken up by tumor cells via receptor-mediated endocytosis. The DOX was released after the dissolution of CaP within the intracellular lysosome. The RE element further endows NHs with the ability to visualize tumor sites. Cited from reference 64.*

1.3. The biological applications of metal–organic frameworks (MOF)

MOF endowed with attractive properties has become a new research hotspot during the past decades, which is largely attributed to their controllable pore size, high surface area and versatile functions. The pore size between 0.4 and 6 nm [65]resulted from the connection between the metals and organic linker is ideal for capture, separation and delivery (Figure 1-10)[66]. The low *in vitro* and *in vivo* toxicity stimulate scientists to continuously pursue and expand their biomedical applications. Nonetheless, being short of stability often hampers their potential uses. In addition, controlling of particle size is an important factor, not only for increasing the stability and fabricating reproducible formulations, but also *in vivo* administration that demands of the specific size in case of avoiding embolism. The surface modification provides another solution to stabilizing MOF that can be modified by coating with a hydrophilic polymer, poly(ethylene glycol), to increase affinity with surrounding biological medium and to prolong blood circulation[67].

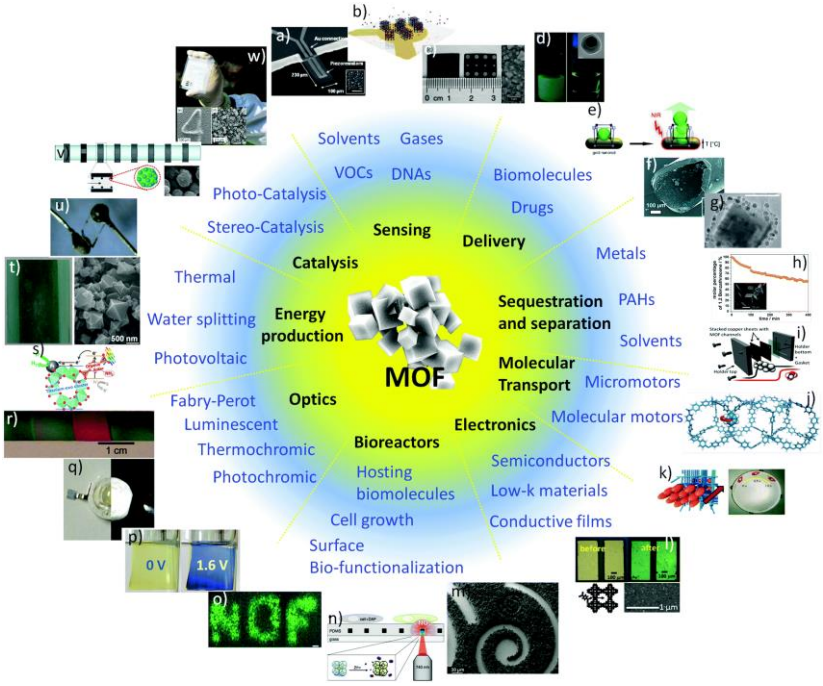

Figure1-10. *The diverse applications of MOF for different fields. The figure was quoted from reference 66.*

On the premise of their uniform porous structure, one major biomedical application of MOF is to function as nanoencapsulators to controllably release agents[68]. MOF demonstrated high drug capacity and perfect behaviors in drug release. Besides, their porosity, biodegradability and versatility enable them to exhibit a high potential for drug/gene delivery applications[69]. In the past, the fluorescent sensor often suffers from self-quenching and low quantum yields. Nevertheless, recent studies indicated that the immobilization of MOF could be conducive to this domain[70]. The organic ligands, metal ions and the interaction between metal ions and organic ligands endow MOF with fluorescence, which has been proved to change with intracellular pH value, and can thus be used for tracking pH value in biological environment[71, 72]. Zr-MOFs were adopted as scaffolds to load and stabilize ultra-small copper nanoparticles. What's more, triphenylphosphonium owing to its specific targeting ability for mitochondria, was further used for surface modification (Figure 1-11)[73]. This platform can realize localized drug synthesis by site-specific copper-catalyzed azide-alkyne cycloaddition (CuAAC) reaction in mitochondria. The in-situ fabrication of the drug from prodrugs in cellular organelles has competitive advantages in minimizing the unwanted side effects and heightening their efficacy. In summary, MOF had been widely utilized to biological and medical fields. Consequently, a more thorough comprehension of their biological mechanism helps MOF to meet the standards of a given administration, which is essential for real applications.

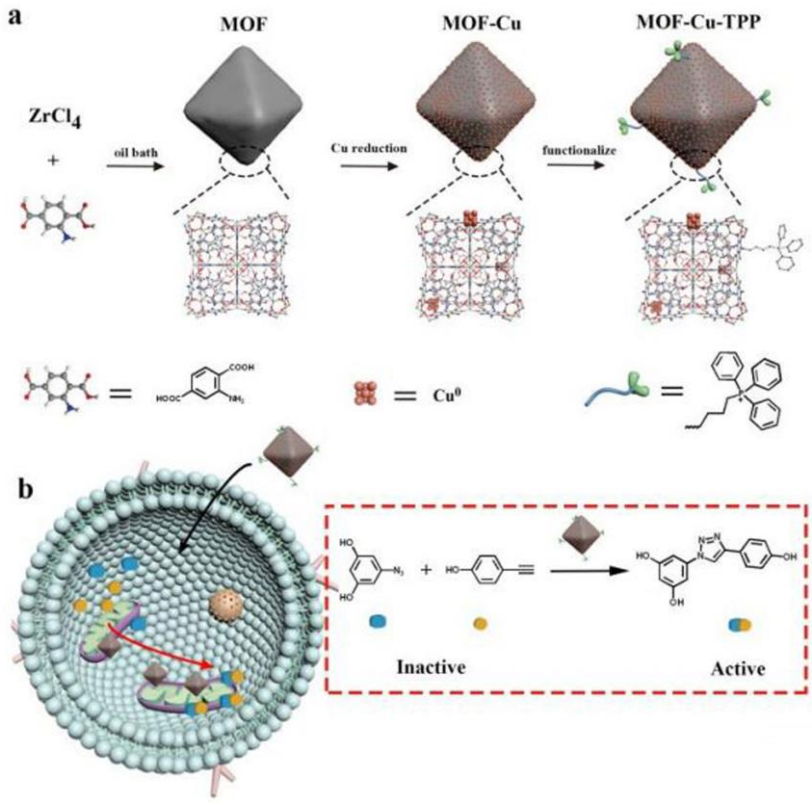

Figure 1-11. *Scheme illustration of fabricating of mitochondria-targeted CuAAC nanocatalysts and the in-situ drug synthesis under subcellular mitochondria Intracellular bioorthogonal reaction for in-situ drug synthesis catalyzed by the designed system. The in-situ reaction in subcellular organelles largely eliminated side effects and increased their uptake efficiency. Extracted from reference 73.*

1.4. Aim of the study

1.4.1. Research purpose and significance

Recently, the biological applications of NHs have aroused increasing curiosity and also attracted attention from most studied field. The attractive properties of NHs enable them to finish the expected tasks, such as controllable manipulation in drug release, compatible carrier for gene as well as precise detection of diseases. However, satisfactory employment of NHs in any of the above fields has not been achieved, for which one major hindrance should be blamed, namely, the change of NHs in the biological environment. Once NHs are administered *in vivo*, the original surface properties will be totally changed. For one thing, NHs will interact with proteins resulting in the formation of PC[74, 75]. For another, low pH value and presence of the digestive enzyme can gradually modify the shape and structure of NHs[76]. Additionally, some inert NHs, such as gold NHs, will be excreted out from the body by liver or kidney. Last but not least, the biotransformation and biodegradation hamper the translation from the chemical design of NHs to commercially available products.

To address the above-mentioned problems, some studies have been devoted to exploring the biological manners of NHs, most of which are focused on the *in vivo* biodistribution of NHs over months[77-79]. However, the extremely complex *in vivo* condition prevents us from making clear the effective biodegradation of NHs at cellular scale. Cellular degradation is the first step of NHs decomposition, which is the prerequisite for monitoring the biological behaviors *in vivo*. That is to say, a good command of relevant knowledge concerning cellular degradation facilitates scientists to design more functional nanomaterials and promote the development of NHs applications. Unfortunately, up to now, very few studies have explored the cellular degradation of NHs. In summary, our study focus on the biodegradation of NHs at the cellular scale.

1.4.2. The main research content

Our study is composed of two parts, the degradation of RE-based NHs and Zr-MOF both of which are inorganic-organic hybrid structures.

1.4.3. The degradation of RE-based NHs

The Eu^{3+} and Bi^{3+} doped $GdVO_4$ NHs coated with polyacrylic acid polymer were designed with the assistance of the classic core-shell structure. Recently, rare earth NHs are reported as a promising nanocarrier for cancer therapy and bio-imaging[80], and their unique and excellent features, including desirable biocompatibility, high photostability and perfect narrow emission lines, have gained significant attention. The tailor-made NHs are expected to continuously reveal the following mechanism, 1) the way of shape change of NHs during the degradation process, 2) the bio-dilution of NHs from cell division at cellular scale 3) the difference between exocytosis and biodegradation.

1.4.4. The biodegradation of Zr-MOF at the cellular scale

Among the large family of MOF, Zr-MOF featured with different structure types, long-term stability, attractive properties and applications, are emerging as one of the most promising MOF materials for practical and biological applications, despite that the understanding of biological behaviors of Zr-MOF is still in its early stage of development. Here, we explore the cellular degradation of Zr-MOF and study the relationship between cell growth and biodegradation.

2. The degradation of RE-based NHs

2.1. Introduction

Hundreds of functional NHs have been successfully fabricated for disease diagnosis and therapy; however, most of the desired goals have not been completely achieved. Of note, targeted NHs often exhibit disappointing targeting ability to designed cells *in vitro* and *in vivo*, which should be mainly attributed to the biotranformation and biodegradation. Increasing data shows that degradation changes the original surface features of NHs to a large extent, and further alters their fate in the biological condition[81]. For instance, PC on the surface of NHs can impose an influence on the NHs–cell interaction, initiate the complementary response[82], attach cell receptors and change the biocompatibility[83]. The release of metal ions from degraded NHs is influential to their biosafety and physiological metabolism[84]. Therefore, an in-depth investigation of the degradation is critical for a better understanding of its effects on biological behaviors. Here, the PAA coated Eu^{3+} and Bi^{3+} doped $GdVO_4$ NHs have been adopted as a nanoplatform for degradation studies (Figure2-1).

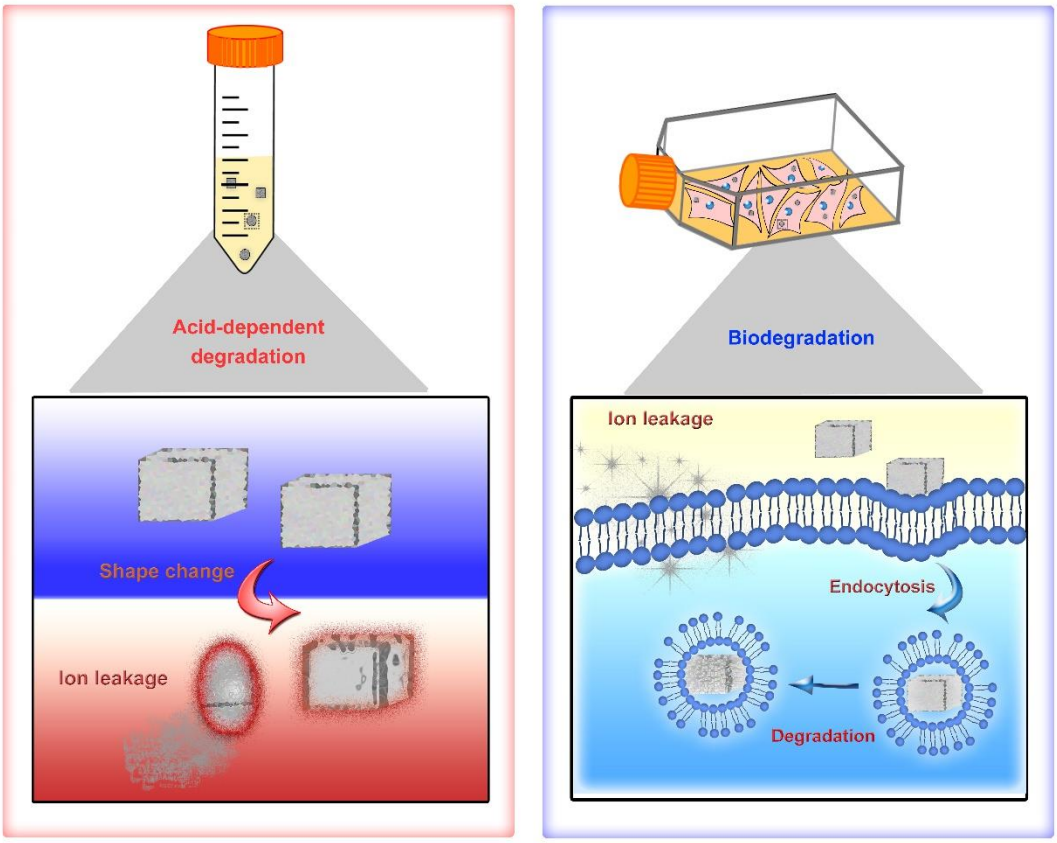

Figure 2-1. *Schematic illustration for our degradation study. It includes two parts, the degradation of NHs in the acid buffer and cellular microenvironment.*

2.2 Major reagents

Name	Purity	Company	Function
$Eu(NO_3)_3{\cdot}5H_2O$	99.90%	Sigma-Aldrich	For synthesize
$Bi(NO_3)_3{\cdot}5H_2O$	99.90%	Sigma-Aldrich	For synthesize
$Gd(NO_3)_3{\cdot}6H_2O$	99.90%	Sigma-Aldrich	For synthesize
Ethylene glycol	>99.5%	Fluka	For synthesize
Na_3VO_4	99.98%	Sigma-Aldrich	For synthesize
Polyacrylic acid	M_w~1800 Da	Sigma-Aldrich	For synthesize
Citric acid	99.90%	Acros	For degradation study
Sodium phospate dibasic	⩾98.5%	Sigma-Aldrich	For degradation study
Nitric acid	67 wt%	Fisher Chemical	For ICP-MS measurement
Hydrochloric acid	35wt%	Fisher Chemical	For ICP-MS measurement
Dulbecco's modified eagle medium		Thermofisher	For cell culture
Penicillin/streptomycin		Sigma-Aldrich	For cell culture
Fetal bovine serum		Biochrom	For cell culture
Resazurin	~80%	Sigma-Aldrich	For cytotoxicity
Phosphate buffered saline		Invitrogen	For cell culture
0.05% trypsin/EDTA		Thermofisher	For cell culture
Triton X-100		Sigma-Aldrich	For degradation study

Chloroquien disphsophate salt	>98%	Sigma-Aldrich	For degradation study
Ammonium chloride		Sigma-Alrich	For degradation study
Pepstatin A	≥90%	Sigma-Alrich	For degradation study
Glutaraldehyde	70% in H2O	Sigma-Alrich	For degradation study
Sodium cacodylate trihydrate	98%	Sigma-Alrich	For degradation study

2.3. Key instruments

Name	Model	Company	Function
Inductively coupled plasma mass spectrometry (ICP-MS)	7700 Series	Agilent	For ICP-MS measurement
Transmission electron microscopy (TEM)	JEM-1400PLUS	JEOL	For degradation study
Dynamic light scattering (DLS)	NANO ZS	Malvern	For degradation study
Fluorescence meter	Fluorolog-3	Horiba Jobin Yvon	For degradation study
Flow cytometry	BD LSRFortessa	BD Biosciences	For degradation study

2.4 Experiments and methods

2.4.1. Synthesis and characterizations of NHs

The rare earth nanoparticles were synthesized as previously reported[85]. The synthesis was performed by aging appropriate RE and orthovanadate precursors in ethylene

glycol (EG)/water mixtures at 120 °C in the presence of PAA. Briefly, 121 mg of $Gd(NO_3)_3 \cdot 6H_2O$ (99.99%, Sigma-Aldrich#451134, Germany) were dissolved in 8 mL of ethylene glycol (EG, >99.5%,Fluka #03750, Germany), and 14 mg of $Eu(NO_3)_3 \cdot 5H_2O$ (99.9%,Sigma-Aldrich #207918, Germany) and 48 mg of $Bi(NO_3)_3 \cdot 5H_2O$ (99.99%, Sigma-Aldrich, #254150, Germany) were dissolved in 1 mL of EG each, respectively" The solutions were gradually heated at 80 °C under continuous magnetic stirring to dissolve the reagents completely. Meanwhile, 368 mg of Na_3VO_4 (99.98%, Sigma-Aldrich #450243, Germany) and 40 mg of PAA (average molar mass $M_w \sim 1800$ Da, Sigma, Germany) were dissolved in 6 mL Milli-Q water and 4 mL of EG solution (volume ratio 3:2). The concentrations of the used materials are given in Table 2-1. Next, the sample was cooled to room temperature (RT), and was mixed together. All solutions were cooled toRT, and mixed. Final precursor concentrations are given in Table 2-1. It should be mentioned that an excess of vanadate was used in order to tune the particle size. The solution was divided into four portions of 5 mL each, which were aged for 5 h in tightly closed test tubes using an oven preheated at 120 °C, and finally cooled down to RT. After this, the solution the dispersions containing the precipitated nanoparticles were centrifuged at 7690 rcf (relative centrifugal force) for 15 min and washed two times with ethanol and once with water (Milli-Q water) to obtain the resulting PAA modified $EuBiGdVO_4$ NPs. To do so, around 10 mL of the corresponding liquid was added to the content of each reaction tube, followed by centrifugation and removal of the supernatants. Finally, the resulting PAA modified nominally $Eu_{0.08}Bi_{0.25}Gd_{0.67}VO_4$ NHs were dispersed in water. For further experiments, the nanoparticle concentrations were determined by drying known volumes of the corresponding dispersions.

Next, the obtained NHs were functionalized with the green fluorophore fluoresceinamine (FA, excitation/emission at λ_{ex} = 450 nm, λ_{em} = 520 nm).For that, the NHs solution was centrifuged (10000 rcf, 10 min), and the precipitated NHs were redispersed in MES (2- (N-morpholino) ethanesulfonic acid) buffer (20 mM, pH 6.5) at NHs concentration of 1.5 mg/mL. Then, 290 µL of EDC solution (0.5 M in MES buffer, freshly prepared) was added to 6 mL of NPs solution (1.5 mg/mL in MES buffer), and the mixture was stirred for 15 min at 37 °C in a thermo-shaker for activating carboxyl groups of the PAA on the surface. Next, the solution was centrifuged (10000 rcf, 10 min), the precipitated NHs were redispersed in 6 mL of HEPES (4-(2-hydroxyethyl)-1-piperazineethanesulfonic acid) buffer (20 mM, pH 8.5), and 1.16 mL of FA solution (1 mM in HEPES buffer) was immediately added. The mixture was incubated overnight with gentle stirring at RT. In this step, the primary amine groups of the FA will react with the previously activated carboxyl groups on the surface of NHs via amide bond formation. The next day, the NHs were collected by centrifugation (10000 rcf, 10 min), the precipitated NHs were washed twice with Milli-Q water, and finally the purified FA-labelled NHs were redispersed in Milli-Q water and stored at 4 °C until use. Prior to performing cell assays, the NHs were transferred to sterilized Milli-Q water by centrifugation (10000 rcf, 10 min) and redispersion in sterilized water. In the following, the NHs with FA-labelled polymer shell will be referred to as FA-NHs, whereas the NHs

with unlabelled polymer shell will be referred to as NHs.

Table 2-.1 Experimental conditions for the synthesis of RE-based NHs

Sample	c(Eu^{3+}) [M]	c(Bi^{3+}) [M]	c(Gd^{3+}) [M]	c(VO_4^{-3}) [M]	c(PAA) [mg/mL]	EG:H_2O Volumetric ratio
$EuBiGdVO_4$ NPs	0.0016	0.005	0.013444	0.1	2	3.5:1.5

The physicochemical characterizations of NHs were conducted with different methods. Firstly, the hydrodynamic diameter d_h of NHs was measured by dynamic light scattering (DLS, Malvern NANO ZS, England) using a UV-Kuevette, ZH 8.5mm Deckel (Sarstedt, Germany).[27] Briefly, 1 mL of NHs solution (C_{NHs}: 1.5 mg/mL) dispersed in Milli-Q water was equilibrated for 5 min at 25 °C. The samples were measured in Milli-Q water at 173° backscatter settings, using a 633 nm laser. Both, the number $d_{h(N)}$ and the intensity $d_{h(I)}$ distributions were recorded (Figure 2-3). Data are provided as mean value ± standard deviation (SD). A Malvern Zetasizer was used to measure the ζ-potential ζ of the NHs with laser Doppler anemometry (LDA). For that, 1 mL of NHs solution (C_{NHs}: 1.5 mg/mL) dispersed in Milli-Q water was equilibrated for 5 min at 25 °C before measurements. The distribution of ζ was shown in Figure 2-3. The ζ values are summarized in Table 2-6. The experiments had been conducted three times (n=3).

Secondly, the size distribution of the NHs cores and their shape was investigated by transmission electron microscopy (TEM) as previously reported[48]. The average size distribution of the side length d_c of the NHs was obtained by counting a 150 NHs for the TEM images. Briefly, for that, 10 µL of NHs solution was dried on top of the cooper grid. TEM images were captured by a JEM-1400PLUS HC TEM (JEOL, Germany). The corresponding histograms were calculated by open software Image J. Illustrative TEM images of the NHs and its corresponding size distributions are represented in Figure 2-4.

Then, we turned to investigate the optical properties of NHs. The fluorescence spectra $I_{Eu}(\lambda)$ and $I_{FA}(\lambda)$ of NHs-FA was evaluated as a function of pH. For this purpose, 1 mL NHs-FA at C_{NHs} (1.5 mg/mL) were dispersed in pH 3.5, 5 and pH7.4 Citric acid-Na_2HPO_4 buffer respectively. Then, the fluorescence spectra $I_{Eu}(\lambda)$ and $I_{FA}(\lambda)$ was measured by a fluorescence meter (Fluorolog-3, Horiba Jobin Yvon, USA), samples were excited at 330, 355 nm and 450 nm to characterize Europium $I_{Eu}(\lambda)$ and FA fluorescence $I_{FA}(\lambda)$ respectively (Figure 2-5). The experiments had been conducted three times (n=3).

Lastly, the concentrations of NHs were detected by ICP-MS[28]. For this purpose, the NHs were prepared to the diluted samples with a serial of concentrations. 50 µL of diluted

samples were digested with 150 µL of aqua regia (HNO_3 (67 wt%, Fisher Chemical, USA) and HCl (35 wt%, Fisher Chemical, USA) with a volume ratio of 1:3) overnight. Diluted the digestive samples with 1.8 mL of 2% HCl (35 wt%, Fisher Chemical, USA) to get the final samples. Transferred the samples to perfluoroalkoxy alkane (PFA) tubes and tested it by ICP-MS (ICP-MS, Agilent 7700 Series, USA).For detecting the concentrations of samples, the calibration curve for elements Eu,Bi and Gd including 9 concentration points (2500 to 0 µg/mL) have been used. We adopted element standard solutions to prepare calibration curves from Agilent. One sample was tested five times. The results are shown as the average value of five measurements. The correlations between the concentration of NHs C_{NHs} and the amount of Eu C_{Eu}, Bi C_{Bi} and Gd C_{Gd} were shown in Figure 2-6. The experiments had been conducted more than three times (n≥3).

2.4.2. The test of NHs degradation at different pH values

In order to evaluate the potential degradation of NHs, the effect of different pH buffer solutions on the optical properties as well as particle sizes were investigated by means of fluorescence spectra measurements $I_{Eu}(\lambda)$ and DLS ($N(d_h)$) and TEM respectively. Briefly, NHs were diluted at different C_{NHs} in pH 3.5, 5 and pH 7.4 (Citric acid-Na_2HPO_4) buffer respectively (at final V= 0.5 mL). See Table 2-2 for detail information of the C_{NHs} used. The effect of pH on the fluorescence of NHs was evaluated at RT for over 30 days. The $I_{Eu}(\lambda)$ of the samples were recorded every 3 days (Figure 2-7). The experiment had been conducted one time (n=1).

Table 2-2. Concentration and density range C_{NHs} and D_{NHs} of the NHs used for the degradation study in different pH buffers. A dilution series of factor 2 was prepared. The dose is expressed in three different metrics: i) the concentration C_{NHs} of NHs in terms of µg per mL, ii) the density D_{NHs} of NHs in terms of the quantity per L and iii) the concentration C_{NHs} of NHs in terms of mol per L. The dilution of NHs is a two-fold serial dilution.

Samples	C_{NHs} [µg/mL]	D_{NHs} [#/L]	C_{NHs} [mol/L]
1#-22#	9.54×10^{-4}-2.00×10^{3}	4.89×10^{9}-1.03×10^{16}	8.12×10^{-15}-1.70×10^{-8}

In order to evaluate the effects of the temperature on the degradation of the NHs, 0.5 mL of NHs at concentration C_{NHs} of 250 µg/mL was dispersed at pH 3.5, pH 5 Citric acid-Na_2HPO_4 buffer and Milli-Q water respectively over 30 days at 37 °C and RT. After the desired times, $I_{(Eu)}(\lambda)$ was recorded at excitation 355 nm and emission 618 nm. The $d_{h(N)}$ of each sample was also tested by DLS as previously described (Figure2-8). The results presented as number mean. Each data point includes three measurements of

DLS (each with 11 runs). The experiments had been conducted twice (n=2).

The degradation at 37°C is more obvious than the one at RT. Thereafter, we try to further investigate the evolution at 37°C. The NHs [250 µg/mL] incubated with 0.5 mL of pH 3.5 Citric acid-Na_2HPO_4 buffer for 0, 2,9,15 and 30 days at 37°C . The shape change of NHs during the degradation time period was characterized by TEM (Figure 2-9). At exact time points, samples were collected and sonicated for a short time. A drop of samples was dried on the surface of the grid. We adopted the JEM-1400PLUS HC transmission electron microscope to take TEM images. During the TEM measurement, the EDX spectra were simultaneously acquired in TEM mode to visualize the elemental mapping (Figure2-10- Figure2-12). Fitted the data with curves including three elements and all elements separately. The experiments had been conducted twice (n=2).The ζ of NHs were tested by DLS (Figure2-14). The method is the same with the previous measurements. Then, we turned to study the elemental change in the course of degradation. The samples were centrifuged at 21.1×10^3g for 5min with centrifugal filters (cutoff M_w:100kDa, Merck, Germany). Collected the supernatant and digested 50µL of samples with 150 µL aqua regia (HNO_3 (67 wt%, Fisher Chemical, USA) and HCl (35 wt%, Fisher Chemical, USA) with a volume ratio of 1:3) overnight. Diluted the samples with 1.8 mL 2% HCl (35 wt%, Fisher Chemical, USA), transferred it to PFA tubes. Determined the concentrations of elements by ICP-MS(Agilent 7700 Series, USA). The results were presented as the ratio between elemental concentrations at x days divided by 0 days (Figure2-13). The experiments had been conducted three times (n=3).

For further investigation of degradation behaviors of free FA, FA (Sigma#201626, Germany) at different concentrations C_{FA} (150, 75, 37.5, 18.75……. 0.036621, 0.018311 µg/mL) were treated with pH 3.5, 5 and pH 7.4 Citric acid-Na_2HPO_4 buffer respectively (final V= 0.5 mL) for 30 days. The FA fluorescence $I_{(FA)}$ (λ) was determined every three days by fluorescence meter(Fluorolog-3, Horiba Jobin Yvon, USA). The samples were excited at 488 nm, which consistent with the lasers at flow cytometry. The intensity at emission of 520 nm was recorded and plotted (Figure2-15). The experiment had been conducted one time (n=1).

2.4.3. TEM calculation

To be more precise, the shape parameters have been introduced to calculate the shape evolution of NHs. Firstly, make a mask of images by Image J. Then, the shape parameters were quantified by the open software cell profiler[86]. Next, adopt Photoshop to enlarge the distance between NHs (Figure2-16). The angles of NHs were defined and calculated by Matlab. The following shape parameters have been calculated. For one data, we have calculated more than 100 NHs (Figure2-17-Figure2-29).

a) Area (A_{NHs}, Figure2-30)

b) Eccentricity (Ec_{NHs}, Figure2-31)[87]: a parameter to determine how much a conic shape deviates from being a circle. For a circle, the Ec_{NHs} should be 0. The Ec_{NHs} of an ellipse is in the range from 0 to 1. At Ec_{NHs} =1, we can get the parabola.

c) Extent (Ex_{NHs}, Figure2-32)[88]: extent is the ratio between the area of a fitting the smallest rectangle and the area of the object. It showed the protrusion situation.

d) F factor (F_{NHs}, Figure2-33)[89]: the area and perimeter of the object should be measured. From this information, F_{NHs} was calculated as $4*\pi*Area/Perimeter^2$. F factor equals 1 for a perfect circle.

e) Solidity (S_{NHs}, Figure2-34)[90]: solidity is the ratio between the area of an object and the area of the convex hull. This parameter presents the indentation of the object.

f) Z factors (Z^0_{NHs}, Figure2-35)[91]: Zernike polynomials using coefficients was adopted to describe a binary object. In this study, we only calculated the 0^{th} moment Z to describe whether the object is similar to a circle (Z^0_{NHs} =1)or more fusiform-like (Z^0_{NHs} =0.25)shape

g) Compactness (C_{NHs}, Figure2-36)[92]: compactness was calculated as the mean radial distance of the object's pixels from the centroid divided by the object area. As for a filled circle, the C_{NHs} equals 1. The irregular shape or objects with holes having C_{NHs} more than 1.

h) Angle (α_{NHs}, Figure2-30)

Then, we defined the average area of the group with Milli-Q water as a threshold. The threshold separate NHs into two groups, single NP and aggregated NHs, which provide a clear picture of change in shape parameters according to different situations. For each condition, more than 100 NHs have been analyzed.

2.4.4 Cell culture and cell viability

Human epithelial cell line Hela was obtained from American Type Culture Collection (ATCC) (Manassas, VA, USA). Hela cells were cultured in Dulbecco's modified eagle medium (DMEM, Thermofisher, USA), supplemented with 10% fetal bovine serum (FBS, Biochrom, UK), 1% penicillin/streptomycin (P/S, Sigma-Aldrich, Germany). Cells were grown in the incubator at 37 °C and 5% CO_2.

For *in vitro* viability assay, the biocompatibility of NHs was tested by resazurin assay[53]. HeLa cells were seeded in 96-well plates (Sarstedt, Germany) with a growth area 0.32 cm^2 at a density of 7,500 cells in 100 µL medium per well overnight. The NHs were diluted at different concentrations in complete cell medium. The concentrations are provided in Tables 2-3. Remove the supernatant of cells in each well and expose the NHs with serials concentrations to cells (100 µL medium per well). After incubation for

24 hours and 48 hours respectively, the cells were washed with phosphate buffered saline (PBS, Gibco, Invitrogen, Belgium) once (0.1 mL per well). The DMEM medium was mixed with the resazurin salt solution (Sigma-Aldrich, USA) at a concentration of 0.25 mg/mL solution (10:1) to obtain the working solution. The working solution was added to each well (100 µL), and the plates were incubated at 37 °C for 4 hours. The experiments had been conducted three times (n=3).

To detect the metabolic activity of cells, the blue nonfluorescent resazurin reagent is converted to red highly fluorescent due to the reduced cellular microenvironment[93939392]. The emission fluorescence spectra was monitored from 572 nm to 650 nm by fluorescence meter(Fluorolog-3, Horiba Jobin Yvon, USA) with excitation at 560 nm. The data was analyzed by Matlab software. Results for viability V are represented as fluorescence intensity of cells incubated with NHs, normalized to the fluorescence intensity of control cells (Figure2-37).

Table 2-3. The concentration and density of used NHs C_{NHs} and D_{NHs} for cytotoxicity study. The concentrations are presented at different units in terms of µg/mL, #/L (Number of NHs per liter) and mol/L. The relationship between the mass concentration of Eu C_{Eu}, Bi C_{Bi}, Gd C_{Gd} and the mass concentration of NHs $C_{NHs.}$ The dilution of NHs is a two-fold serial dilution.

Samples	C_{NHs} [µg/mL]	D_{NHs} [#/L]	C_{NHs} [mol/L]
1#-20#	9.54×10^{-4}-5.00×10^{2}	4.89×10^{9}-2.56×10^{15}	8.12×10^{-15}-4.26×10^{-9}

C_{Eu}[µg/mL]	C_{Bi}[µg/mL]	C_{Gd}[µg/mL]
6.33×10^{-5}-7.26×10^{0}	1.15×10^{-4}-2.94×10^{1}	3.59×10^{-4}-5.44×10^{1}

2.4.5. The procedures of biodegradation study

Firstly, the used concentrations of NHs for biodegradation study were determined by ICP-MS as previously described. The working concentrations of NHs were given in Table 2-4.

Then, cells were seeded at a 24-well plate or 6-well plate. On the next day, the NHs at working concentrations were exposed to cells for different exposure time intervals t_{exp} of 6, 24, 48 hours in the incubator at 37°C and 5% CO to study the uptake efficiency. For the degradation study, we aspirated the supernatant at t_{exp}=24 hours. The cells were washed with PBS (1 mL/well for 24 well-plate, 2 mL/well for 6 well-plate) three

times and added fresh medium (0.5 mL/well for 24 well-plate, 2 mL/well for 6 well-plate). Keep another incubation time t_{inc} for 0, 24, 48 and 72 hours.

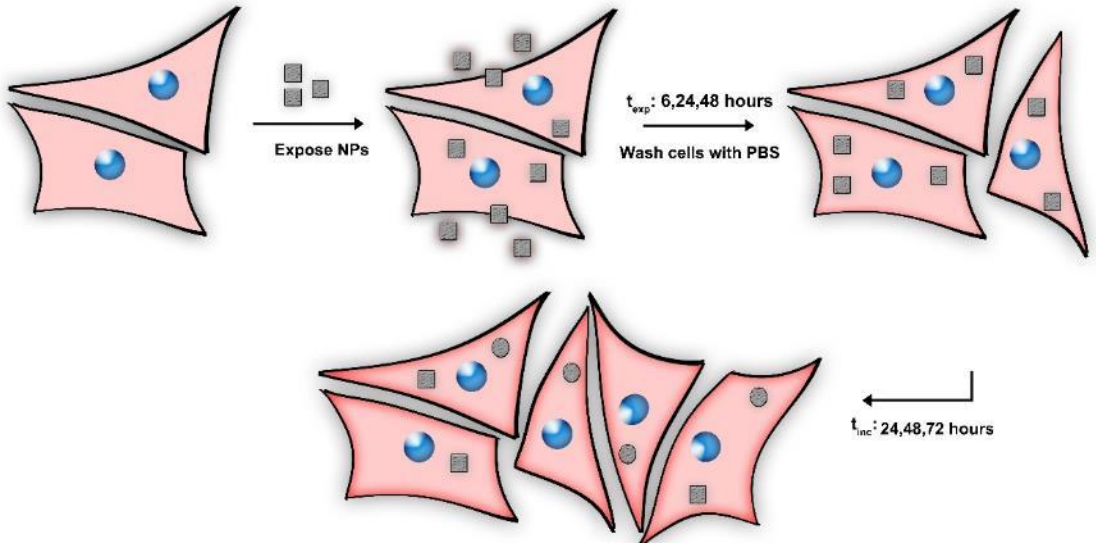

Figure 2-1. *Schematic illustration of uptake and biodegradation study. For uptake study, NHs at different concentrations were exposed to cells for 6, 24 and 48 hours (t_{exp}). For biodegradation study, remove the supernatant of cells for 24 hours (t_{exp}) incubation with NHs and add fresh medium. Keep the additional incubation of NHs for 24, 48 and 72 hours (t_{inc}).*

Table 2-4. The working concentration and density of NHs C_{NHs} and D_{NHs} for biodegradation study. The concentrations are presented at different units in terms of μg/mL, #/L and mol/L. The relationship between the mass concentration of Eu C_{Eu}, Bi C_{Bi}, Gd C_{Gd} and the mass concentration of NHs C_{NHs}.

Samples	C_{NHs} [μg/mL]	C_{NHs} [#/L]	C_{NHs} [mol/L]	C_{Eu} [μg/mL]	C_{Bi} [μg/mL]	C_{Gd} [μg/mL]
1#	2.50	1.28×10^{13}	2.13×10^{-11}	0.04	0.15	0.27
2#	5.00	2.56×10^{13}	4.26×10^{-11}	0.07	0.29	0.54
3#	10.00	5.13×10^{13}	8.52×10^{-11}	0.15	0.59	1.09
4#	20.00	1.03×10^{14}	1.70×10^{-10}	0.29	1.18	2.18
5#	40.00	2.05×10^{14}	3.41×10^{-10}	0.58	2.35	4.35
6#	80.00	4.10×10^{14}	6.81×10^{-10}	1.16	4.71	8.70

7#	160.00	8.21×10^{14}	1.36×10^{-9}	2.32	9.41	17.40

2.4.6.NHs uptake and degradation tested by flow cytometry

To further investigate the cellular behaviors of NHs, we adopted the flow cytometry (BD LSRFortessa™, BD Biosciences, US) to detect the uptake and degradation of NHs-FA[33]. Hela cells were seeded at a density of 40,000 cells per well with a volume of 1 mL into 24-well plate (surface area 1.82 cm^2, Sartstedt, Germany). On the next day, the procedures of biodegradation study had been conducted. At exact time points, cells were washed with 1 mL of PBS three times and digested with 0.05% trypsin/EDTA solution (Thermofisher, USA) in a volume of 0.1 mL. Trypsin was neutralized with 1mL of complete cell medium. Detached cells were collected in flow cytometry tubes (Falcon, Germany) and centrifuged at 300 g for 5 min to get the cell pellet. The cells were resuspended in PBS with a volume of 0.3 mL. The cell number of each sample have been counted. For this purpose, 10 µL of cell suspension solution was added to the cell counting chamber (Neubauer Chamber, Celeromics Technologies, Spain) and the cell number for each sample was counted by the microscope one by one. The resuspended cells were then characterized by flow cytometry (with laser 355nm and laser 488 nm,). Data were analyzed by Flowjo software (Figure2-40). Data subtracted the fluorescence of control cells to obtain the mean Eu fluorescence $I_{Eu/cell\ (intra)}(\lambda)$ and mean FA fluorescence $I_{FA/cell\ (intra)}(\lambda)$ (Figure2-38). In the meantime, we recorded cell growth during the degradation study. From these data, the mean Eu fluorescence $I_{Eu/cell\ (intra)}(\lambda)$ and mean FA fluorescence $I_{(FA)}(\lambda)$normalized by cell growth were calculated and summarized in Figure2-39. Briefly, we defined growth factor as the cell number at t_{inc}=x hours divided by the value at t_{inc}=0 hour. Then, the mean Eu fluorescence $I_{Eu/cell\ (intra)}(\lambda)$ and mean FA fluorescence $I_{FA/cell(intra)}(\lambda)$multiply with the growth factor respectively to obtain the normalized Eu fluorescence $I_{Eu/cell\ (normalized)}(\lambda)$and normalized FA fluorescence $I_{FA/cell\ (normalized)}(\lambda)$.The experiments had been conducted four times (n=4).

2.4.7. Biodegradation of NHs characterized by fluorescence meter

To evaluate the biodegradation of NHs-FA by Hela cells, the fluorescence originating from NHs-FA inside cells was quantified by fluorescence meter. Therefore, Hela cells were seeded on a 24-well plate at the density of 40,000 cells per well in a volume of 1 mL. On the next day, we conducted the experiment with the procedure of biodegradation study. From the data quantified by flow cytometry, we can know the fluorescence at low concentration (2.5 and 5 µg/mL) of NHs is low. Thereafter, we chose the part of concentration (10-160 µg/mL) to continue the biodegradation study detected by fluorescence meter. After the desired time, cells were washed three times with 1 mL of PBS buffer and lysed with 100 µL of 0.2 M NaOH containing 0.5%

Triton X-100 (T87875, Sigma, Germany)for 30 min at RT. Next, added PBS with a volume of 430 µL to each well and collected the samples in 2 mL Eppendorf tubes (Sarstedt, Germany). The Eu fluorescence I_{Eu} (λ)and FA fluorescence I_{FA} (λ)of samples were measured by fluorescence meter (Fluorolog-3, Horiba Jobin Yvon, USA) with excitation 355 nm/488 nm and emission 618 nm/520 nm (Figure2-41). The experiments had been conducted twice (n=2).

2.4.8. Study the effect of intracellular pH value on the fluorescence of cells

In order to distinguish the fluorescence change between NHs-FA degradation and intracellular pH variation, we further study the effect of intracellular pH value on the fluorescence of cells. Cells were seeded in 24 well plate (surface area 1.82 cm^2,Sarstedt, Germany).at density of 40,000 cells in a volume of 1 mL. On the following day, cells were incubated with NHs-FA at a dose of 160 µg/mL for 24, 24+24 and 24+48 hours (presented as $t_{exp} + t_{inc}$). Afterward, the medium was replaced with PBS and cells were washed with 1 mL of PBS twice. Cells were rinsed with 150 mM NaCl aqueous solution with a volume of 1mL, detached with 100 µL of 0.05% trypsin/EDTA and collected with 300 µL of 150 mM NaCl aqueous solution in flow cytometry tubes. The tubes were centrifuged at 300g for 5 min in order to get the pellet. The pellet was redispersed in different pH buffer and 150 mM NaCl aqueous solution with a volume of 300µL respectively. To make a pH calibration curve, buffers were prepared by mixing DPBS (pH 7.4) with MES buffer (pH 4.0; 50 mM MES, 150 mM NaCl, 4 mM KCl, and 1 mM $MgSO_4$). Monensin and nigericin (dissolved in Ethanol) were added into different pH buffers at final concentrations of 20 µM and 10 µM respectively to equilibrate the intracellular environment to the extracellular pH buffer. To compare with the cells exposed to NHs-FA, the cells without NHs-FA were also collected and resuspended in pH clamp buffer and 150 mM NaCl aqueous solution by the same method. As controls, the Hela cells with or without NHs-FA were collected in the normal way. Briefly, cells were rinsed with 1 mL of PBS three times, trypsinated with 100µL of 0.05% trypsin/EDTA and normalized with 0.5 mL of FBS supplemented cell medium. Detached cells were gathered in flow cytometry tubes and centrifuged at 300g 5min. Then cell pellet was resuspended in 300 µL of PBS buffer. All the samples were characterized by flow cytometry (with laser 355 nm and laser 488 nm). The mean Eu fluorescence $I_{Eu/cell\ (intra)}$ (λ) and mean FA $I_{FA/cell\ (intra)}$ (λ) fluorescence were analyzed and plotted by flowjo software. These data have already normalized by the control value (Figure2-42). The experiment had been conducted once (n=1).

2.4.9. The impact of lysosome inhibitors on NHs degradation inside cells

In order to investigate the effect of lysosome inhibitors on the cell viability, 7,500 Hela cells were seeded per well in 96-well plates (growth area 0.32 cm^2, sarstedt, Germany), dispersed in 100 µL of FBS supplemented DMEM medium. In the next day, the supernatant was removed and 100 µL of fresh medium containing the NHs-FA at a

concentration of 80 μg/mL was added. Cells were incubated with NHs-FA for 24 hours (t_{exp}) in the incubator with 5% CO_2 at 37 °C. Then, the old medium was removed and washed the cells with PBS (100μL per well) three times. A part of cells were incubated with 100μL per well of full cell medium containing Chloroquine (CQ, ＞98%, Sigma-Alrich#C6628, Germany), Ammonium chloride (NH_4Cl, Sigma-Alrich#A9434,Germany) and Pepstatin A (PA, ≥90%, Sigma-Alrich#P5318, Germany) at desired concentrations (C_{CQ}, C_{NH4Cl}, C_{PA}) for 24, 48 and 72 hours respectively (t_{inc}). The concentration range of lysosome inhibitors was listed in Table 2-5. Another part of cells was treated with serum-free medium (SF) for 24, 48 and 72 hours (t_{inc}). As controls, cells without NHs-FA were also exposed to lysosome inhibitors and serum-free conditions for 24, 48 and 72 hours. After the incubation time, cells were washed once with PBS (100 μL) and then the diluted resazurin salt solution was added in each well (100 μL per well) and incubated the plate for 4 hours at 37 °C. Next, the fluorescence was measured at 560 nm excitation and 590 nm emission wavelengths using fluorescence meter (Fluorolog-3, Horiba Jobin Yvon, USA). The data analysis is the same as mentioned above (Figure2-45). The experiments had been conducted three times (n=3).

Table 2-5. The concentration range of lysosome inhibitors

Sample	C_X 1	C_X 2	C_X 3
C_{CQ}	5 μM	2.5 μM	1.25 μM
C_{NH4Cl}	40 mM	20 mM	10 mM
C_{PA}	10 μg/mL	5 μg/mL	2.5 μg/mL

Hela cells were seeded into 24-well plate (surface area 1.82 cm^2, Sarstedt,Germany) with an amount of 40,000 cells per well with 1 mL of complete cell medium. On the next day, NHs- FA in a volume of 0.5mL at concentrations of 80 μg/mL and 40 μg/mL were exposed to cells for 24 hours (t_{exp}). Then, we removed the supernatant and washed the cells with 1 mL of PBS three times. Cells were partially added the complete cell medium with inhibitors at different concentrations (Table 2-5) with a volume of 0.5 mL for 24, 48 and 72 hours (t_{inc}). A portion of cells was treated with serum-free cell medium for 24, 48 and 72 hours (t_{inc}). For comparison with cells contained NHs-FA, the control cells were also incubated the lysosome inhibitors and serum-free medium for 24, 48 and 72 hours (t_{inc}). After incubation, cells were washed with 1 mL of PBS three times and detached with 100 μL of 0.05% trypsin/EDTA solution. Trypsin/EDTA was neutralized with 1 mL of complete cell medium. Resuspended cells were transferred to flow cytometry tubes and centrifuged at 300 g for 5 minutes. The supernatant was removed and 300 μL of PBS was added to each tube. Every sample was counted by the

counting chamber. We then used flow cytometry with laser 355 nm and 488 nm to characterize the samples. The mean Eu fluorescence intensity $I_{Eu/cell\ (intra)}(\lambda)$ and mean FA fluorescence $I_{FA/cell\ (intra)}(\lambda)$ intensity coming from the Hela cells were corrected by the control group and calculated with Flowjo software (Figure2-43). Normalized Eu fluorescence $I_{Eu/cell\ (normalized)}(\lambda)$ and normalized FA fluorescence $I_{FA/cell\ (normalized)}(\lambda)$ were obtained by the method as described above (Figure2-44). The experiments had been conducted three times (n=3).

2.4.10. NHs uptake and degradation determined by ICP-MS

To assess the cellular fate of NHs, we adopted ICP-MS to characterize the uptake and degradation[5]. Hela cells were seeded in 6 well plates (growth area: 8.87 cm^2, Sartstedt, Germany) at a density of 207,890 cells per well in 2 mL of FBS supplemented cell medium. Then, the procedures of biodegradation study were also carried out. To investigate the biodegradation of NHs for a longer time point (Figure2-2), cells in 6-well plates were partially exposed NHs at the same working concentrations (Table 2-4) for 24 hours (t_{exp}). The cell medium was aspirated and added fresh medium. After 48 hours of incubation time (t_{inc}), collected the supernatant. Cells were washed with 2mL of PBS three times, digested it with 0.05% trypsin-EDTA with a volume of 200 µL and removed the trypsin. Gently blowed the cell with cell medium in a volume of 1 mL, collected the cell suspension solution and resuspended in T-25 flask (Growth area: 25 cm^2, Sarstedt, Germany). Added 2.6 mL of cell medium and the collected supernatant of original well with a volume of 2 mL to make the final volume of flask is 5.6 mL. Kept it for another incubation time (t_{inc}) of 72 hours (total incubation time t_{inc}: 120 hours).At different time points, the supernatant was collected. The cells were washed with PBS (2mL for 6-well plates, 4 mL for T-25 flasks) three times and detached from the bottom of the plates by 0.05% trypsin-EDTA (200 µL for 6-well plates, 600 µL for T-25 flask). When the cells were detached, we added PBS (1 mL for 6-well plate, 3 mL for T-25 flask) to count the cells in each well. Then, the samples were centrifuged at 4000 rpm for 10 min and the supernatant was removed. As for the cell pellet, it was digested with 75 µL HNO_3 (67 wt%, Fisher Chemical, USA) overnight, added 150µL HCl (35 wt%, Fisher Chemical, USA) to the solution. Keep the cell pellet with concentrated acid for overnight. Diluted it with 2.275 mL 2% HCl (35 wt%, Fisher Chemical, USA) transferred the sample with a final volume of 2.5 mL to 6 mL PFA tubes. As for the supernatant, 50µL of samples were digested with 150 µL of aqua regia overnight. Diluted the concentrated samples with 1.8 mL of 2% HCl (35 wt%, Fisher Chemical, USA) to get the test sample with a final volume of 2 mL. The samples were detected by the ICP-MS machine with the argon gas as flow. The experiments had been conducted more than three times ($n \geqslant 3$).

To compare the elemental concentration in pellet and supernatant, we need to consider the volume factor. For the supernatant, the volume in each well is 2 mL, which

is the same as the volume of test samples. Whereas, the medium volume in wells is 2 mL for the cell pellet samples, which is inconsistent with the test samples in a volume of 2.5 mL. The data of cell pellet samples should multiply with 1.25 to normalize the dilution. The ratios between Eu, Bi and Gd were plotted and calculated for the cell pellet and supernatant (Figure2-46-Figure2-49).

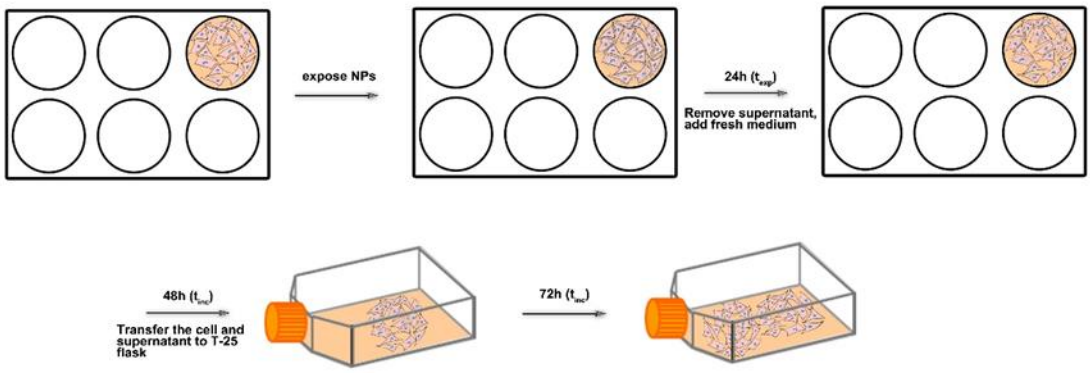

Figure 2-2. *Scheme illustration of procedures for biodegradation study by ICP-MS for a longer time. NHs at working concentrations were incubated with cells for 24 hours (t_{exp}).Remove the supernatant and add the new cell medium. Keep the incubation time for 120 hours (t_{inc}).*

2.4.11. Cellular degradation of NHs followed by TEM

Hela cells were seeded into culture flask (growth area 25 cm^2, Sarstedt, Germany) at a density of 589,935 cells per flask with a medium volume of 5.6 mL. The next day, cells were exposed to NHs (160 µg/mL) for 6 and 24 hours (t_{exp}) respectively to visualize the shape change during uptake process. For the biodegradation study, the supernatant of cells was removed at 24 hours (t_{exp}) and washed the cells with 3 mL of PBS three times. Added fresh complete cell medium with a volume of 5.6 mL to each flask and kept the incubation time for 72 hours (t_{inc}). To get an insight into the biodegradation of NHs for a longer time, cells incubated with NHs for 24 hours and replaced the old medium with a new one. NHs at t_{inc}=48 hours were detached with 0.05 % trypsin-EDTA and resuspended in new culture flask (growth area 75 cm^2 , Sarstedt, Germany) for another 72 hours of incubation time (the total incubation time t_{inc} is 120 hours). After different time points, cells were rinsed in PBS buffer for three times and fixed in 3% glutaraldehyde (prepared from glutaraldehyde solution, 70% in H_2O, Sigma-Aldrich#G7776) in 0.1 M sodium cacodylate buffer (pH 7.4) for 30 min at RT. Cells were detached from culture flask by careful scraping and collected by centrifugation at 300 g for 5 min. The cell pellets were resuspended in 1 ml of fixation buffer (3% glutaraldehyde in 0.1 M sodium cacodylate buffer). To embed the samples in agarose, we firstly prepare 2% agarose in Soreson's phosphate buffer. Centrifuge cells at 0.8 g for 5 min, remove the supernatant and resuspend it in 2% agarose. Mixed the solution

gently, centrifuge it at 0.8 g for 1 min. Cooling the samples to RT and put it at 4 °C overnight. Cut the samples at about 1 mm^3 cube and put them in an Eppendorf tube. The pellets were post-fixed in 1 mL of 0.6% osmium tetroxide and kept it in ice and dark for 1 hour. Then, the samples dehydrated in ethanol with a range of concentrations followed by acetone, embedded in Spurr's resin and cured at 60 ºC in a vacuum oven overnight. Ultrathin sections were cut on a Leica UC7/FC7 microtome (Leica Microsystems, Germany). Digital images were collected using the TEM (JEM-1400PLUS, from JEOL, Japan) (Figure2-50).The cell TEM images were also analyzed and calculated by the above method. For one data, we calculated more than 170 NHs (Figure2-51-Figure2-55). The experiments had been conducted twice (n=2).

2.5. Results and discussions

2.5.1. The synthesis and characterizations of NHs

PAA coated Eu- and Bi-doped $GdVO_4$ NHs were constructed and characterized as described in our previous work[94]. In brief, the core-shell NHs were obtained by a one-pot synthesis with the surface functionalization of PAA. It can be achieved by a specific design for releasing the anions or cations within the solution. To measure the degradation behaviors of surface polymer, FA was linked to the PAA. As shown by TEM, the NHs displayed well-defined cubic shapes with side length of 32.9± 4.14 nm (Figure2-3), which was close to the side length of 33.17±0.65 nm obtained via DLS. The zeta potential of NHs was -32.30±2.42 mv (Figure 2-4). Judging from fluorescence spectra, we can find NHs contained two fluorescence, the typical luminescence of Eu(III) and the fluorescence from FA, whose intensity were gradually reduced with a descending pH value (Figure2-5).In general, we successfully constructed the tailor-made NHs with defined cubic shape, narrow size distribution and two fluorescences. The relationship between the concentration of NHs C_{NHs} and the amount of Eu C_{Eu}, Bi C_{Bi} and Gd C_{Gd} further give the information about the elemental composition (Figure2-6). The ratio of C_{Eu}/C_{NHs}, C_{Bi}/C_{NHs} and C_{Gd}/C_{NHs} is 1.66, 6.28 and 12.17, respectively.

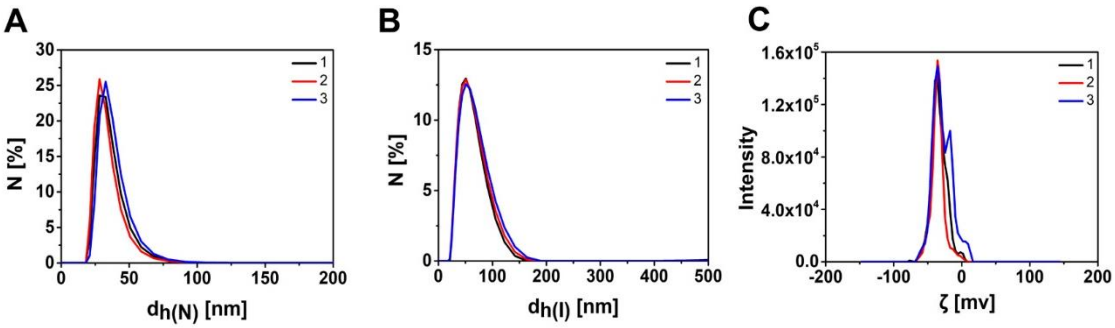

Figure2-3. *The hydrodynamic diameter d_h of NHs as determined with DLS in Milli-Q water. Number distribution $d_{h(N)}$ (A), Intensity distribution $d_{h(I)}$ (B)and ζ-distribution ζ of NHs (C). The results represent three measurements are shown.*

Table2-6. The hydrodynamic diameter d_h of NHs as determined with DLS in Milli-Q water. Number distribution $d_{h(N)}$, Intensity distribution $d_{h(I)}$ and ζ-distribution ζ of NHs. The results represent three measurements are shown.

Sample	$d_{h(N)}$ [nm]	$d_{h(I)}$ [nm]	PDI	ζ [mV]	d_{TEM} [nm]
$EuBiGdVO_4$	33.17±0.65	54.62±0.85	0.23±0.00	-32.30±2.42	32.9± 4.14

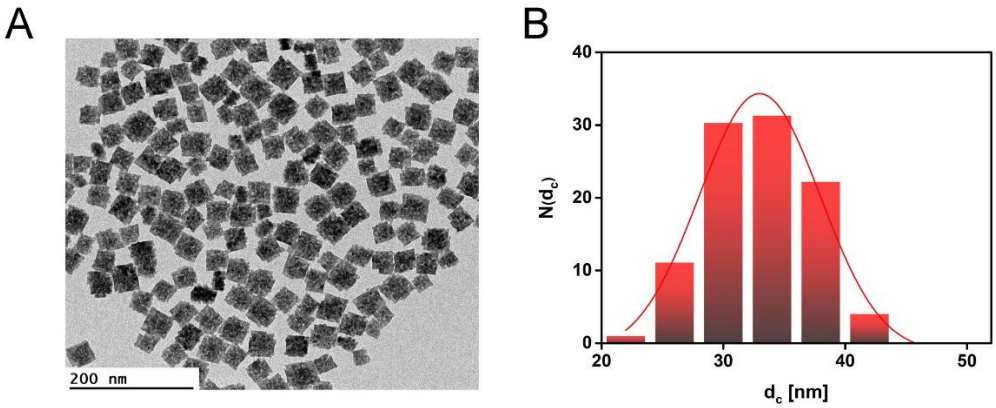

Figure2-4. *The TEM image of NHs (A) and side length histogram distribution of NHs as measured by TEM (B).*

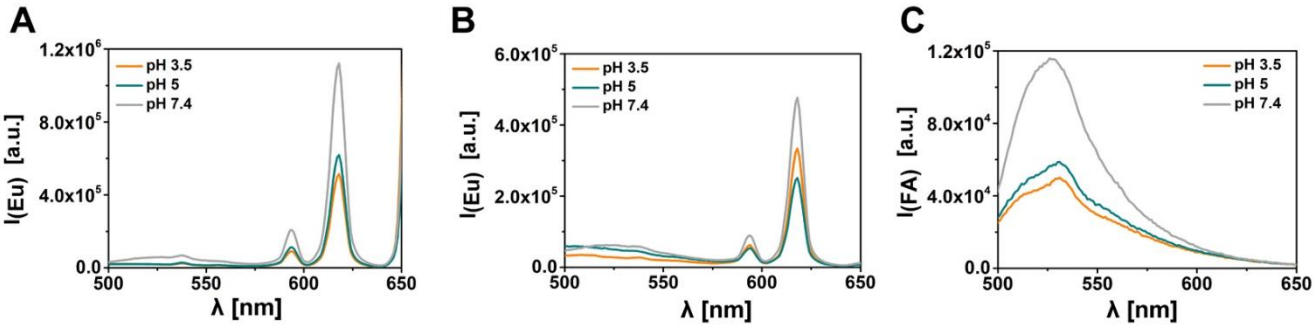

Figure 2-5. *Fluorescence spectrum of NHs-FA. Representative Eu and FA fluorescence spectrum $I_{EU}(\lambda)$ and $I_{FA}(\lambda)$ of NHs at C_{NHs} (1.5 mg/mL) at pH 3.5, 5 and 7.4 at t = 0 h after immersion in buffer. Spectra resulting from FA-NHs solution exited at λ_{330} (A), λ_{355} (B) and λ_{450} (C) respectively.*

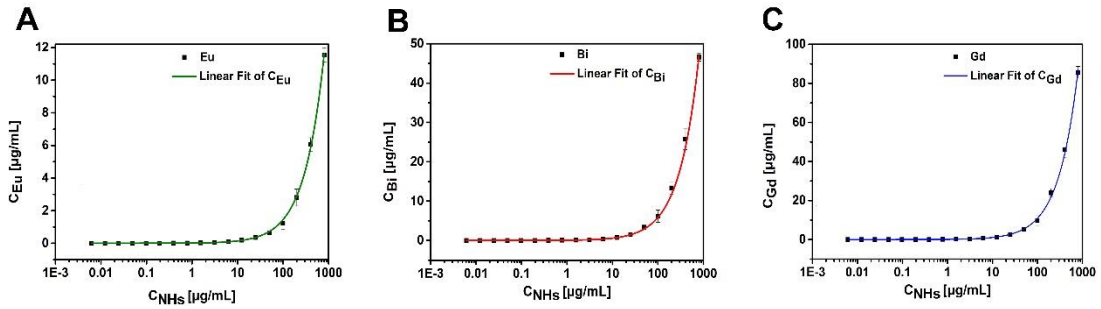

Figure2-6. *The standard curves of correlations between the concentration of NHs C_{NHs} and the amount of Eu C_{Eu}, Bi C_{Bi} and Gd C_{Gd}., determined by ICP-MS. For the relationship between C_{Eu} and C_{NHs}, the equation is $y=0.01452x+4.945\times10^{-5}$ $R^2=0.9961$ (A). For the relationship between C_{Bi} and C_{NHs}, the equation is $y=0.05884x+5.929\times10^{-5}$ $R^2=0.9984$ (B). For the relationship between C_{Gd} and C_{NHs}, the equation is $y=0.1088x+2.548\times10^{-4}$ $R^2=0.9965$ (C).*

2.5.2. NHs degradation at different pH buffers

Rare earth metals are commonly featured with dissolution in the acid buffer, which may lead to the destruction of rare earth nanoparticles. It is expected that the structure of rare earth nanoparticles will collapse and diminish under an acid condition. To evaluate the acid-dependent degradation for the inorganic core, the NHs of serial dilutions were directly immersed in the buffer with different pH values (pH 3.5, 5 and 7.4). In buffer with pH 3.5 buffer, the NHs were significantly degraded, as evidenced by a sharp decrease in Eu fluorescence $I_{(Eu)}$ (λ) . It was also found the pH 5 buffer had a comparatively slight effect on $I_{(Eu)}$ (λ), whereas no obvious fluctuation was found in data in pH 7.4 buffer. Interestingly, the decrease in fluorescence was NHs concentration-dependent. The reduce in $I_{(Eu)}$ (λ) can be observed in NHs at 0.00195-0.5 mg/mL. Comparatively, the intensity of $I_{(Eu)}$ (λ)displayed the irregular value at the high concentration with 1-2 mg/mL. It was hypothesized that the high concentration caused severe sedimentation, and thus decreased the opportunity for NHs to react with acid buffer. Thereafter, the acid buffer becomes less able to dissolve the sedimentation.

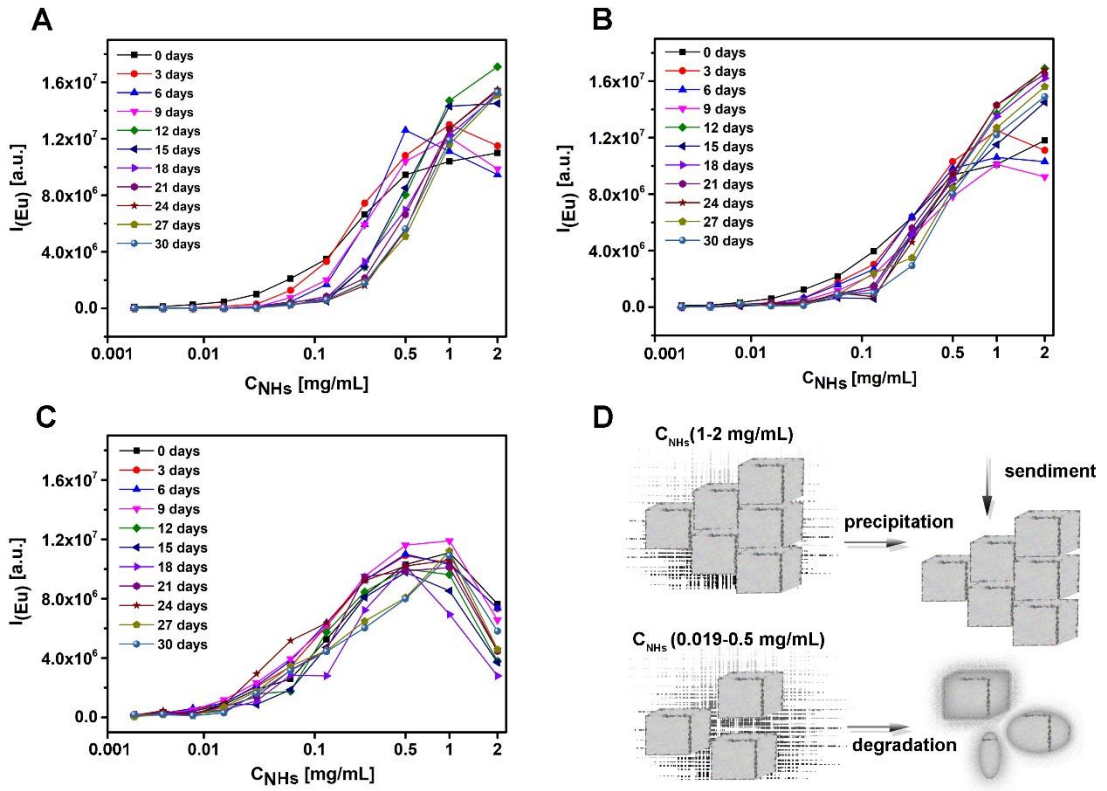

Figure 2-7. *NHs degradation at different pH buffers evaluated by means of fluorescence intensity measurements. Fluorescence spectrum $I_{(Eu)}$ (λ) of NHs at different concentration C_{NHs} dispersed in the different buffers, at pH 3.5 (A), pH 5 (B) and pH 7.4 buffer (C) for 30 days at RT. Sketch illustrating the effect of C_{NHs} on the degradation of NHs. The high concentration induces the precipitation of NHs (D). It is difficult for the precipitation to react with acid buffer completely. So, the $I_{(Eu)}$ (λ) of NHs at high concentration didn't decrease with time*

Next, we turned to explore the effect of temperature on acid-dependent degradation. Core-shell NHs were exposed to citric acid – Na_2HPO_4 buffer with different solutions (pH 3.5, 5 buffers and Milli-Q water) for 30 days at RT and 37°C. The degradation process was monitored by the fluorescence assay based $I_{(Eu)}$ (λ) and size measurement. As displayed in Figure 2-8, the decrease of $I_{(Eu)}$ (λ) was substantially accelerated under pH 3.5 condition compared with that in pH 5 and Milli-Q water. Besides, a moderate decline in $I_{(Eu)}$ (λ) was observed at pH 5. These data were in line with the previous one. Notably, the high temperature also contributed to the decrease of $I_{(Eu)}$ (λ). The degradation behavior of NHs under the concurrent pH 3.5 buffer with 37°C was the most obvious one. Similar to the fluorescence data, the size analysis demonstrated the same tendency since an overt loss of size also can be observed under pH 3.5 condition. The carboxyl group on the surface is sensitive to the acidity, which enables the significant aggregation with 1260 nm to come into being in pH 3.5 buffer. It can be found the aggregation was gradually dissolved at pH 3.5.

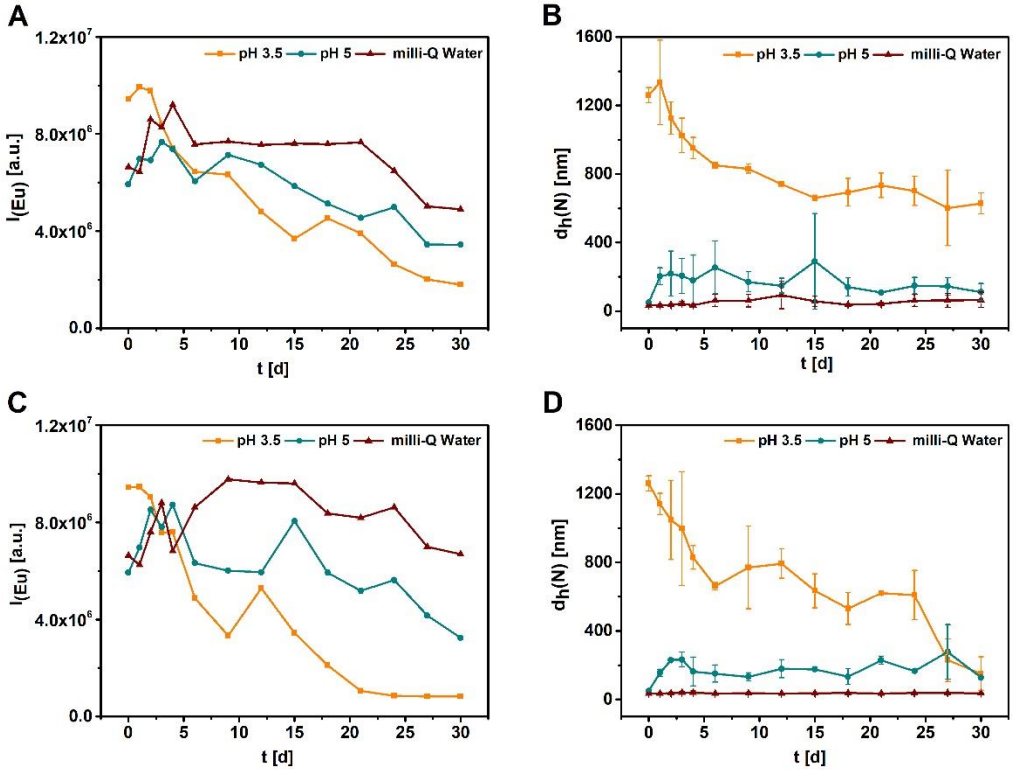

Figure2-8. *The degradation of NHs [250 µg/mL] at pH3.5,pH5 buffer (citric acid-Na_2HPO_4 buffer) and Milli-Q water. The change of hydrodynamic diameter $d_{h(N)}$ of NHs at RT (B) and 37 °C (D). Variation in Eu fluorescence $I_{(Eu)}$ (λ) of NHs at RT (A) and 37 °C (C).*

In consequence, we specifically selected the pH 3.5 buffer in the following studies because the most pronounced degradation occurs in pH 3.5 buffer. We treated NHs with pH 3.5 buffer at RT and 37°C for 30 days respectively. The degradation was determined by TEM, EDX as well as ICP-MS. The structural evolution of NHs was visualized by TEM, which is a favorable choice for exploring the in-situ degradation of NHs at the nanoscale. According to the obtained TEM images, the structure of NHs was found to collapse and fuse with each other in pH 3.5 condition, while the NHs kept the well-dispersed cubic shape in Milli-Q water (Figure2-9). What's more, the NHs displayed a distinct cubic edge at 2 days with incubation of pH 3.5 buffer, while the edge became more rounded and merged to the surrounding NHs at 30 days. The defined cubic shape NHs converted to irregular aggregation. No significant difference between RT and 37°C can be observed during the acid-dependent degradation process.

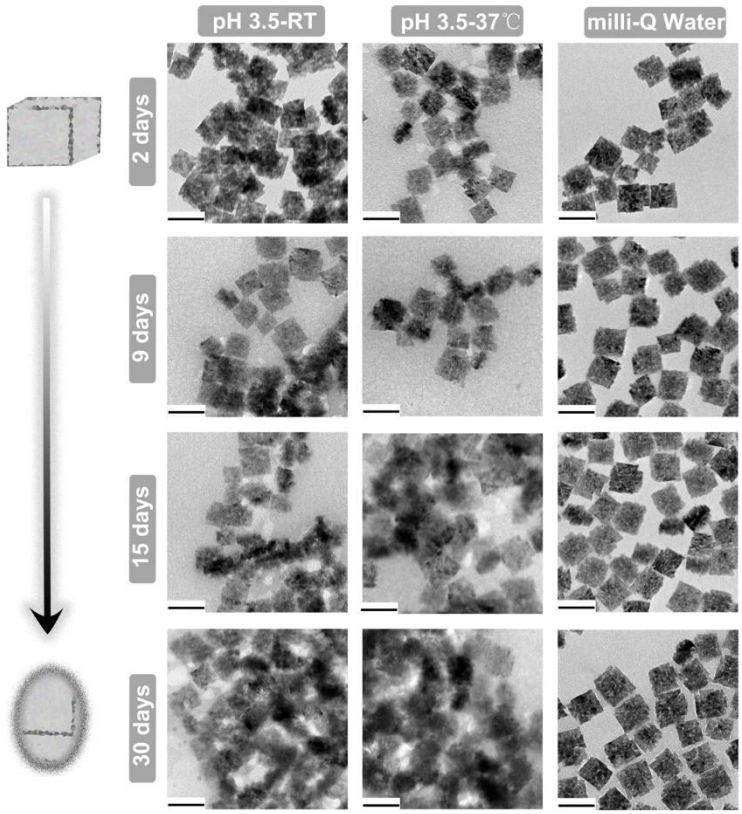

Figure2-9. *Representative shape evolution for the NHs [250 μg/mL] in pH 3.5 buffer (citric acid-Na_2HPO_4 buffer) at RT and 37°C with label bar 50 nm. The NHs in Milli-Q water at RT was used as a control group.*

The change in the concentrations of Eu, Bi and Gd was conducted by EDX. The red, green and blue signals were evenly distributed, revealing these components were uniformly distributed within the inorganic core of NHs (Figure2-10). The signal was further semiquantitatively analyzed by fitting for three elements (Figure 2-11) and all elements (Figure 2-12) respectively, with no significant influence on the amounts of Eu,Bi and Gd being observed during the acid-dependent degradation. We then detected the transformation of elements by ICP-MS, which indicated that the release of Bi was faster than that of Eu as well as that of Gd, that was inconsistent with the results from EDX (Figure2-13). The differences may originate from the sensitivity and limitation between the two techniques. Such degradation behavior was attributable to the crystal structure, revealing the distinguishable structure of Bi. The crystal structure of Eu and Gd is similar, while that of Bi is totally different. When the “runaway” opportunity arises, Bi becomes highly motivated.

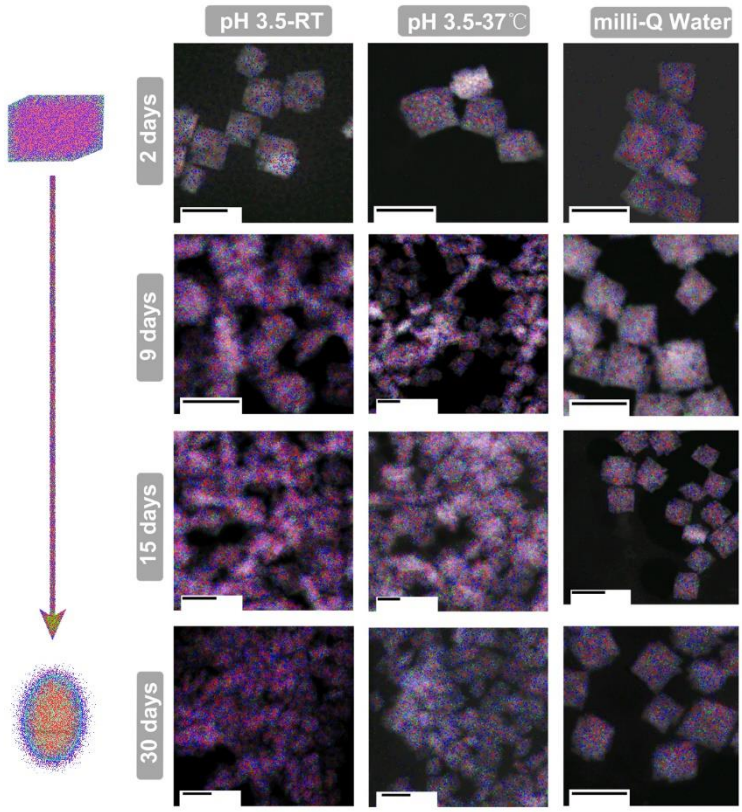

Figure2-10. *EDX elemental maps (Eu in green, Bi in red, Gd in blue) of NHs in the incubation of pH 3.5 buffer and Milli-Q water at 37 °C and RT for different time periods (label bar:50 nm)*

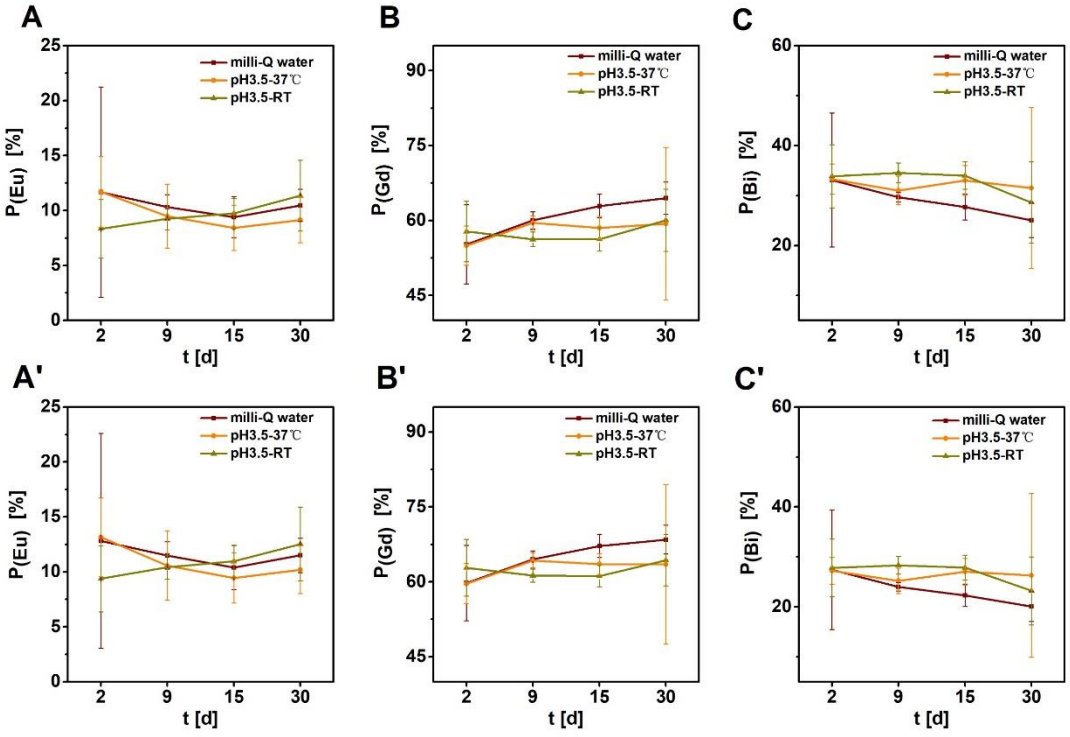

Figure2-11. *The relative percentage of Eu $P_{(Eu)}$(A and A'), Gd $P_{(Gd)}$(B and B') and Bi $P_{(Bi)}$*

(C and C') in EDX elemental mapping in terms of weight (A-C) and atomic (A'-C') which fitting for three elements.

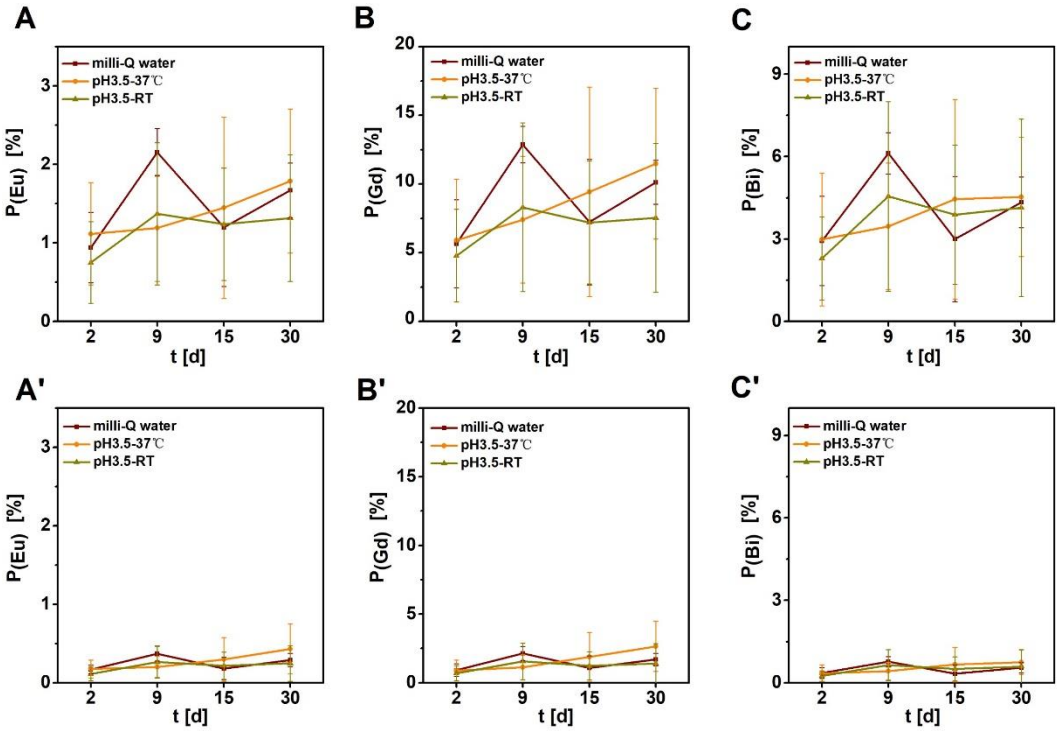

Figure2-12. *The relative percentage of Eu $P_{(Eu)}$ (A and A'), Gd $P_{(Gd)}$ (B and B') and Bi $P_{(Bi)}$ (C and C') in EDX elemental mapping in terms of weight (A-C) and atomic (A'-C') which fitting for all elements*

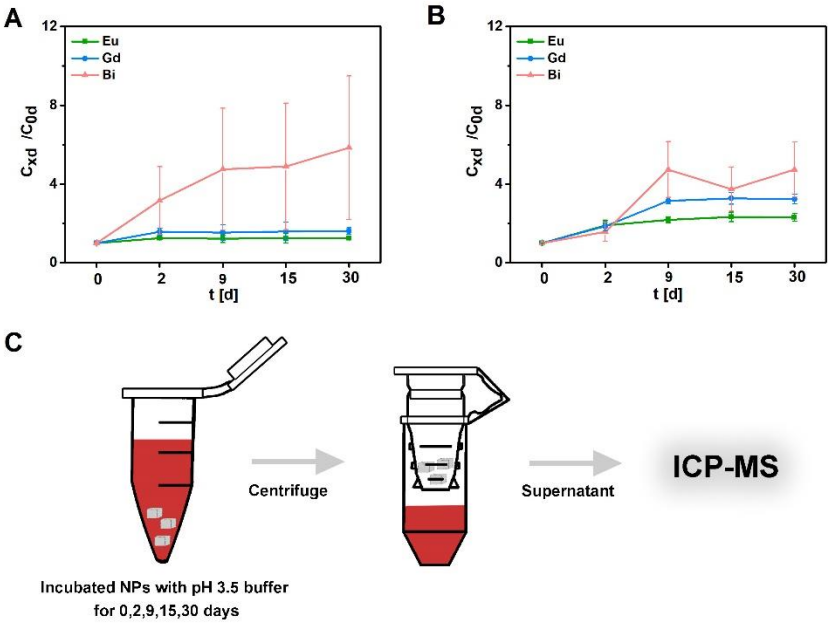

Figure 2-13. *The ratio of metal elements in the supernatant of the NHs at concentration of 250 µg/mL (A) and 160 µg/mL (B) incubated with pH 3.5 buffer at 37°C for the*

degradation study. The data was presented as the ratio between metal concentration at X days and the one at 0 day. Schematic illustration for the NHs degradation in pH 3.5 condition. Incubated NHs with pH 3.5 buffer for 0, 2, 9, 15 and 30 days. Adopt centrifuge filters (cut-off weight 30KDa) to collect the supernatant (21.1×10^3 g, 5 min). Measured the concentration of elements in the supernatant by ICP-MS (C).

In the light of the organic shell on the surface of NHs, we adopted surface zeta potential and FA fluorescence $I_{(FA)}$ (λ) to characterize the degradation. In principle, the PAA on the surface of NHs won't display the acid-dependent degradation behavior. The results from zeta potential also confirmed that the change of surface potential was marginal (Figure2-14). As is described previously, the FA has been linked to the PAA on the surface of NHs. The variation of fluorescence originating from free FA incubated with different pH buffer for 30 days was also assessed. In pH 3.5 condition, the fluorescence displayed a mild increase. There is no regular tendency of fluorescence variation under the other two conditions (Figure2-15).

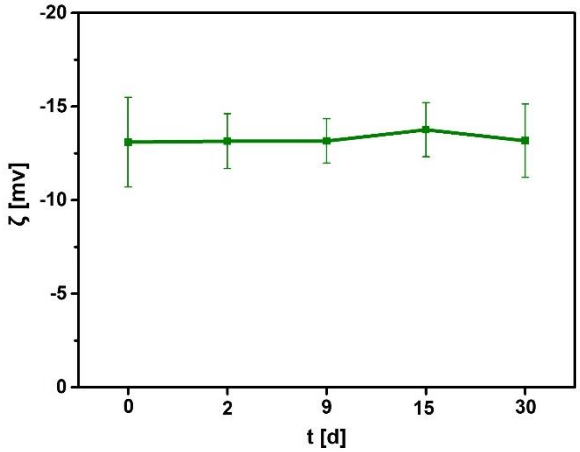

Figure2-14. *The change in ζ of NHs [250 μg/mL] with pH 3.5 buffer at 37 °C for 30 days. Surface charges were monitored by Malvern Zetasizer.*

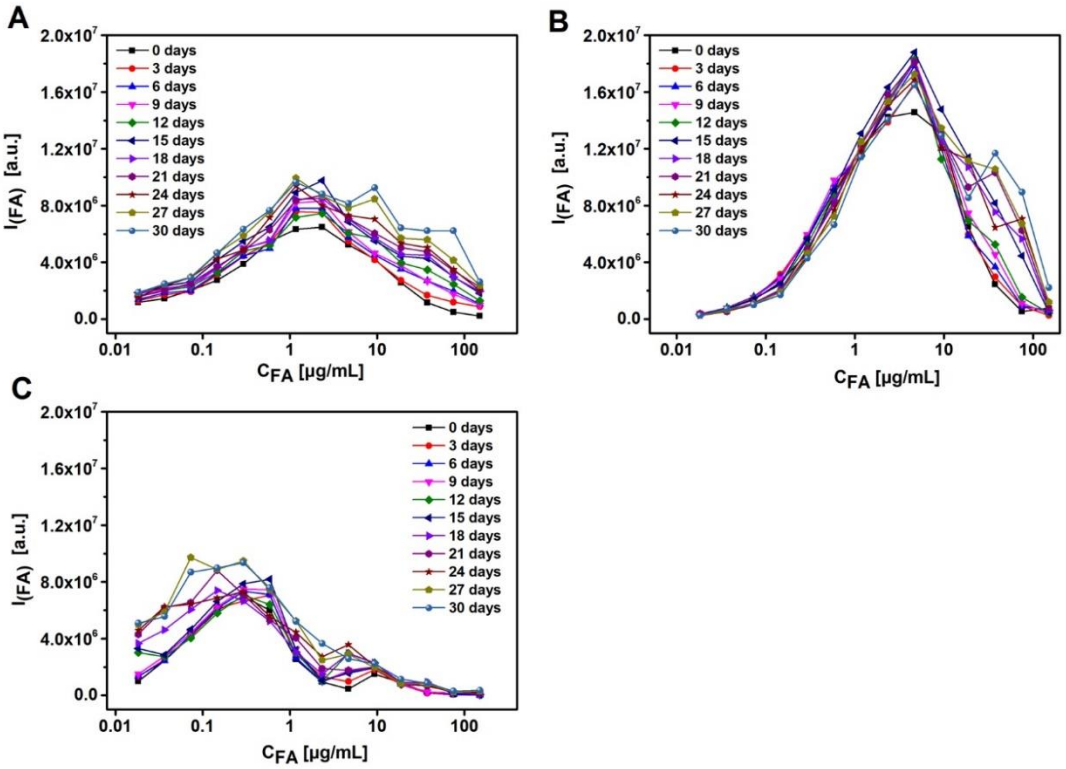

Figure2-15. *The variation of FA fluorescence $I_{(FA)}(\lambda)$ originated from the free FA at pH 3.5 (A), pH5 (B) and pH 7.4 (C) buffer for 30 days. The fluorescence has been quantified for every three days.*

It was concluded that the acid buffer significantly decreased Eu fluorescence, effectively shrank acid responsive aggregation, totally reconstructed the shape of NHs and largely changed the elemental composition. In conclusion, the NHs can be successfully degraded and changed by acid buffer at pH 3.5.

2.5.3. The results of TEM calculation

With the help of cell profiler and Matlab, the fingerprint of shape change in NHs degradation can be calculated to precisely describe the evolution. Firstly, we need to make a mask for all images by Image J. The masks should be analyzed by cell profiler to calculate the shape parameters, Area (A_{NHs}), Eccentricity (Ec_{NHs}), Extent (Ex_{NHs}), F factor (F_{NHs}), Solidity (S_{NHs}), Z factors (Z^0_{NHs}) and Compactness (C_{NHs}). Next, we enlarged the distance between NHs by Photoshop to avoid analyzing two NHs as one. In the last, the angles in the image can be identified and calculated by Matlab. We used one code to find the corners (points) of the object. Then, these points were sorted in order. After which points can connect the nearest one to form a line. What follows is to calculate the inner angels between two lines by the Arctan function.

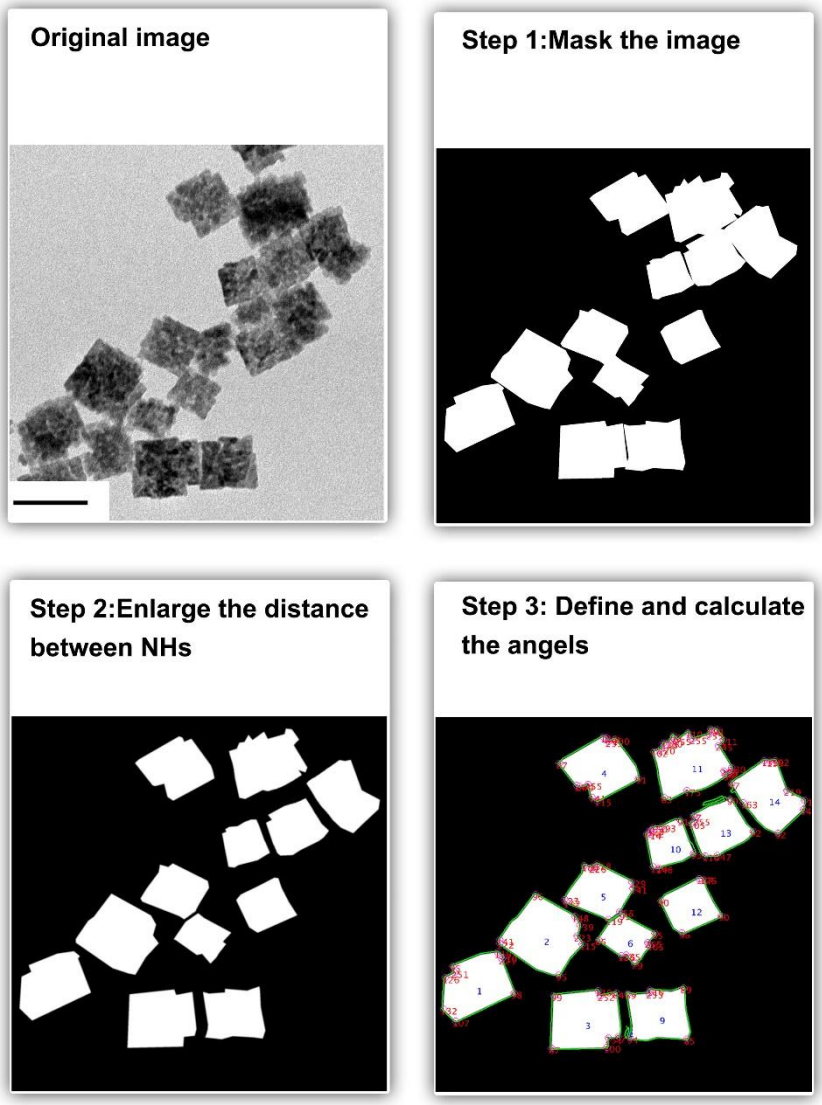

Figure 2-16. *One example of the calculation of TEM image. There are three steps in the procedure.*

For one condition, we analyzed and calculated 6 images (n=2) through the above steps to get the shape parameters. The analyzed images for all groups are listed in the following.

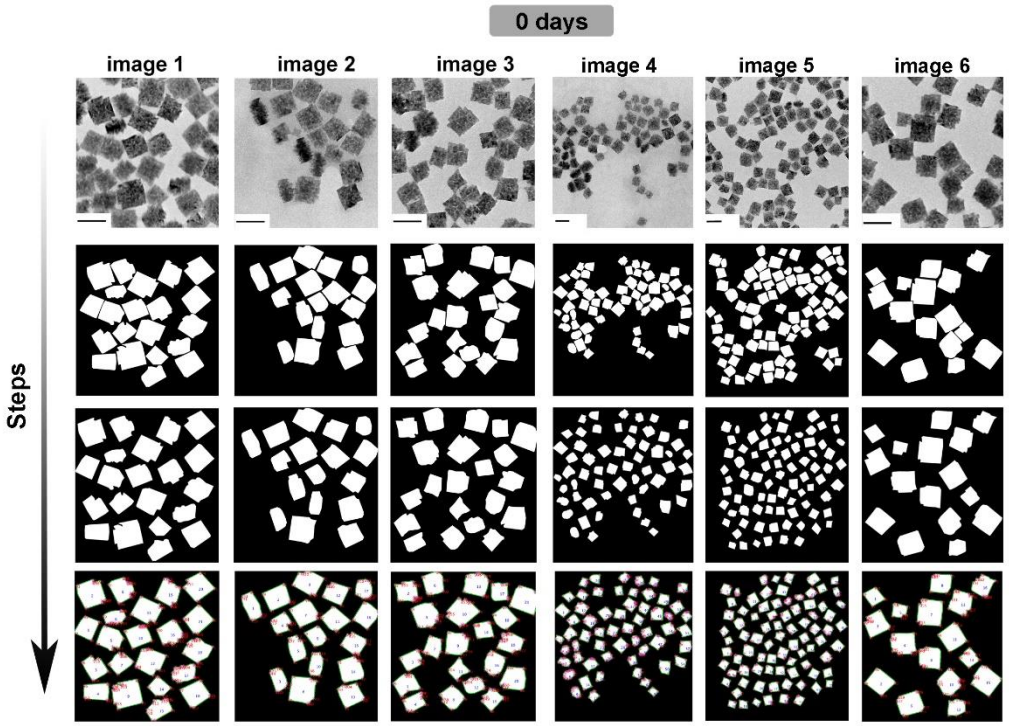

Figure 2-17. *The steps of TEM calculation for NHs at 0 days with label bar 50 nm.*

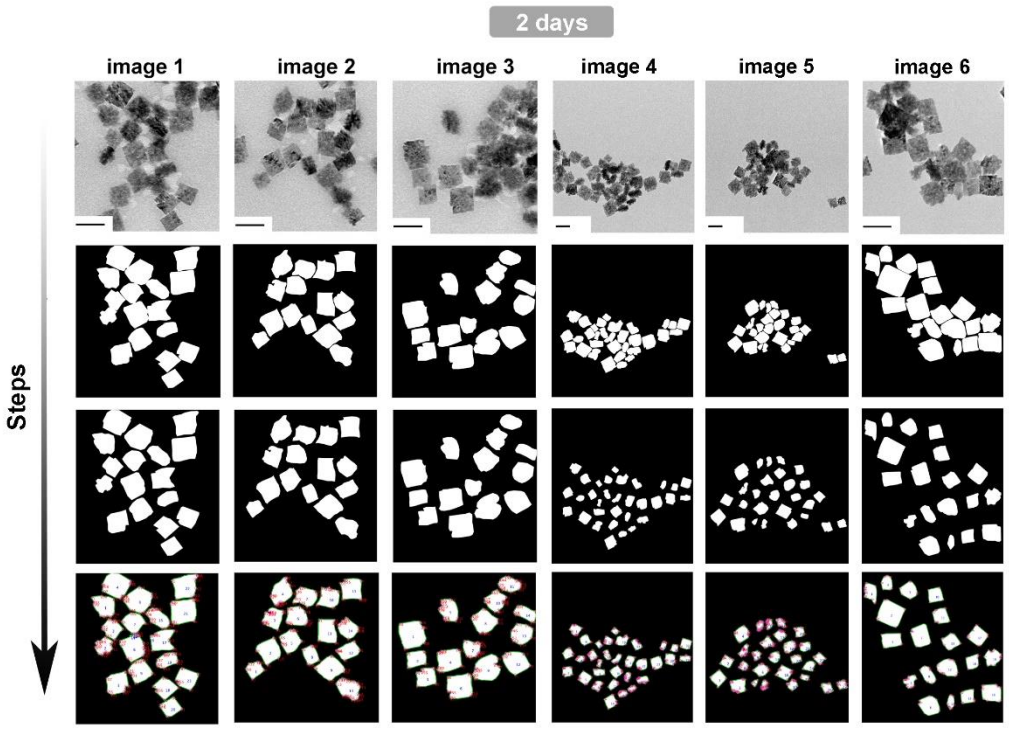

Figure 2-18. *The steps of TEM calculation for NHs incubated at Milli-Q water for 2 days at RT. The label bar is 50 nm.*

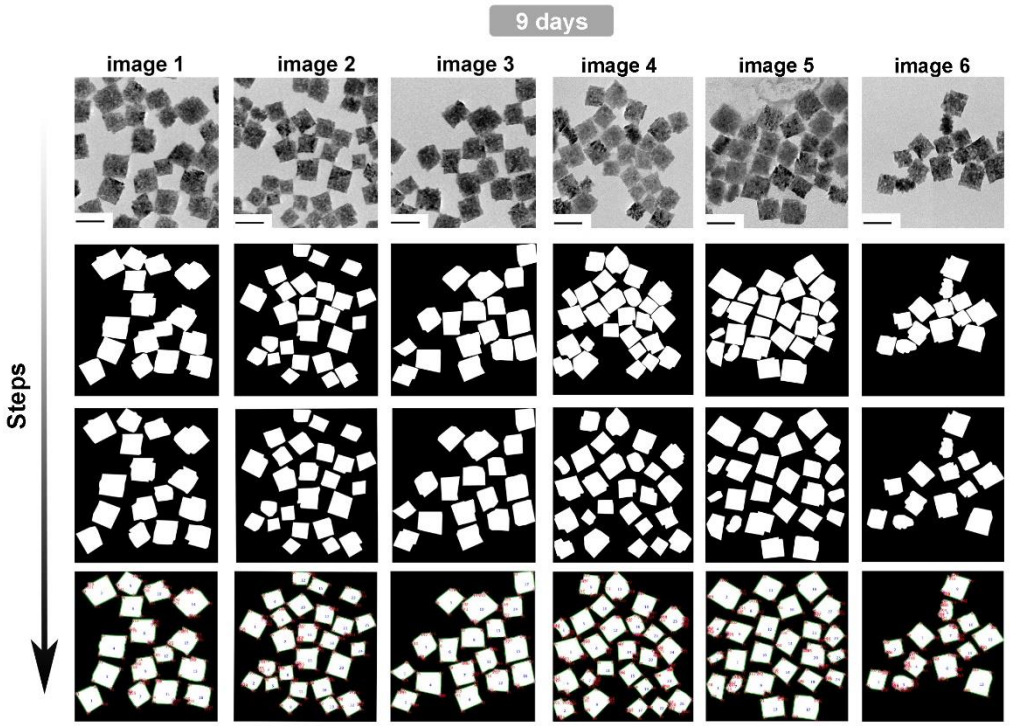

Figure 2-19. *The steps of TEM calculation for NHs incubated at Milli-Q water for 9 days at RT. The label bar is 50 nm.*

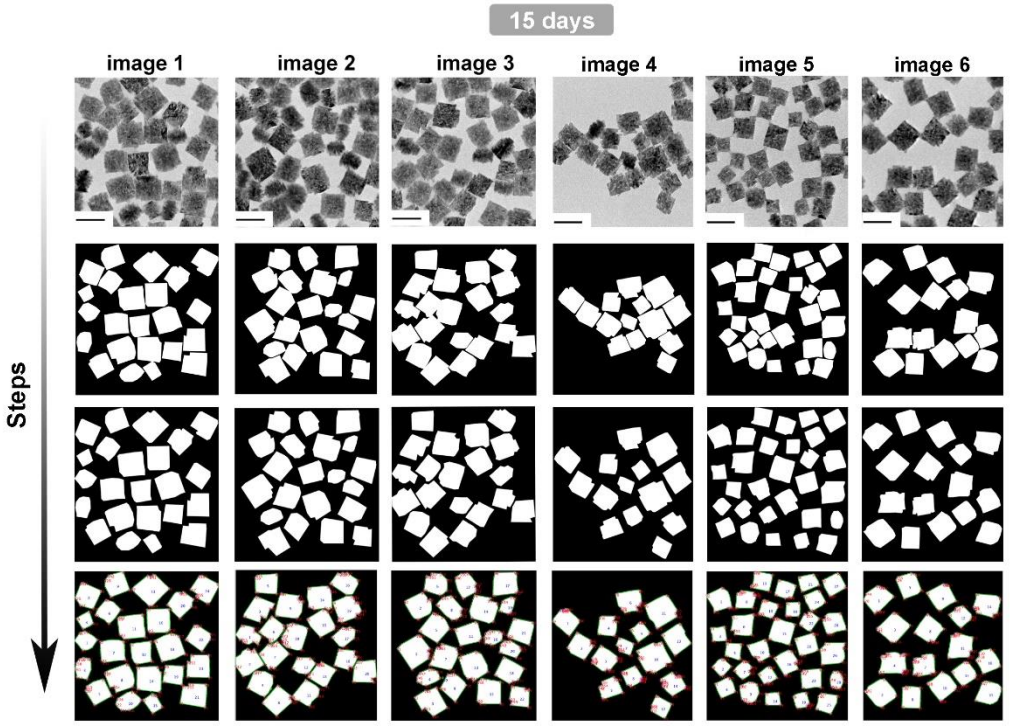

Figure 2-20. *The steps of TEM calculation for NHs incubated at Milli-Q water for 15 days at RT. The label bar is 50 nm.*

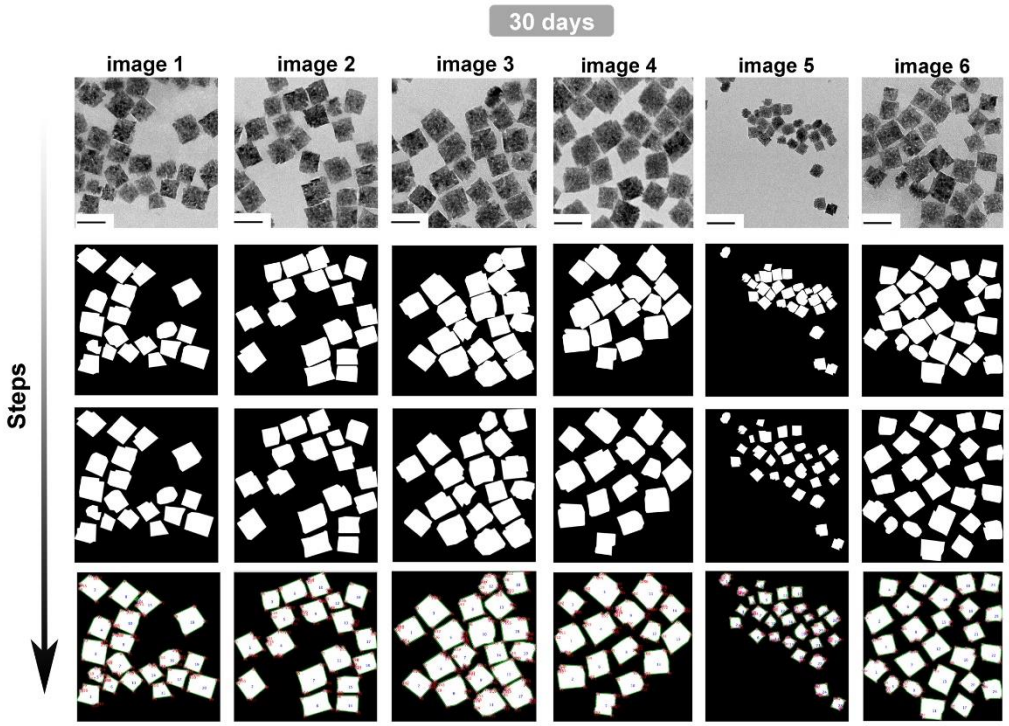

Figure 2-21. *The steps of TEM calculation for NHs incubated at Milli-Q water for 30 days at RT. The label bar is 50 nm.*

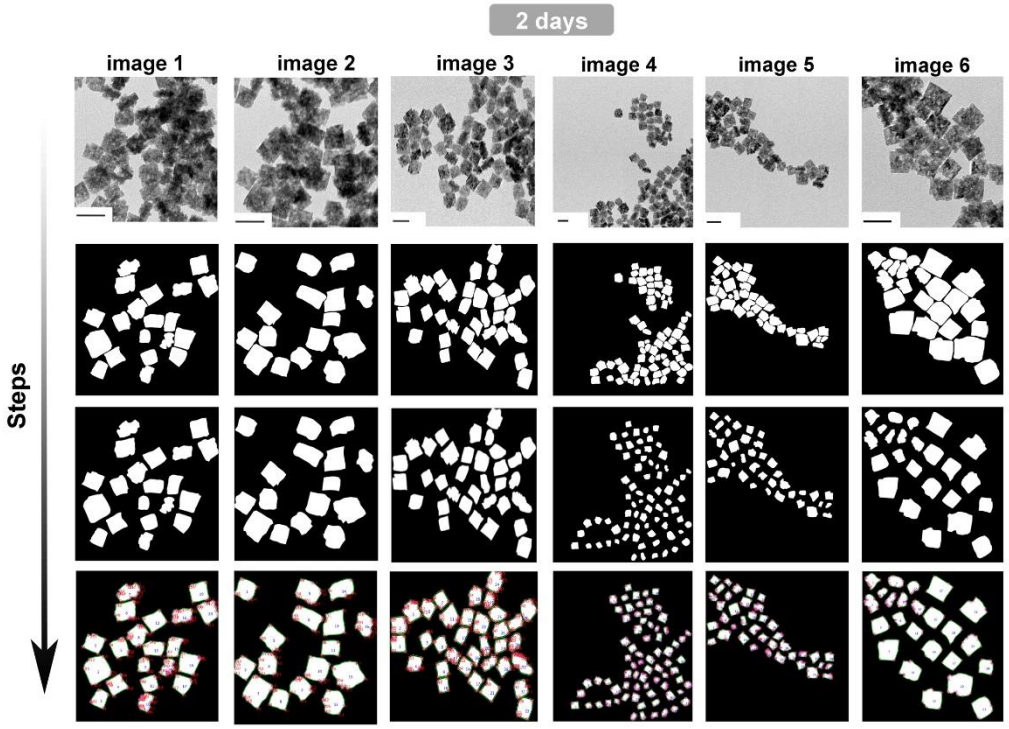

Figure 2-22. *The steps of TEM calculation for NHs incubated at pH 3.5 buffer for 2 days at RT. The label bar is 50 nm*.

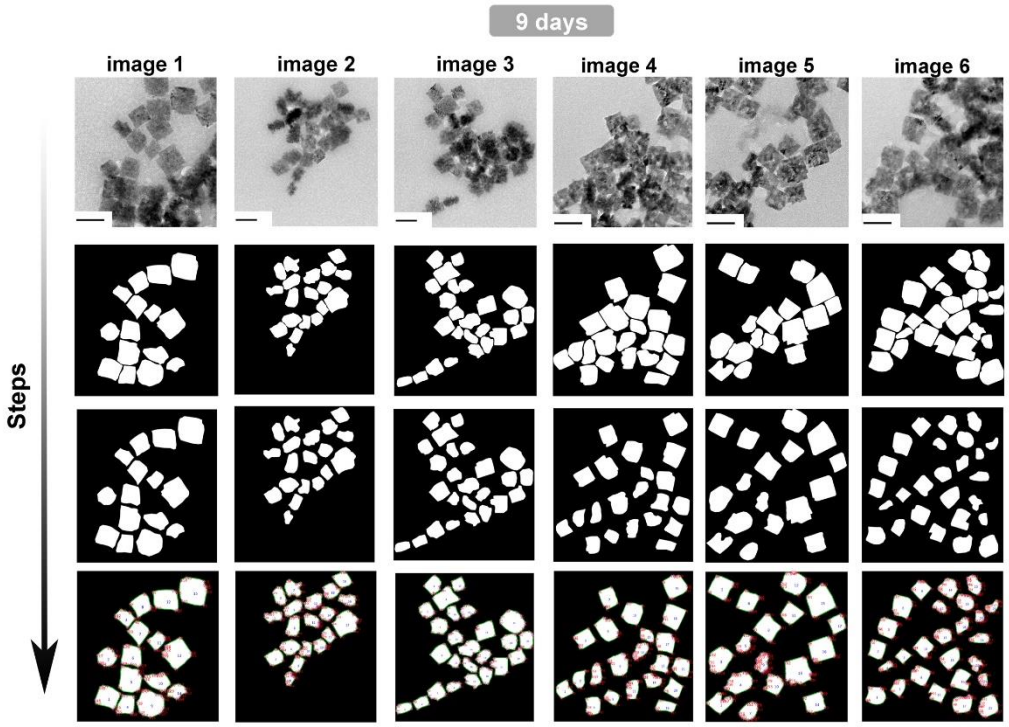

Figure 2-23. *The steps of TEM calculation for NHs incubated at pH 3.5 buffer for 9 days at RT. The label bar is 50 nm.*

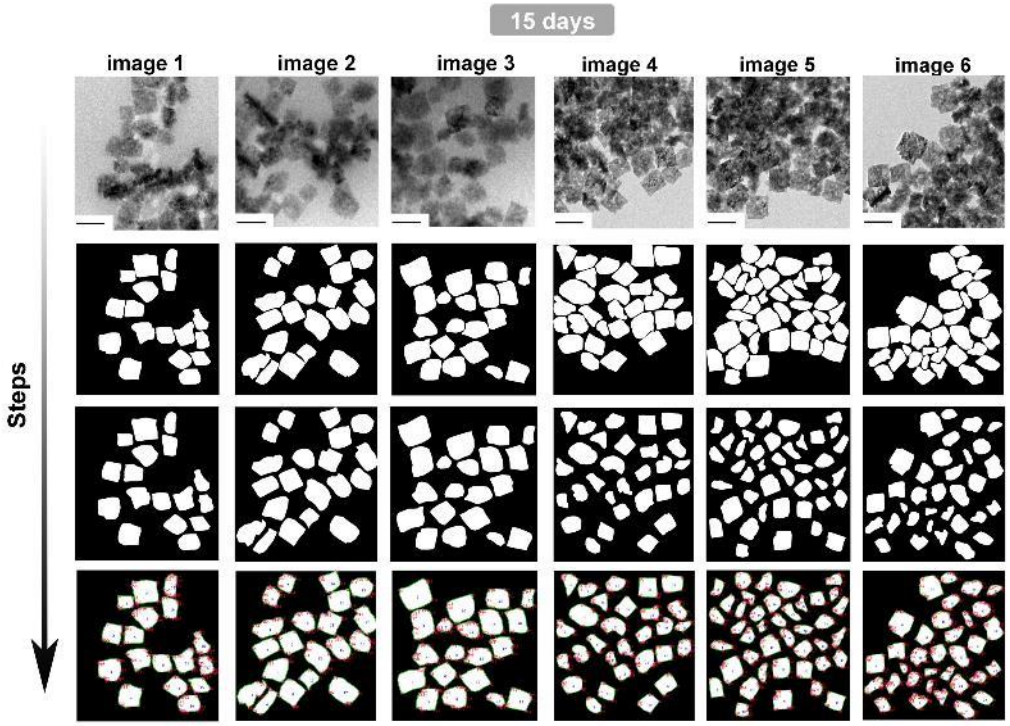

Figure 2-24. *The steps of TEM calculation for NPs incubated at pH 3.5 buffer for 15 days at RT. The label bar is 50 nm.*

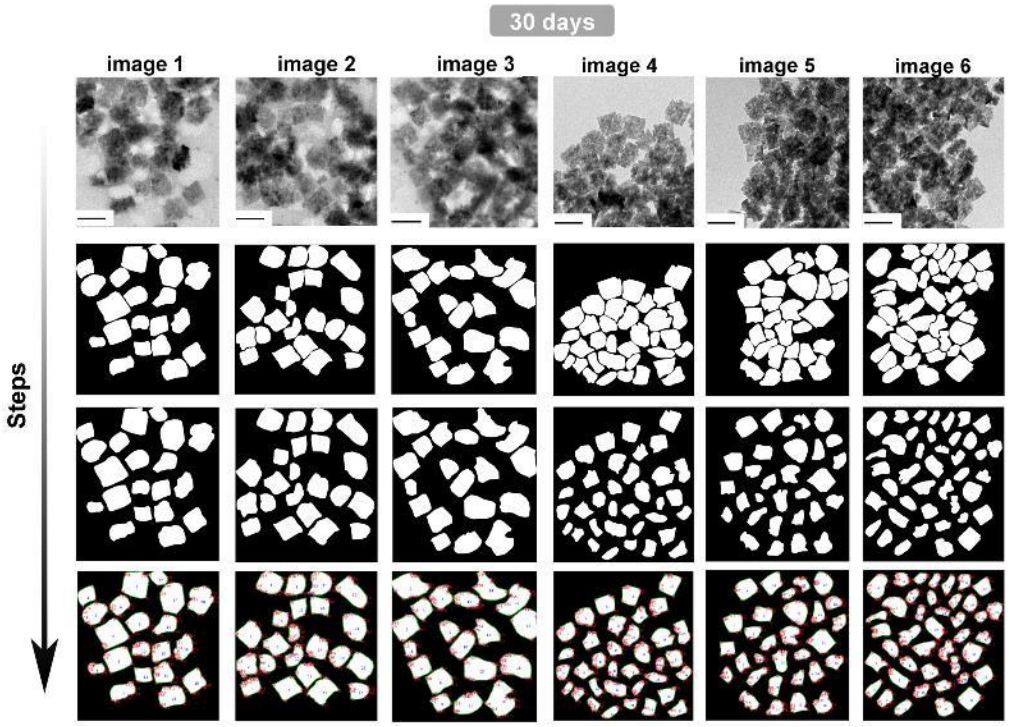

Figure 2-25. *The steps of TEM calculation for NHs incubated at pH 3.5 buffer for 30 days at RT. The label bar is 50 nm.*

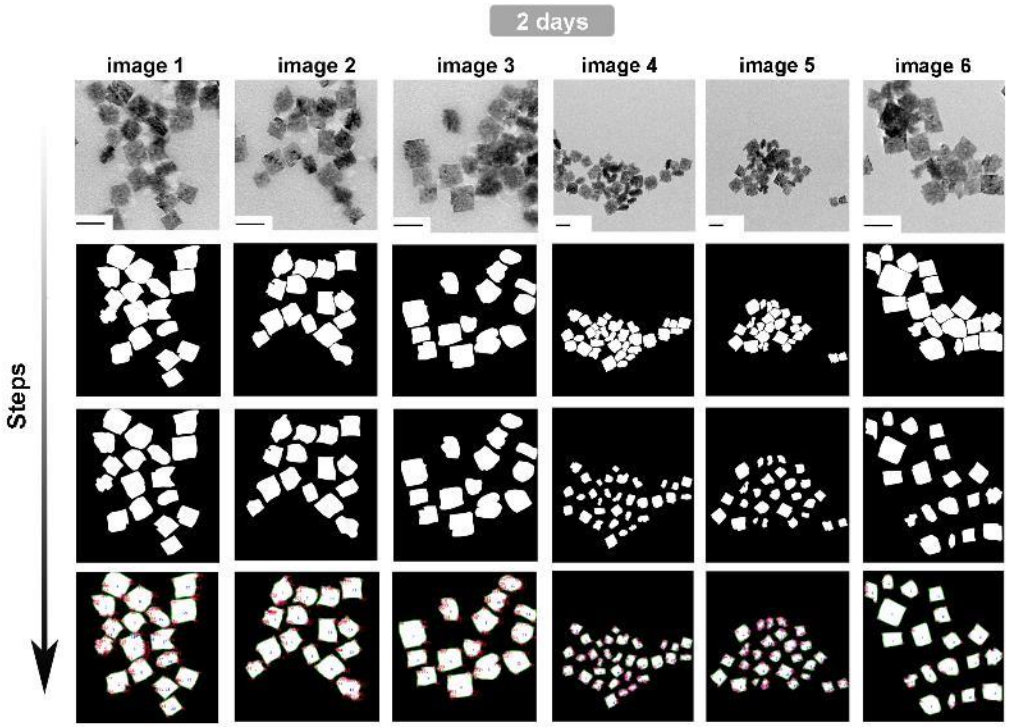

Figure 2-26. *The steps of TEM calculation for NHs incubated at pH 3.5 buffer for 2 days at 37 ℃. The label bar is 50 nm.*

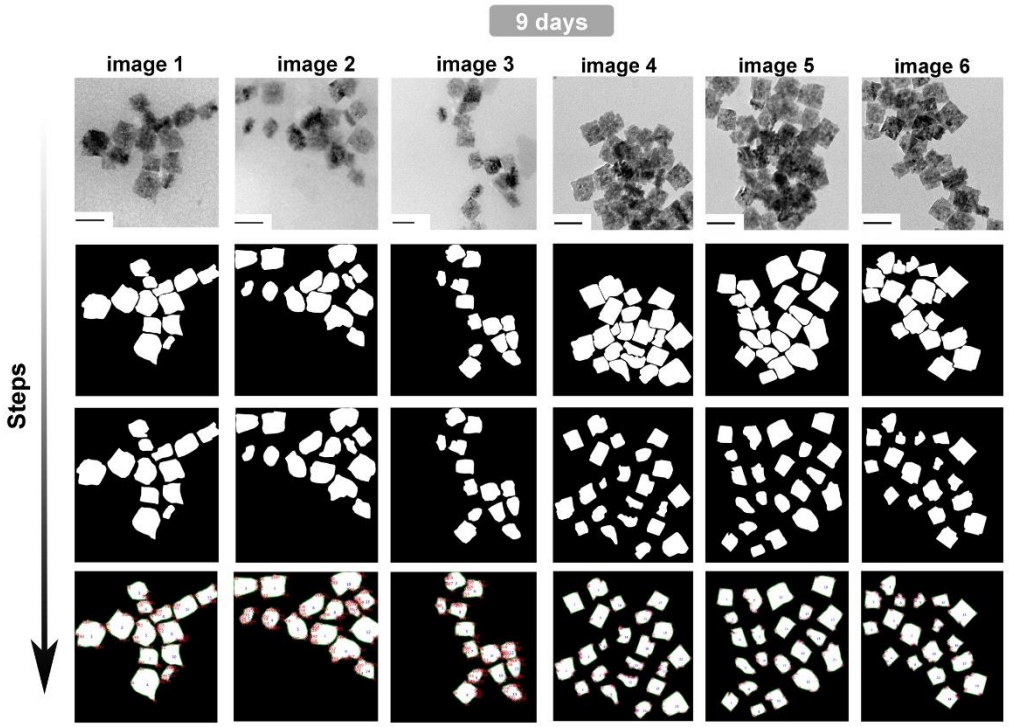

Figure 2-27. *The steps of TEM calculation for NHs incubated at pH 3.5 buffer for 9 days at 37 ℃. The label bar is 50 nm.*

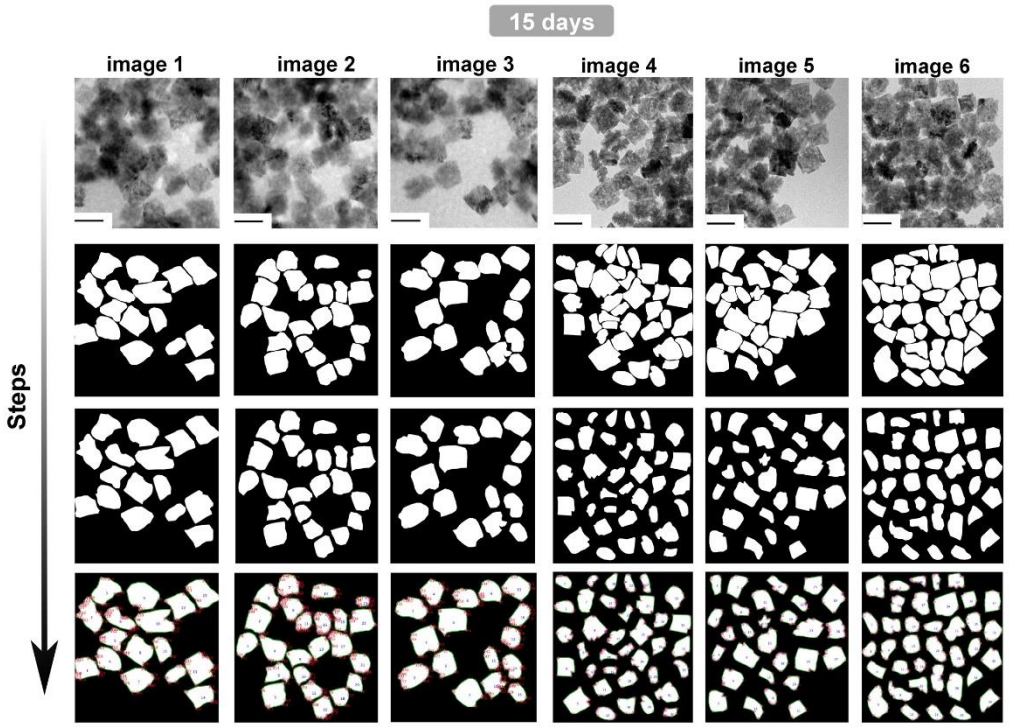

Figure 2-28. *The steps of TEM calculation for NHs incubated at pH 3.5 buffer for 15 days at 37 ℃. The label bar is 50 nm (n=2)*

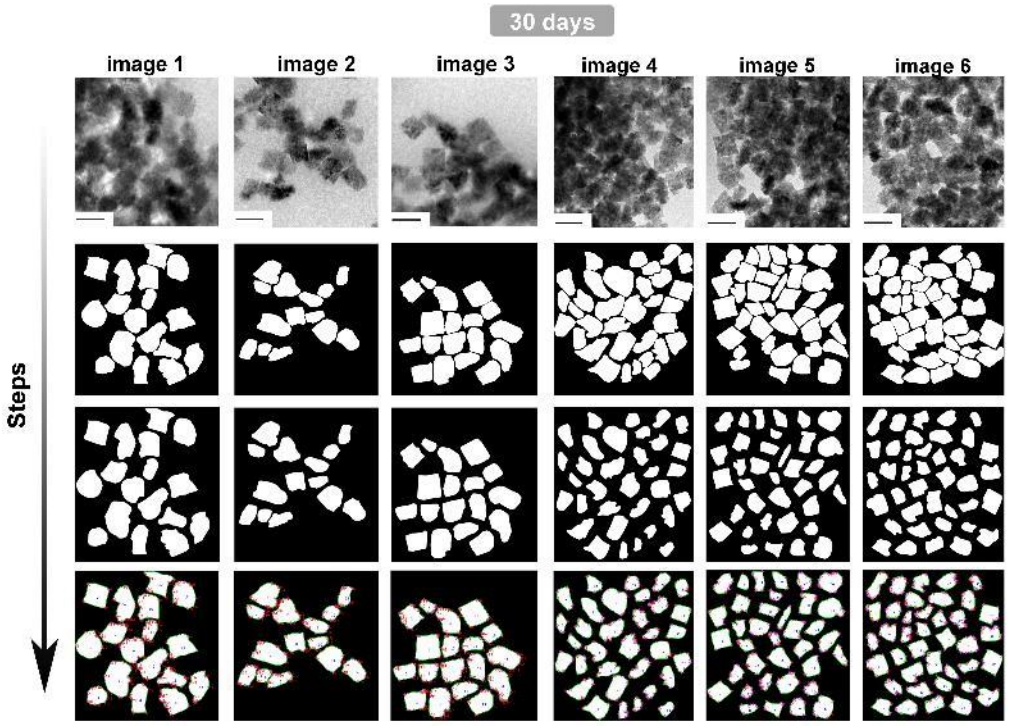

Figure 2-29. *The steps of TEM calculation for NHs incubated at pH 3.5 buffer for 30 days at 37 ℃. The label bar is 50 nm.*

As the pH 3.5 buffer gives rise to the acid-responsive aggregation, it is necessary to analyze coherent NHs and single NH respectively. For this purpose, the threshold (the average area of NHs in Milli-Q water) was conducted during the analysis. It is due to the threshold that, there are more single NHs in the group of area ≤threshold. Accordingly, the percentage of aggregated NHs is high in the group of area > threshold. It was interesting to find that the degradation process drastically enlarged the α_{NHs} of NHs from about 105° to about 130°, compared with the negligible influence they have at area (Figure2-30). In addition, the Ec_{NHs} of NHs increased during the degradation, suggesting the NHs turn to a more elongated shape (Figure2-31). The minor decrease in Z^0_{NHs} further confirmed the tendency of NHs to elongation (Figure2-35). Furthermore, it was also observed that the slight elevation in C_{NHs}, which is the parameter represents the irregularity (Figure2-36). Comparatively, the insignificant variation in S_{NHs} and Ex_{NHs} revealed that the protrusion and indentation of objects kept unchanged during the degradation process (Figure2-32 and Figure2-34). Since the area and perimeter didn't alter as time went by, the F_{NHs} stayed constant (Figure2-33). In terms of groups of whole NH, aggregate NHs and single NH, the same tendency was observed accounting for the change of NHs distortion.

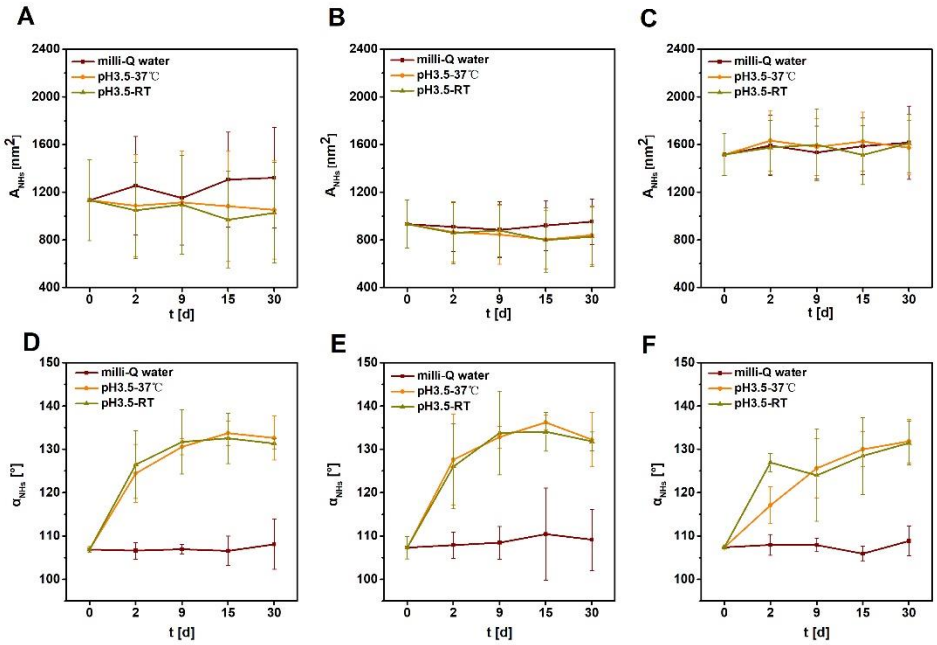

Figure 2-30. *A_{NHs}(A-C) and α_{NHs}(D-F) of NHs in the condition of pH 3.5 buffer and Milli-Q water at RT and 37 ℃ over 30 days. In order to exclude the calculation of aggregations, one threshold (the average area of control NHs: 1259 nm^2) have been adopted to group the results, all NHs (A and D), the area ≤ threshold (B and E) and the area > threshold (C and F).*

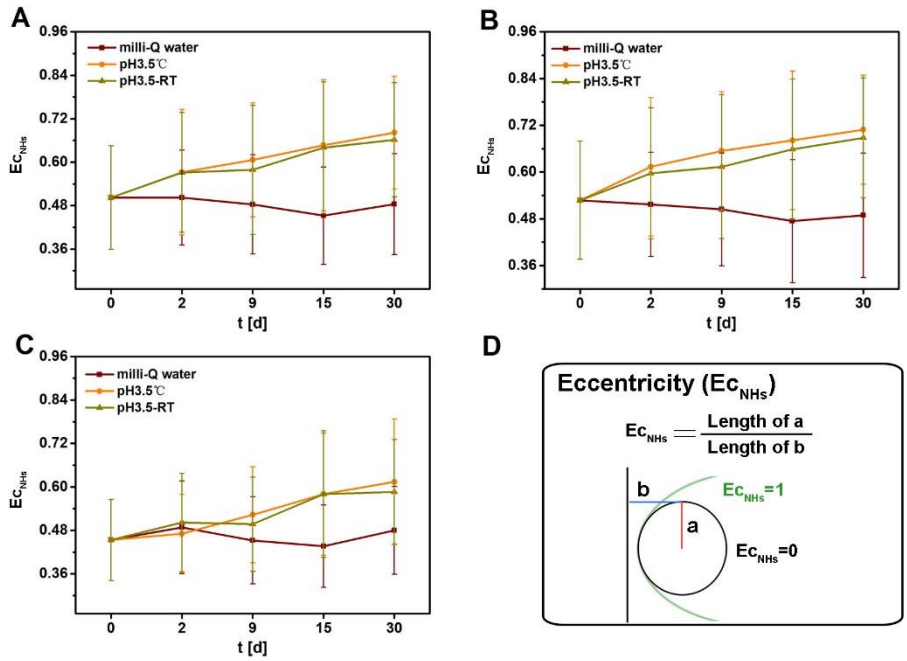

Figure 2-31. *Ec_{NHs} of NHs incubated with pH 3.5 buffer and Milli-Q water at RT and 37 ℃ over 30 days. The results contain all NHs (A), the area ≤ threshold (B) and the area >*

threshold (C).The explanation for Ec_{NHs} (D).

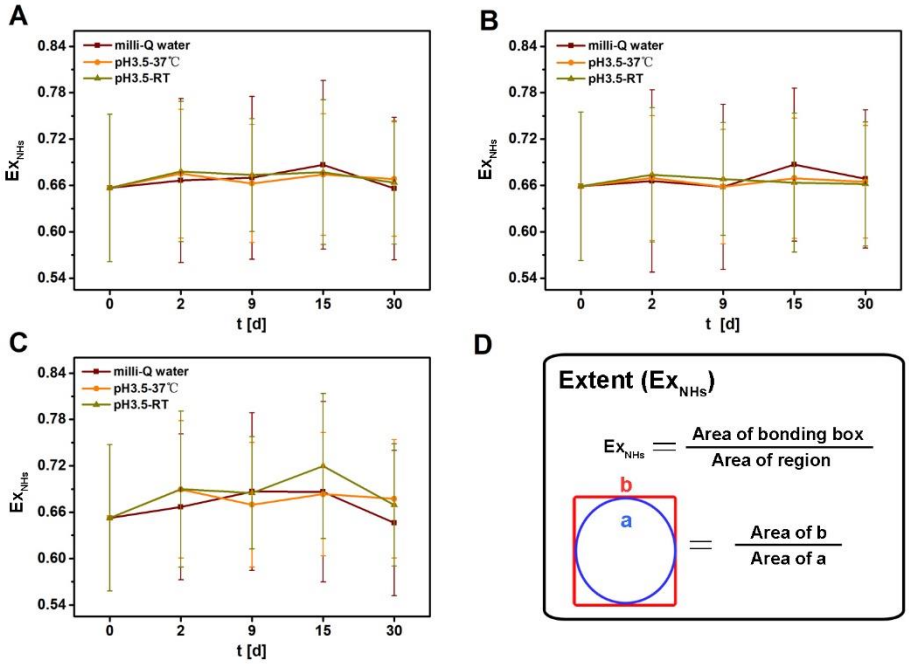

Figure 2-32. *Ex_{NHs} of NHs incubated with pH 3.5 buffer and Milli-Q water at RT and 37 ℃ over 30 days. The results contain all NHs (A), the area ≤ threshold (B) and the area > threshold. The explanation for Ex_{NHs} (D).*

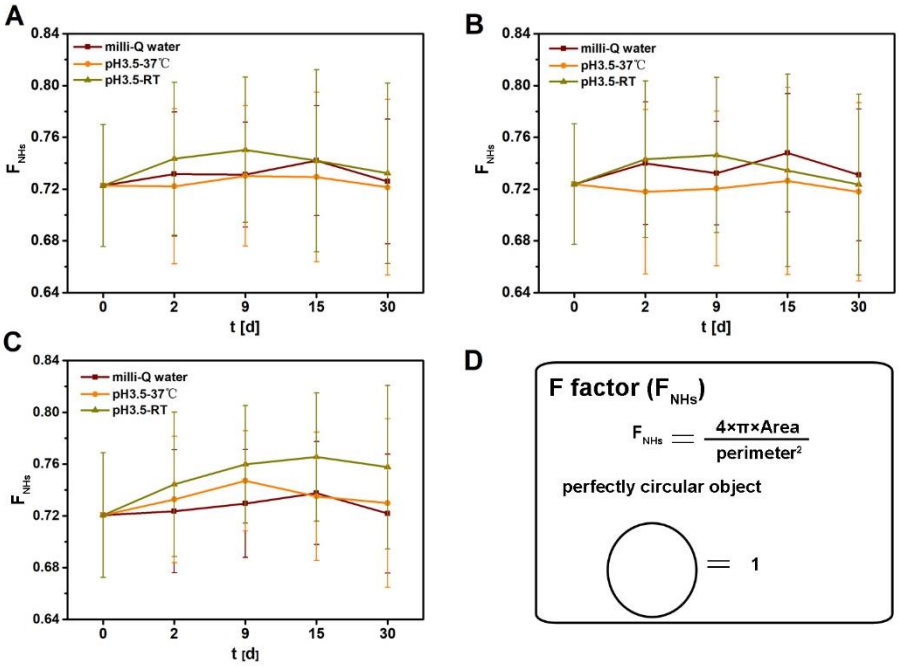

Figure 2-33. *F_{NHs} of NHs incubated with pH 3.5 buffer and Milli-Q water at RT and37 ℃ over 30 days. The results contain all NHs (A), the area≤threshold (B) and the area > threshold (C). The explanation for F_{NHs} (D).*

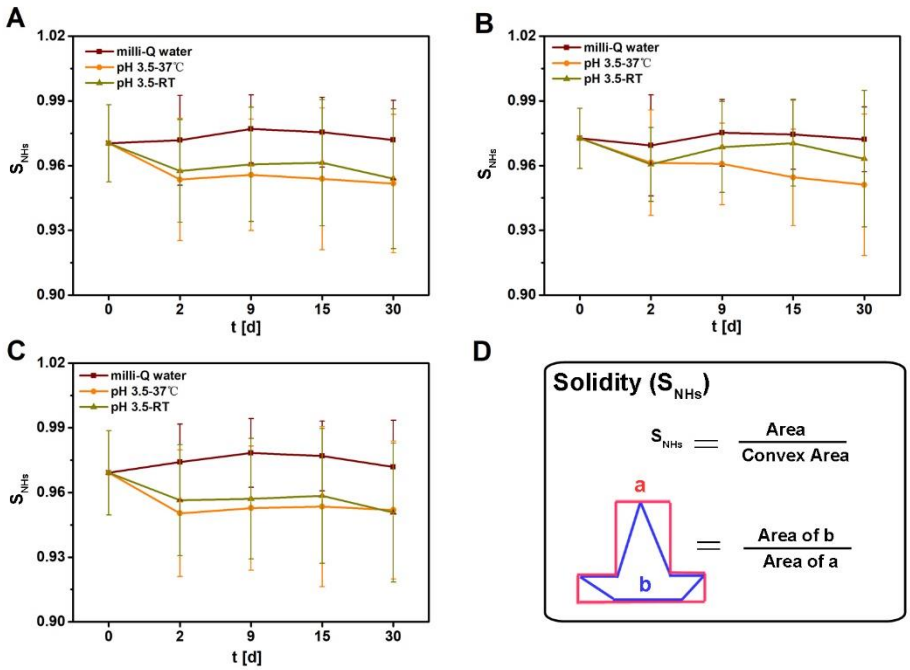

Figure 2-34. *S_{NHs} of NHs incubated with pH 3.5 buffer and Milli-Q water at RT and 37 ℃ over 30 days. The results contain all NHs (A), the area ≤ threshold (B) and the area > threshold (C). The explanation for S_{NHs} (D).*

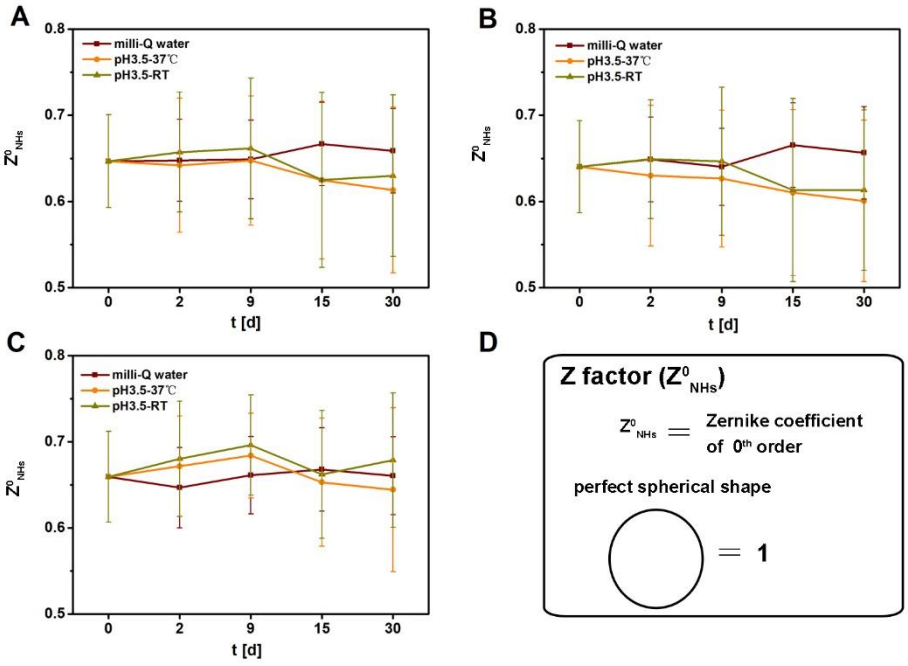

Figure 2-35. *Z^0_{NHs} of NHs incubated with pH 3.5 buffer and Milli-Q water at RT and 37 ℃ over 30 days. The results contain all NHs (A), the area ≤ threshold (B) and the area > threshold (C). The explanation for Z^0_{NHs} (D).*

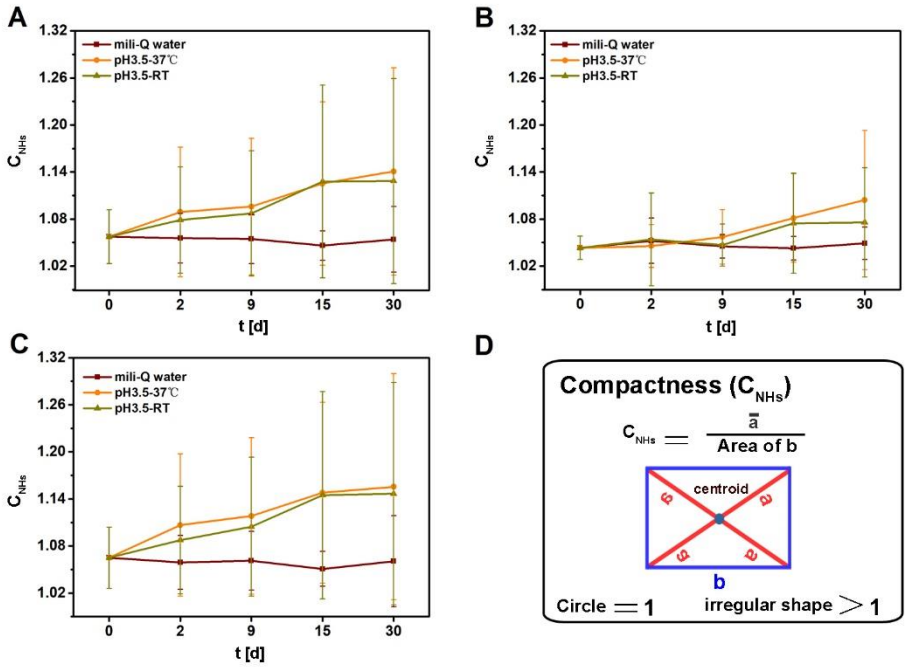

Figure 2-36. *C_{NHs} incubated with pH 3.5 buffer and Milli-Q water at RT and 37 ℃ over 30 days. The results contain all NHs (A), the area ≤ threshold (B) and the area > threshold (C). The explanation for C_{NHs} (D).*

To sum up, the data semiquantitatively exhibited that the acid-dependent degradation significantly enlarged the angles, constantly happened in the same area and mildly increased the degree of ellipticity and irregularity. The gradual shape change is the fingerprint of degradation, which has never been visualized and calculated. Here, we provide the method to track the progressive shape change of degradation. Information relevant to such a model can be also used to describe the structural evolution for proteins, cells and NHs.

2.5.4. Biodegradation behaviors of NHs monitored by fluorescence

Encouraged by results at acid buffers, we sought to further explore the *in vitro* biodegradation ability of NHs. The good biocompatibility of NHs guarantees their satisfactory performance on biodegradation study (Figure2-37). The cellular internalization is a critical first step for NHs biodegradation, which is directly related to the biodegradation. We established the method to study uptake and biodegradation synchronically. Briefly, NHs with used concentrations were exposed to the cells for 6, 24 and 48 hours respectively (t_{exp}: 6, 24 and 48 hours) to probe uptake efficiency. In the case of biodegradation, the supernatant of cells incubated with NHs at 24 hours (t_{exp}) was removed, and then fresh medium was added to cells, which was subsequently incubated for 24, 48 and 72 hours (t_{inc}:24,48,72 hours). At desired time points, we made use of flow cytometry, fluorescence meter, ICP-MS and TEM to

inspect the biodegradation.

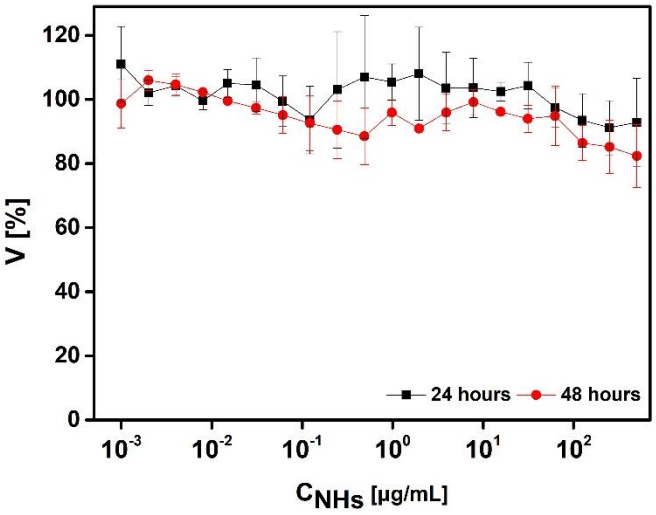

Figure2-37. *Cell Viability V of Hela cells exposure to NHs for 24 hours and 48 hours. Hela cells were incubated with NHs at different concentrations in complete cell medium. The cell viability was determined by resazurin assay*

Next, the uptake and biodegradation processes were characterized by flow cytometry. To clarify how we analyze and plot the data, one example has been shown in Figure 2-38.

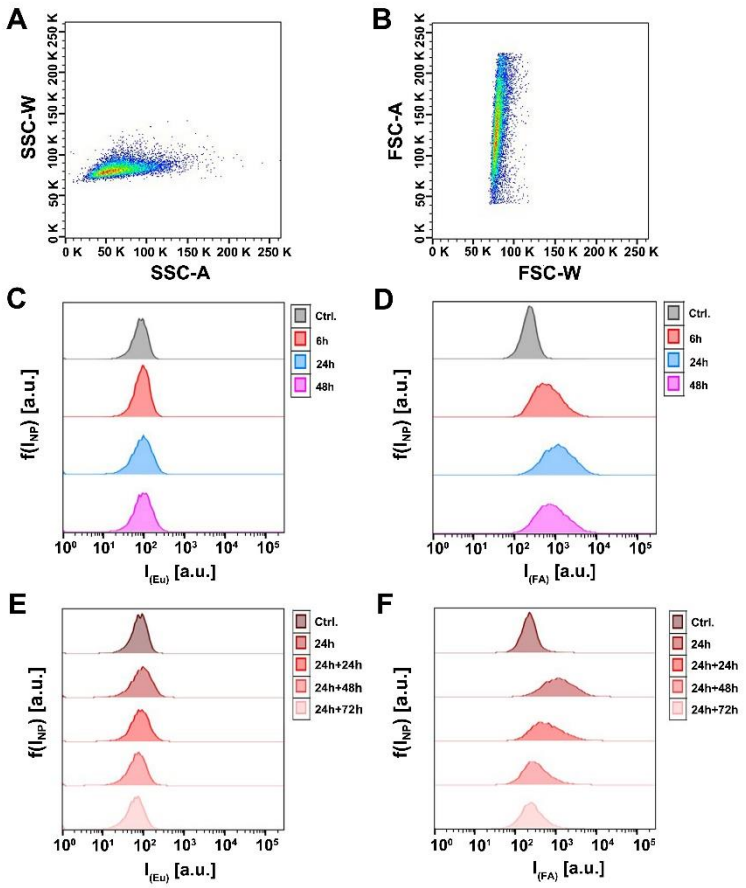

Figure2-38. *Gating strategy of NHs-FA fluorescence measurements* $I_{Eu/cell\ (intra)}$ *(λ) and* $I_{FA/cell\ (intra)}$ *(λ) of Hela cells exposed to NHs-FA (A and B). Example of one distribution of e* $I_{Eu/cell\ (intra)}$ *(λ) (C, E) and* $I_{FA/cell\ (intra)}$ *(λ) (D, F) from Hela cells incubated with NHs-FA at a concentration of 160 µg/mL for different time periods.*

As is shown in Figure2-39, the uptake efficiency of NHs at 24 hours is higher than 6 hours and 48 hours on the basis of quantitative intracellular fluorescence from flow cytometry measurement, which means that the exocytosis affects the uptake procedures. The Eu and FA fluorescence ($I_{Eu/cell\ (intra)}$ (λ) and $I_{FA/cell\ (intra)}$ (λ)) were decreased to ≈10% in the course of biodegradation study, which largely contributed to the cell division. In addition, the amount of NHs in one mother cell passes to two daughter cells during the cell division, revealing that cell growth significantly dilutes the concentration of NHs in the individual cell. On account of the obstacle imposed by cell division on our interpretation of effective biodegradation, the growth factor was introduced to normalize the factor of cell growth. Encouragingly, the normalized Eu and FA fluorescence ($I_{Eu/cell\ (normalized)}$ (λ) and $I_{FA/cell\ (normalized)}$ (λ)) still manifested about 50% decrease in the course of biodegradation (Figure2-40).

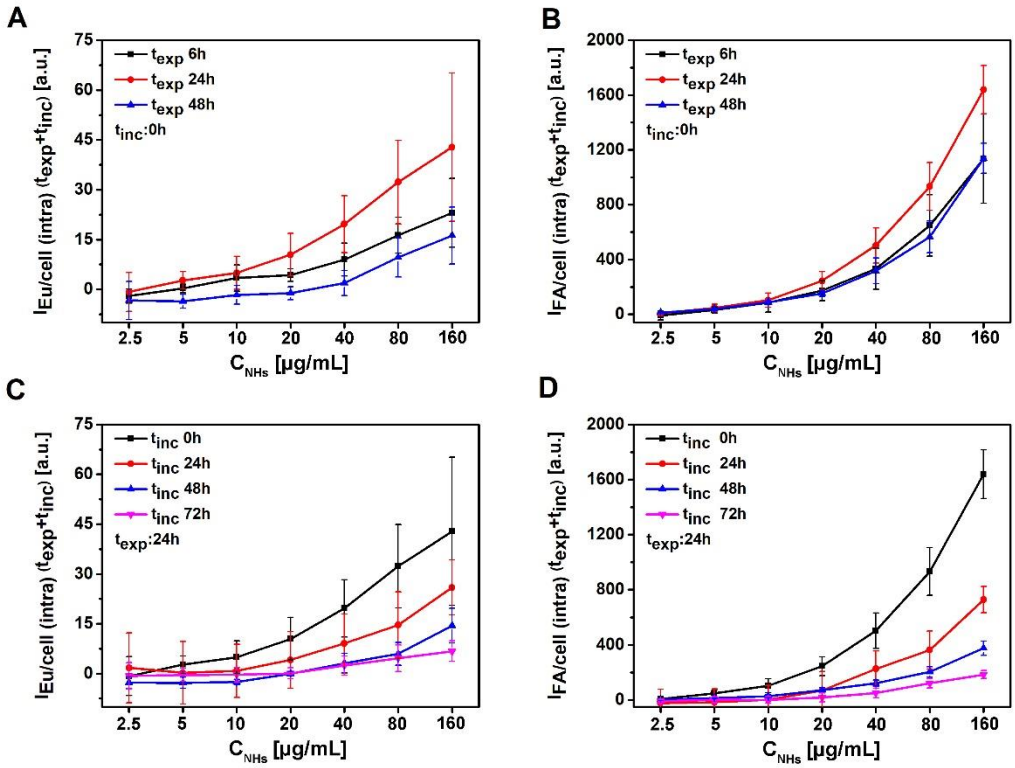

Figure2-39. *NHs-FA uptake and biodegradation inside Hela cells cultured in serum-supplemented medium, quantified by mean Eu fluorescence $I_{Eu/cell\ (intra)}$ (λ) and mean FA fluorescence $I_{FA/cell\ (intra)}$ (λ), determined by flow cytometry analysis. Uptake of NHs-FA for different time periods characterized by $I_{Eu/cell\ (intra)}$ (λ) (A) and $I_{FA/cell\ (intra)}$ (λ) (B). Biodegradation of NHs-FA inside Hela cells characterized by $I_{Eu/cell\ (intra)}$ (λ) (C) and $I_{FA/cell(intra)}$ (λ) (D).*

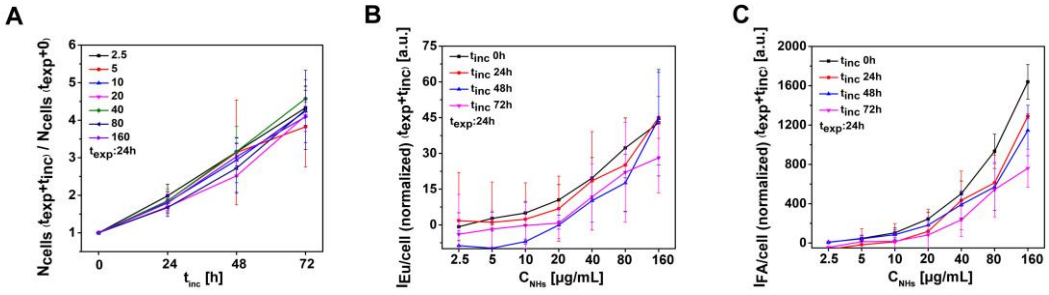

Figure 2-40. *The growth factors are termed as the cell number at X hours (t_{inc}) divided the one at 0 hours (t_{inc}). The growth factor during the time period of biodegradation study (A). $I_{Eu/cell\ (intra)}$ (λ) and $I_{FA/cell\ (intra)}$ (λ) multiplied with corresponding growth factor to obtain the $I_{Eu/cell\ (normalized)}$ (λ) and $I_{FA/cell\ (normalized)}$ (λ) (B and C).*

Furthermore, the experiment applying the same method was conducted to test the total fluorescence by fluorescence meter, which was intended to exclude the influence

of cell growth. The data further confirmed the loss of NHs' fluorescence during their cellular journey (Figure2-41). As has been illustrated out by the previous data, the fluorescence of NHs changed with pH value. The pH variation has also happened to the tumor microenvironment from the extracellular part to the lysosome. To confirm that the reduction in fluorescence is the signal of biodegradation instead of pH change, the intracellular fluorescence from NHs at different pH buffer was tested by flow cytometry. The results showed that the $I_{Eu/cell\ (intra)}$ (λ) increased with the decline in pH value, which mismatched with the reduction of in the biodegradation study (Figure2-42). Hence, it can be claimed that the decrease of $I_{Eu/cell\ (normalized)}$ (λ) is a strong indicator of biodegradation.

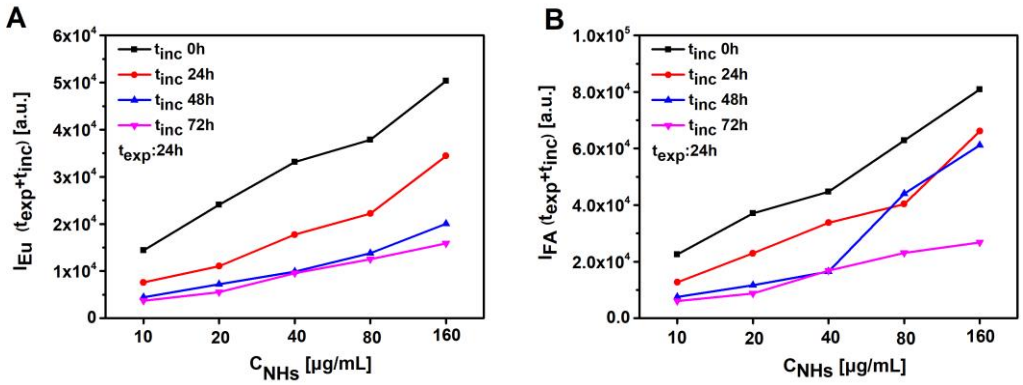

Figure 2-41. *Biodegradation of NHs-FA inside Hela cells cultured in complete cell medium, quantified by Eu fluorescence I_{Eu} (λ) (A) and FA fluorescence I_{FA} (λ) (B), characterized by fluorescence meter. Cells were lysed by Triton and tested the fluorescence from Hela cells incubated with NHs-FA.*

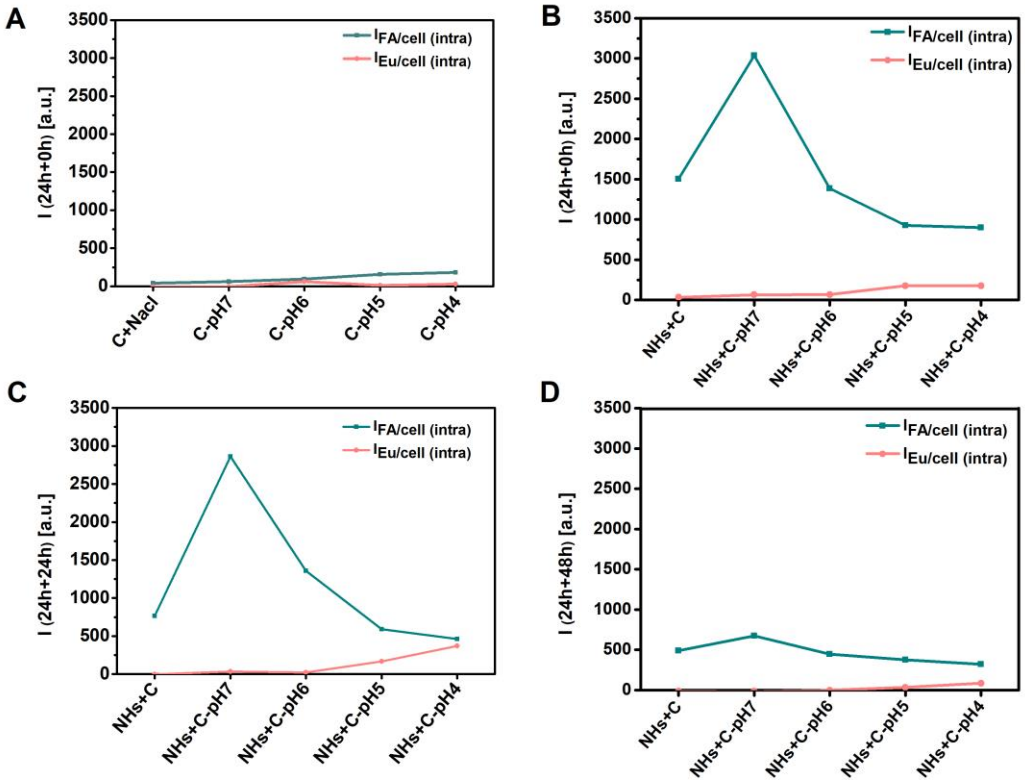

Figure 2-42. *The change of Eu fluorescence $I_{Eu/cell\ (intra)}$ (λ) and FA fluorescence $I_{FA/cell\ (intra)}$ (λ) detected from Hela cells [Control,C].The fluorescence from the C (A) and cells exposed to NHs [160 µg/mL] at pH 7, 6, 5 and 4 buffer (DPBS and MES buffer) for 24 hours (B),24+24 hours (C) and24+48 hours (D). The time is presented as exposure time t_{exp} + incubation time t_{inc}.*

To further probe into the effect of cell growth on biodegradation, we adopted certain lysosome inhibitors to interfere with the lysosome function of Hela cells. As the "digestive stomach" for cells, the lysosome is mostly responsible for biodegradation. In the presence of chloroquine (CQ) and ammonium chloride (NH_4Cl), the decrease of $I_{Eu/cell\ (intra)}$ (λ) and $I_{FA/cell\ (intra)}$ (λ) were completely inhibited. Notably, the inhibition was also a concentration-dependent procedure. Moreover, a modest reduction in $I_{Eu/cell\ (intra)}$ (λ) and $I_{FA/cell\ (intra)}$ (λ) were detected in the group with the treatment of pepstatin A (PA) and serum free (SF) condition. Of note, the impact of inhibitors on the fluorescence of NHs was identical to that on cell growth (Figure2-43). The results were normalized by growth factor as previously described, with no significant reduction being observed in $I_{Eu/cell\ (normalized)}$ (λ) and $I_{FA/cell\ (normalized)}$ (λ) (Figure2-44).The data from cytotoxicity about the lysosome inhibitors was in perfect agreement with the cell numbers (Figure2-45). As a consequence, it can be inferred that the impact of inhibitors would be wrongfully considered as the constraint on biodegradation, which is in essence the result of interferences from lysosome function. In fact, the inhibitors disturb the lysosome function, while it also reduces cell growth in the meantime. Cell proliferation is pivotal

to biodegradation and is decisive to the concentration of NHs per cell. Hence, suppressing cell growth is equivalent to imposing restriction on the power for diluting the NHs amount in an individual cell. Our study depicts a clear picture of the correlation between cell growth and biodegradation.

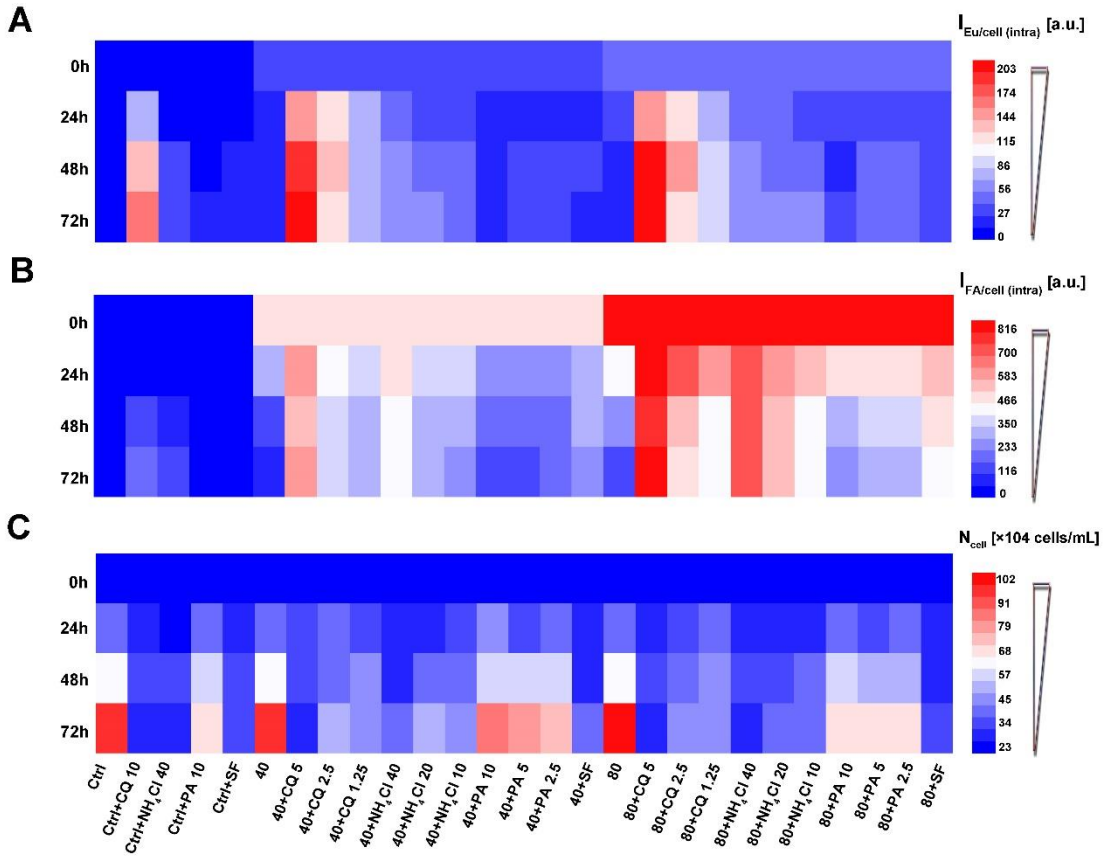

Figure 2-43. *The effect of lysosome inhibitors (Chloroquine: CQ; Ammonium chloride : NH_4Cl; Pepestatin A :PA; serum-free conditions: SF) at different concentrations on the mean Eu fluorescence $I_{Eu/cell\ (intra)}$ (λ) (A) , mean FA fluorescence $I_{FA/cell\ (intra)}$ (λ) (B) and cell growth (C) of the Hela cells incubated with and without NHs-FA at concentration of 80 µg/mL and 40 µg/mL. Incubated NHs-FA with Hela cells for 24 hours (t_{exp}), removed the supernatant and added fresh medium. Measured the $I_{Eu/cell\ (intra)}$ (λ), $I_{FA/cell\ (intra)}$ (λ) and cell growth at different incubation time (t_{inc}) of 0 hour, 24 hours, 48 hours, 72 hours.*

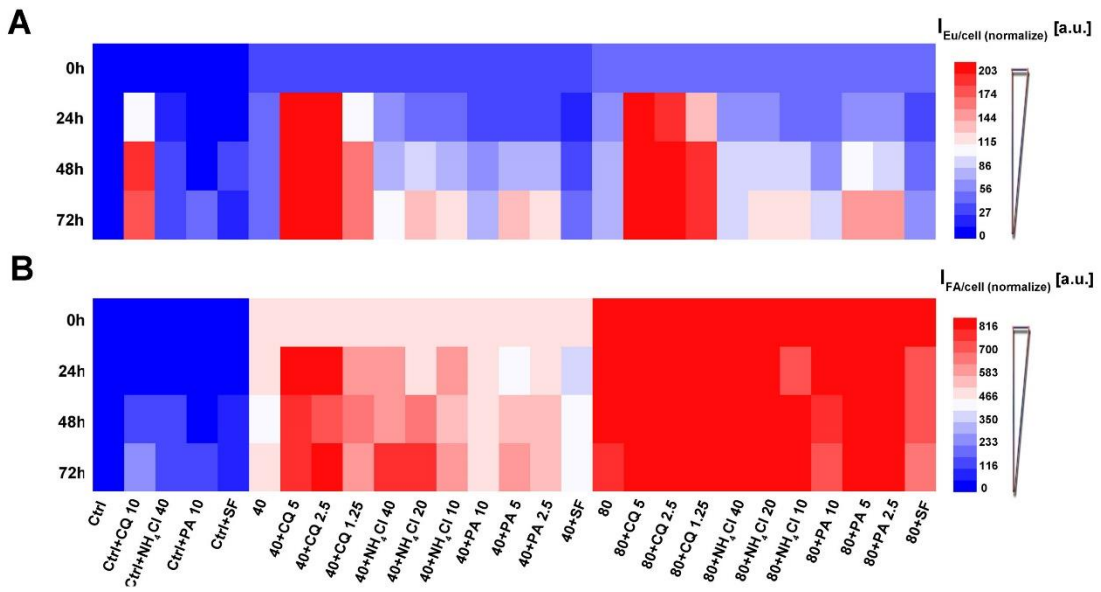

Figure 2-44. *The normalized Eu fluorescence $I_{Eu/cell\ (normalized)}$ (λ) (A) and normalized FA fluorescence $I_{FA/cell\ (normalized)}$ (λ) (B) from the Hela cells co-treated with or without NHs-FA and inhibitors. The data was obtained by mean Eu fluorescence $I_{Eu/cell\ (intra)}$ (λ) and mean FA fluorescence $I_{FA/cell\ (intra)}$ (λ) multiplied with corresponding growth factor.*

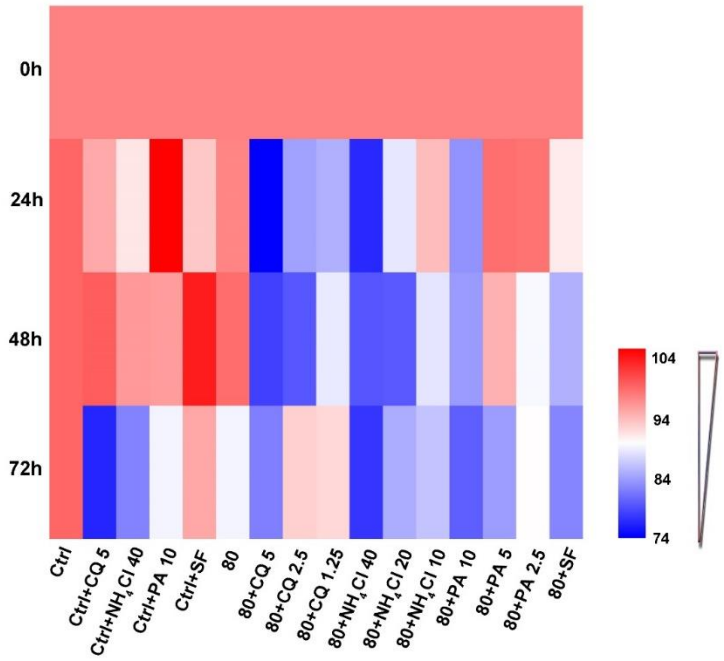

Figure 2-45*. The effect of lysosome inhibitors (chloroquine: CQ; ammonium chlorid : NH_4Cl; pepestatin A :PA; serum-free conditions: SF) at different concentrations on cell viability V of Hela cells with and without NHs-FA at the concentration of 80 µg/mL. Incubated NHs-FA with Hela cells for 24 hours (t_{exp}), removed the supernatant and added fresh medium. Tested the V of Hela cells at different incubation time (t_{inc}) of 0*

hour, 24 hours, 48 hours, 72 hours.

2.5.5. Cellular behaviors of NHs tracked by metal concentrations.

To go on uncovering the biodegradation of the inorganic core, we made use of the ICP-MS to explore the mechanism. First, Hela cells saturated with NHs at 6 hours. The amount of internalized NHs per cell stayed unchanged from 6 hours to 48 hours, accompanied with the constant elemental concentrations in the supernatant, which was inconsistent with the one from flow cytometry. A potential interpretation of this phenomenon lies in the strong attachment of NHs to the cell membrane were also counted as internalized NHs during ICP-MS measurement. For the biodegradation study, we extended the incubation time to 120 hours to have an insight into biological fate for a longer time. It was clear that the concentration of Eu, Bi and Gd per cell ($m_{Eu/cell\ (intra)}$,$m_{Bi/cell\ (intra)}$ and $m_{Gd/cell\ (intra)}$) markedly reduce to ≈10% in the course of biodegradation due to cell growth, which is thus consistent with the fact that cell growth is a powerful way to clear the NHs per cell (Figure2-46).

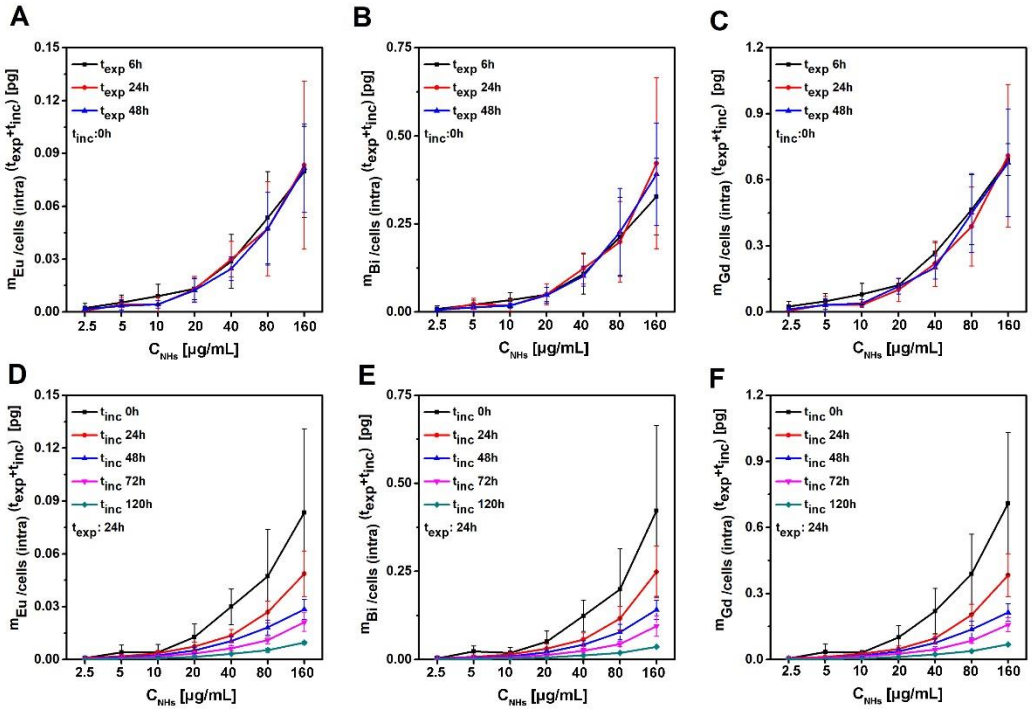

Figure2-46. *Quantitative NHs uptake (A-C) and biodegradation (D-F) in Hela cells in complete cell medium. The mass concentration of Eu per cell* $m_{Eu/cell\ (intra)}$ *(A and D), the mass concentration of Bi per cell* $m_{Bi/cell\ (intra)}$ *(B and E) and the mass concentration of Gd per cell* $m_{Gd/cel\ l(intra)}$ *(C and F) in the cell pellet.*

Then, we shifted our focus to analysis of the total amount of NHs inside Hela cells in

the course of degradation. A slight decline in the cellular concentration of three elements can be observed (Figure2-47). Accordingly, increasing concentration of Eu, Bi and Gd were also found in the supernatant (Figure2-48). There are two possible reasons for this change, exocytosis of degraded NHs and exocytosis of intact NHs. To work it out, the ratio between the elements in the supernatant was calculated and plotted. When the cells secreted out the undamaged NHs, the ratio of elements should be unvaried during the process. However, in fact, the ratio of Bi/Eu and Gd/Bi exhibited considerable change during the biodegradation study, while there was no statistical difference in the ratio of Gd/Eu (Figure2-49). To compare with biodegradation process, it gives negligible variation for three ratios in the supernatant during the uptake procedure. The varied ratios between elements were encouraging and provided direct cues for the biodegradation of cellular NHs. Applying the calculation of elemental ratios, we illustrated how to distinguish the exocytosis of intact NHs and degraded ones in this context.

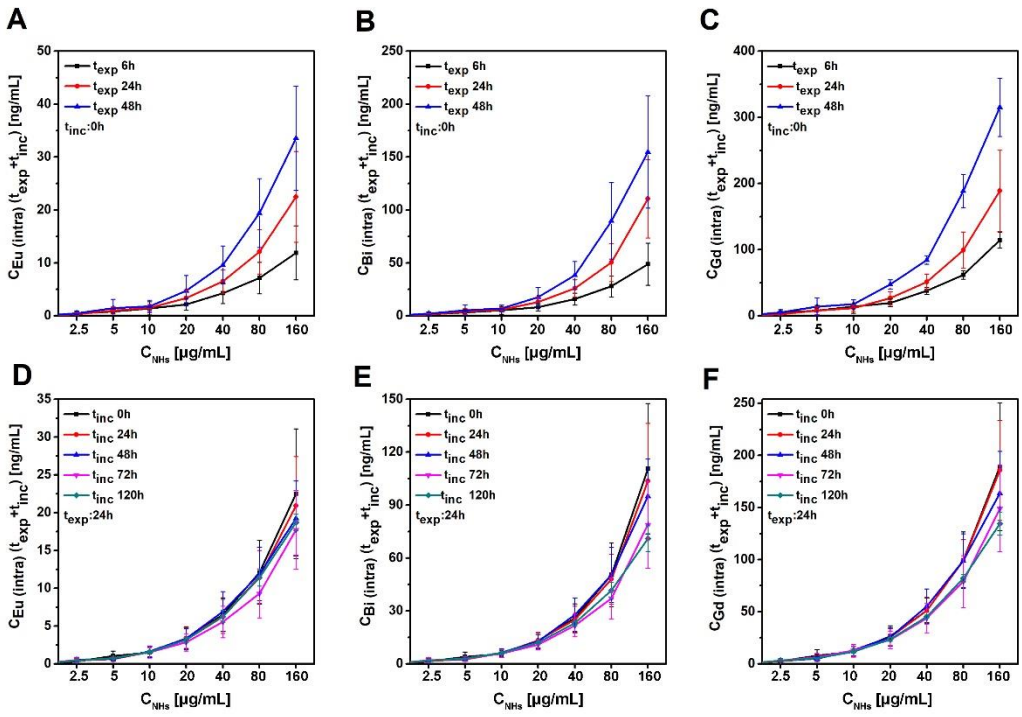

Figure2-47. *Quantitative NHs uptake (A-C)and biodegradation (D-F) in Hela cells in complete cell medium. The total amount of Eu $C_{Eu\ (intra)}$ (A and D), the total amount of Bi $C_{Bi\ (intra)}$ (B and E) and the total amount of Gd $C_{Gd\ (intra)}$ (C and F) inside Hela cells.*

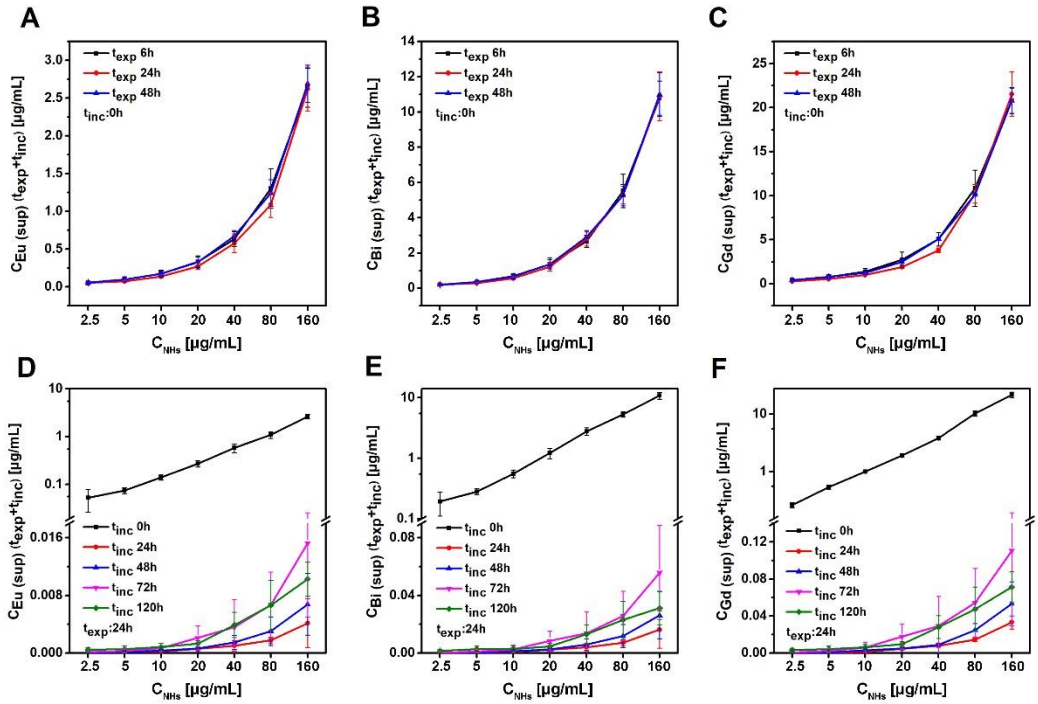

Figure 2-48. *The total amount of of Eu $C_{Eu\ (sup)}$, Bi $C_{Bi\ (sup)}$ and Gd $C_{Gd\ (sup)}$ in the supernatant during the uptake (A-C) and biodegradation (D-F) period.*

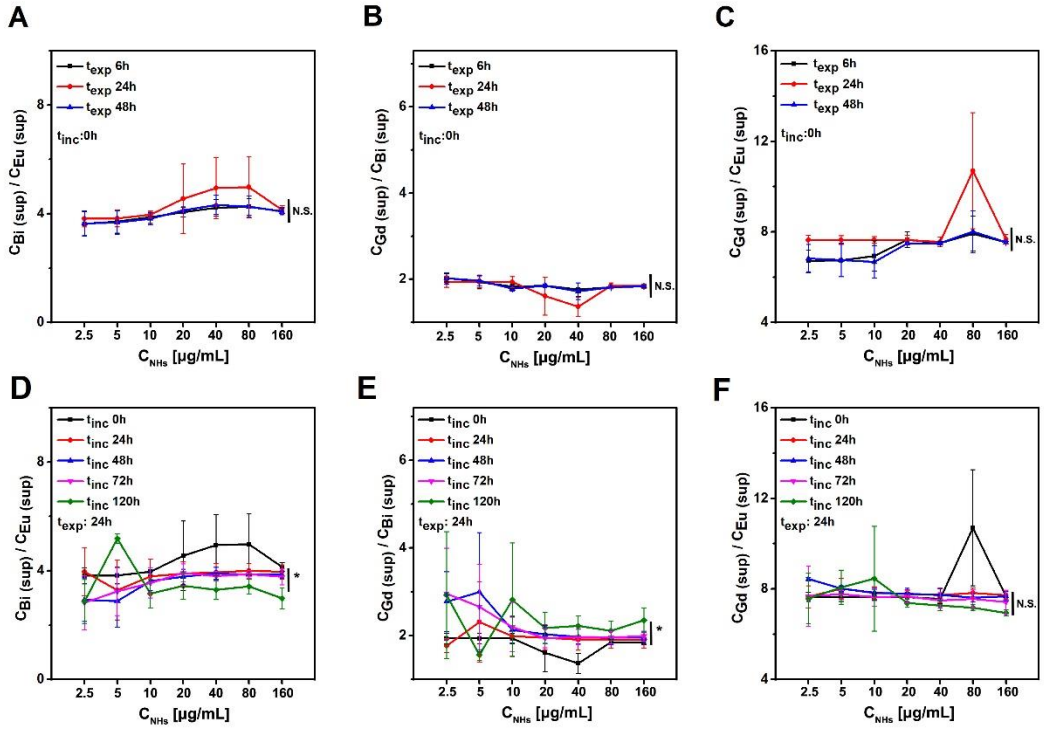

Figure2-49. *The ratio between the total amount of Eu $C_{Eu\ (sup)}$, Bi $C_{Bi\ (sup)}$ and Gd $C_{Gd\ (sup)}$ in the supernatant.*

2.5.6. Shape evolution of NHs during the biodegradation process

Subsequently, TEM was used to follow the structural evolution during the intracellular biodegradation. Figure2-50 directly presented the shape change from 6+0 hours to 24+120 hours. At 6+0 hours, some NHs were randomly distributed in the cytoplasm, while some uninternalized NHs were still attached to the cell membrane. Once internalized by cells at 6 +0 hours, the sharp edges and points of most NHs were blunted. Whereas, all NHs were confined within lysosome from 24+0 hours to 24+120 hours, and progressively loosed the well-defined cubic shape and turned into irregular round-like figures in the course of biodegradation. The degraded NHs were inclined to combine with adjacent NHs to form a large aggregation. Furthermore, the shape parameters were further performed to calculate the shape change in the semiquantitative way (Figure2-51-Figure2-54). The α_{NHs} were drastically enlarged from 6+0 hours to 24+120 hours. The bio-condition had little impact on the A_{NHs} of objects. A small decline was observed in S_{NHs} and Z^0_{NHs}, representing the highest degree in depression and ellipticity (Figure2-55). The Ec_{NHs} and C_{NHs} increased with time, suggesting the enhanced ellipticity and irregularity. Conclusively, the shape parameters proved clearly that NHs changed from well-dispersed cube to disorganized spindle-like shape, which was consistent with the evolution of the test at acid buffer.

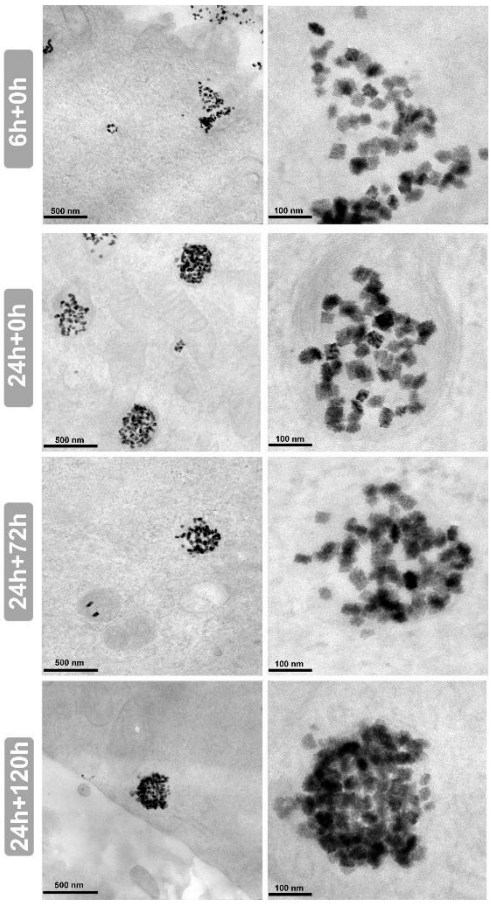

Figure 2-50. *The change in the shape of NHs at a concentration of 160 μg/mL in the*

course of uptake and biodegradation. The time is presented as exposure time t_{exp} + incubation time t_{inc}.

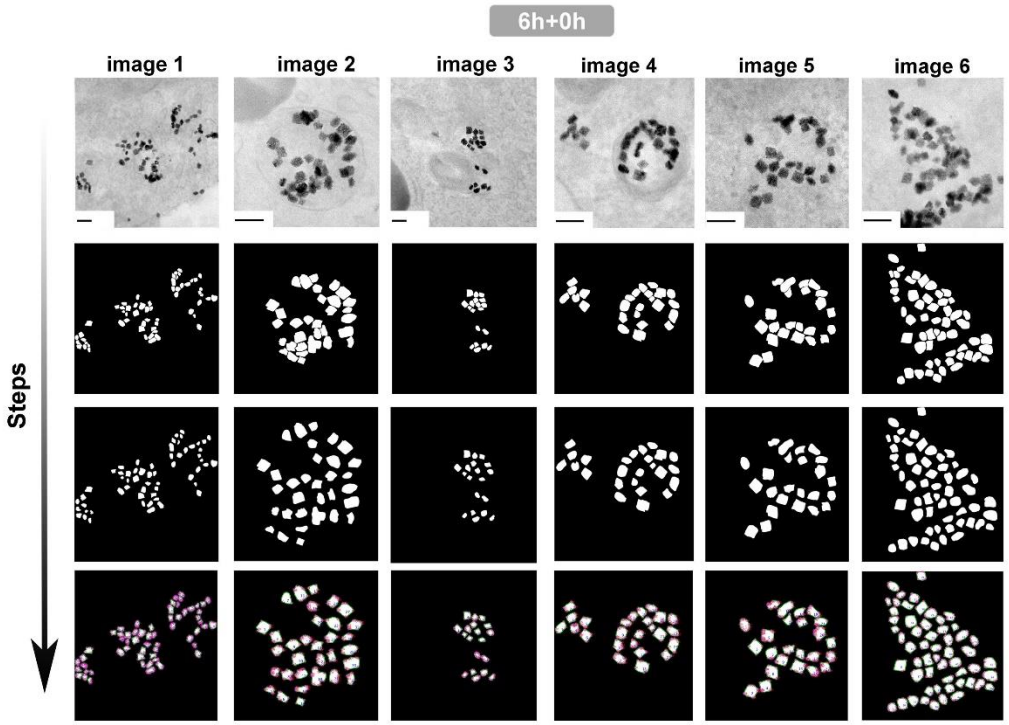

Figure 2-51. *The steps of TEM calculation for NHs inside cells for 6 hours+0 hours. The label bar is 100 nm. The time is presented as exposure time t_{exp} + incubation time t_{inc}.*

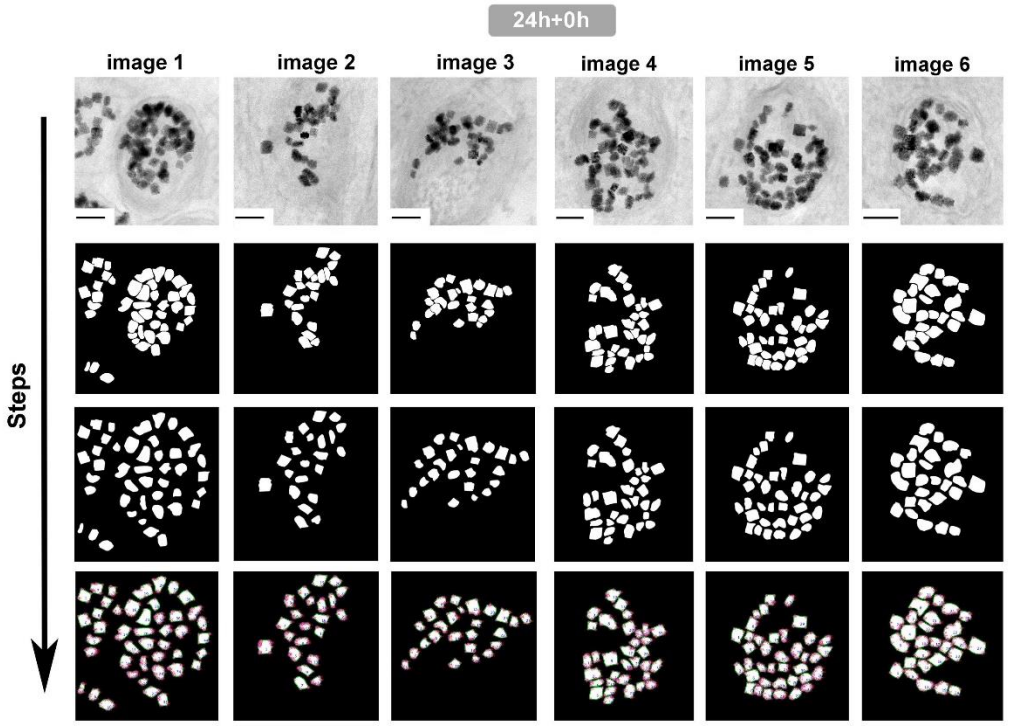

Figure 2-52. *The steps of TEM calculation for NHs inside cells for 24 hours+0 hours. The label bar is 100 nm. The time is presented as exposure time t_{exp} + incubation time t_{inc}.*

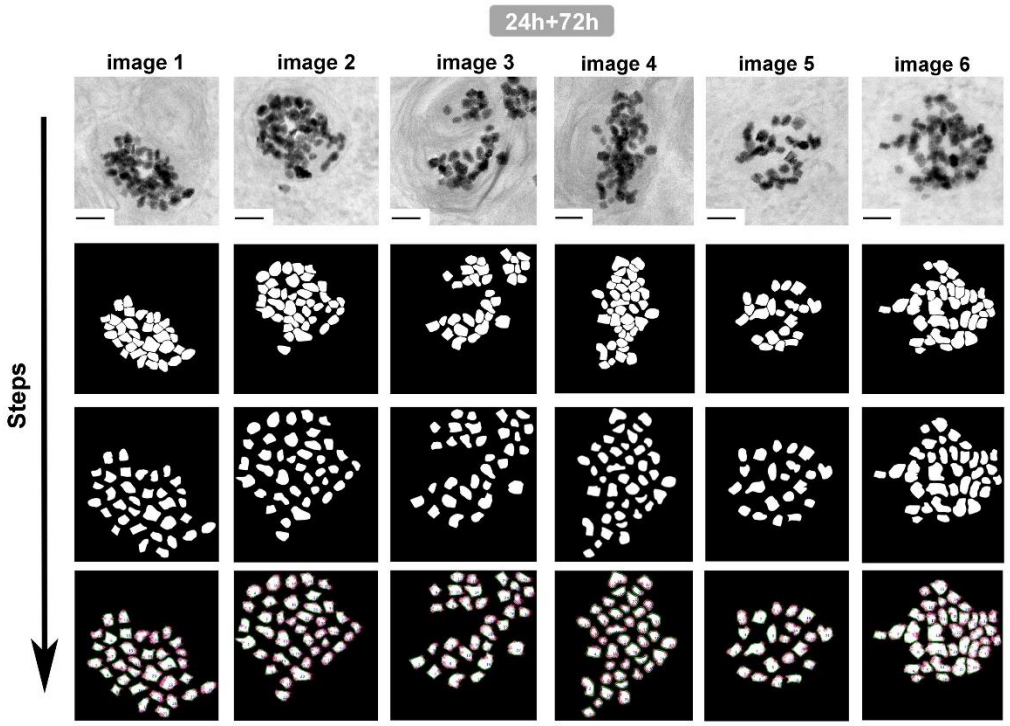

Figure 2-53. *The steps of TEM calculation for NHs inside cells for 24 hours+72 hours. The label bar is 100 nm. The time is presented as exposure time* t_{exp} *+ incubation time* t_{inc}*.*

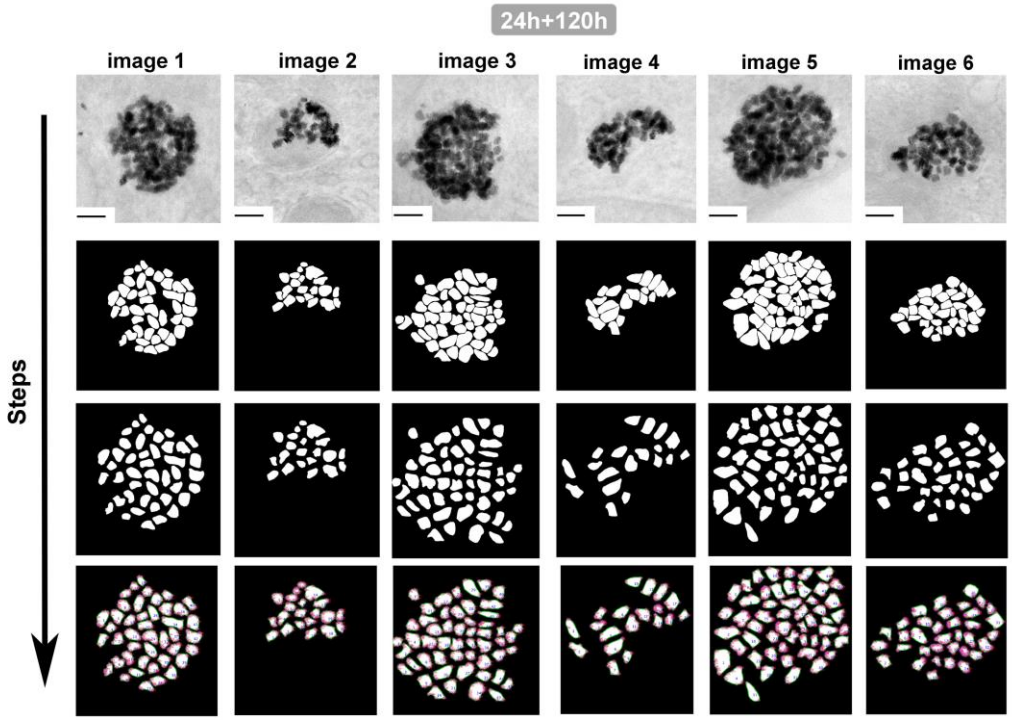

Figure 2-53. *The steps of TEM calculation for NHs inside cells for 24 hours+120 hours. The label bar is 100 nm. The time is presented as exposure time* t_{exp} *+ incubation time* t_{inc} *.*

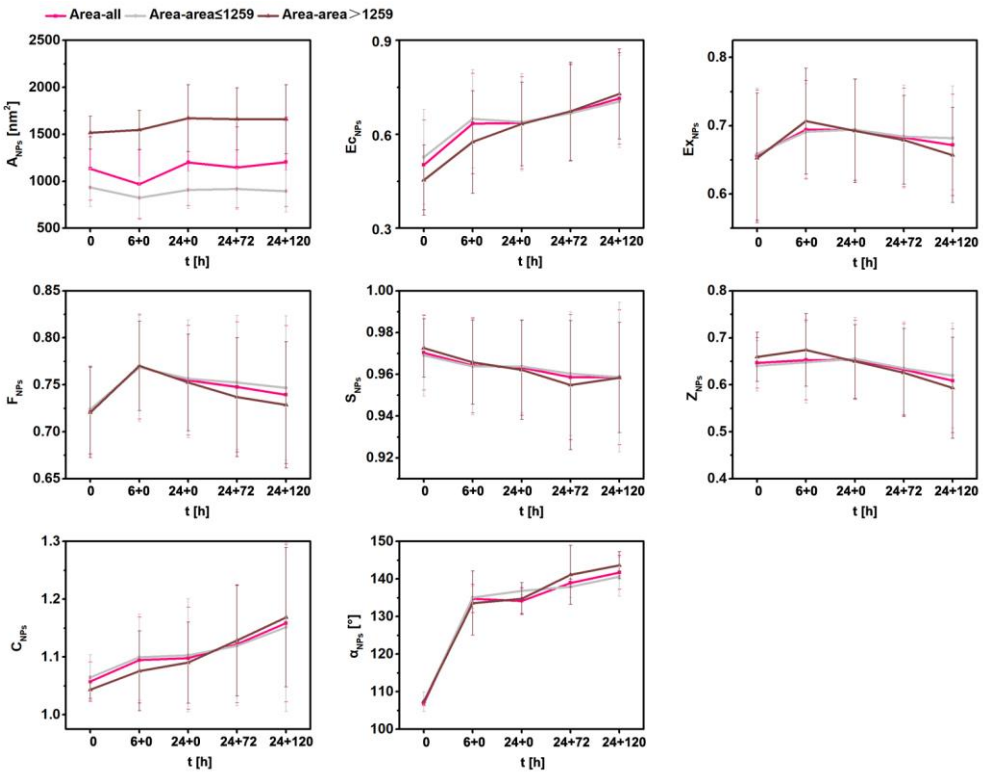

Figure 2-55. *The shape parameters of NHs inside cells for 6+0, 24+0, 24+72 and 24+120 hours. The time is presented as exposure time t_{exp} + incubation time t_{inc}.*

2.6. Summary for Chapter 2

In the present study, we evidenced that RE-based NHs can indeed be degraded at pH 3.5 acid buffer and the cellular environment. Firstly, the well-defined cubic shape NHs with 33.17±0.65 nm were successfully synthesized. To trace the inorganic core and polymeric shell during the process, two major methods, namely, fluorescence and the concentration of metal ions were put to use. The NHs consisted of two fluorescence, Eu fluorescence for the inorganic core and FA fluorescence for the polymeric shell, and three metal ions inside the inorganic core, Eu, Bi and Gd. At the acid buffer, an obvious reduction in Eu fluorescence and size can be observed after about two weeks. Comparatively, the surface FA fluorescence and charge kept constant, indicating the invariable behaviors of the polymeric shell at acid buffer. Making use of Cell profiler and Matlab, we came up with a method to track the shape evolution during the degradation process. By this method, sharp edges and points of the objects can be blunted, revealing that the shape collapses and merges to other NHs. Meanwhile, the acid buffer enlarged the angles of the object without affecting the area. As for *in vitro* condition, the evident decrease in fluorescence and the amount of metal ions started to appear within cells after 72 hours. It is worth mentioning that cell growth and exocytosis obstructed us from probing into the effective degradation. Therefore, growth factor was applied so as to successfully eliminate the effect of cell division. The

ratios between metal ions clearly distinguished degradation from exocytosis. Furthermore, the shape evolution inside cells was in line with the tendency in the acid buffer.

It had been proven that detecting NHs degradation at the cellular scale is demanding for the reason that developing a method to study the effective cellular biodegradation requires considerations of multiple factors, such as cell division and exocytosis. Herein, we displayed a useful way to directly determine the degradation of NHs, which was made of a fingerprint of shape evolution for both test at acid buffer and *in vitro* measurement. It can also be applied to the structure change of proteins and cells. We further demonstrated that the cell growth powerfully reduced the concentration of NHs in the individual cell. The correlation between bio-dilution and biodegradation was paramount in understanding the complex picture of cellular degradation. The quantification of element ratios had the additional advantage of distinguishing the exocytosis between intact NHs and damaged ones. Ultimately, this work developed the strategy to identify the degradation of NHs, creating exciting opportunities to deepen our knowledge about the biological behaviors of NHs in a physiological environment.

3. The degradation of MOF

3.1. Introduction

Zr-MOF with highly porous properties offers numerous opportunities for applications in the fields of catalysis and biology. As a new class of materials, the biological applications of MOF are often hampered by their biocompatibility and toxicology[95]. With regard to Zr, it can be detected in nature and biological systems without difficulty, its rich content makes toxicologically acceptable formulation possible, and in the meanwhile, high stability of Zr meets the prerequisite requirement for medical use. It has been well documented that Zr-MOF can be used as carriers for controllable release of doxorubicin (DOX)[96]. Taking the advantage of the interaction between hydroxyl groups in DOX and Zr in MOF, the DOX-encapsulated Zr-MOF displayed a sustainable drug release and achieve efficient, decent therapeutic efficacy. By the way, the modification of spherical nucleic acid can be also used to enhance the stability and cellular uptake of Zr-MOF[97]. To expand their biological applications, the knowledge related to the physiological fate of MOF is in urgent demand. Degradation processes in the biological environment could ultimately break the structure of MOF, and their degradable fractions and a wide range of side products are likely to exert broader underlying impacts from toxicity to the immunological response. In consequence, it is anticipated that knowledge concerning degradation could give guidance for the in-depth study of MOFs towards practical applications. Based on the above considerations, our study investigates the biological behaviors of Zr-MOF within cells.

3.2. Major reagents

Name	Purity	Company	Function
Zirconium (IV) chloride	≥ 99.0%	Sigma-Aldrich	For synthesis
Fumaric acid	≥ 99.9%	Sigma-Aldrich	For synthesis
Citric acid	99.90%	Acros	For synthesis
Sodium phosphate dibasic	⩾98.5%	Sigma-Aldrich	For synthesis
Nitric acid	67wt%	Fisher Chemical	For ICP measurement
Hydrochloric acid	35wt%	Fisher Chemical	For ICP measurement
Dulbecco's modified		Thermofisher	For cell culture
Penicillin/streptomycin		Sigma-Aldrich	For cell culture
Fetal bovine serum		Biochrom	For cell culture

Resazurin	~80%	Sigma-Aldrich	For cell experiment
Phosphate buffered		Invitrogen	For cell culture
0.05% trypsin/EDTA		Thermofisher	For cell culture
Atto-647		Atto TEC	For synthesis

3.3. Key instruments

Name	Model	Company	Function
Inductively coupled plasma mass spectrometry (ICP-MS)	7700 Series	Agilent	For ICP measurement
Dynamic light scattering (DLS)	NANO ZS	Malvern	For characterization
Fluorescence meter	Fluorolog-3	Horiba Jobin Yvon	For characterization
Flow cytometry	BD LSRFortessa™	BD Biosciences	For degradation study

3.4. Experiments and methods

3.4.1. Synthesis of Zr-MOF

Zr-fum NPs were synthesized according to a procedure reported by Zahn et al[98]. Fumaric acid (180.0 mg, 1.550 mmol) and $ZrCl_4$ (120.5 mg, 0.517 mmol) were dissolved in 10 mL of bidistilled H_2O. Formic acid (1.190 g, 25.85 mmol) in a volume of 0.975 mL was mixed with the solution and the reaction solution was sealed in a glass autoclave (25 mL). Heat the mix solution to 120 °C for 24 h and cool it down to RT afterward. Further, the resulting Zr-MOF were transferred in 15 mL tubes and centrifuged at 7187 g for 10 min. After washing it with 6mL of H_2O, the Zr-MOF was transferred to Eppendorf tubes and centrifuged at 16900 g for 10 min. The solution was washed twice with ethanol and then was stored it in ethanolic solution.

Zr-MOF was dissolved in 1 mL HEPES buffer (20 mM, pH 7.4). DBCO-PEG4-NHS ester

was dissolved in DMSO were added to the Zr-MOF solution. The reaction mixture was incubated for 3 hours at RT under shaking. H6-PEG36-5ANV (HCl salt) was added to the Zr-MOF solution and the mixture was incubated at RT. Purification was continued with the method which combined immobilized metal ion chromatography (IMAC) with size exclusion chromatography (SEC). First, the HisTrapHP 1 mL column was connected to an Äkta purifier system (GE Healthcare Bio-Sciences AB, Sweden) to isolate H6-tagged protein. We then adopted a gradient of binding buffer (20 mM sodium phosphate, 0.5 M NaCl, pH 7.4) as mobile phase and another buffer (20 mM sodium phosphate, 0.5 M NaCl, 0.5 M imidazole, pH 7.4) as elution buffer. The fractions with the highest affinity to the column were collected and concentrated with Amicon Ultra centrifugal filter units (MWCO= 10.000; Millipore, USA). To remove the salt and free H6-PEG36-5ANV, the solution was subjected to SEC using the Sephadex G25 superfine size exclusion column with Äkta purifier system. The HEPES buffer (20 mM, pH 7.4) was adopted as the mobile phase. Targeted fractions were collected and concentrated by Amicon Ultra centrifugal filter units (M_W = 10.000; Millipore, USA). The H6-PEG35-5ANV modified Zr-MOF in HEPES buffer (20 mM, pH 7.4) was prepared. ATTO 647N NHS ester was dissolved in DMSO were added to the H6-Zr-MOF solution. The solution was incubated for 2 hours at RT subsequently SEC (Sephadex G25 superfine) was carried out as described before. The concentration of labeled Zr-MOF was determined by ICP-MS.

3.4.2. The physicochemical characterizations of Zr-MOF

Firstly, the hydrodynamic diameter d_h of Zr-MOF was measured by dynamic light scattering (DLS, Malvern NANO ZS, England) with a UV-Kuevette, ZH 8.5mm. Deckel (Sarstedt, Germany)[29].0.5 mL of NHs solution ($c_{Zr\text{-}MOF}$: 200µg/mL) dispersed in Milli-Q water was equilibrated for 5 min at 25 °C. The samples were measured in Milli-Q water at 173° backscatter settings, using a 633 nm laser. The data were presented as number $d_{h(N)}$ and intensity $d_{h(I)}$ distributions were both recorded (Figure 3-2). A Malvern Zetasizer was adopted to test the ζ-potential ζ of the Zr-MOF with laser Doppler anemometry (LDA). For that, 1 mL of Zr-MOF solution at concentration $C_{Zr\text{-}MOF}$ of 200µg/mL dispersed in Milli-Q water was waited for 5 min at 25 °C for equilibration before measurements. The distribution of ζ was shown in Figure 3-2. The precise data were summarized in Table3-4. Lastly, the relationship between the concentration of Zr-MOF $C_{Zr\text{-}MOF}$ and the concentration of Zr C_{zr} was measured by ICP-MS. For this purpose, the NHs with a serial of dilution were prepared. 50µL of tested samples were mixed with 150 µL of aqua regia (HNO_3 (67 wt%, Fisher Chemical, USA) and HCl (35 wt%, Fisher Chemical, USA) with a volume ratio of 1:3) overnight. Diluted the concentrated samples with 1.8 mL of 2% HCl (35 wt%, Fisher Chemical, USA) to get the final samples. Put the samples to perfluoroalkoxy alkane (PFA) tubes and tested it by ICP-MS (ICP-MS, Agilent 7700 Series, USA). The method has been described above. The correlation between the concentration of Zr-MOF $C_{zr\text{-}MOF}$ and the amount of Zr C_{zr} was

displayed in Figure 3-2. The experiment had been conducted three times (n=3).

3.4.3. Cell culture and cell viability

Hela cells, cervical cancer cells, were adopted for the cellular uptake and biodegradation study, which were purchased from American Type Culture Collection (Manassas, VA, USA).Cells were cultured in Dulbecco's Modified Eagle Medium (DMEM, Thermofisher, USA) supplemented with 10% fetal bovine serum (FBS, Biochrom, UK), and 100 units/mL penicillin/streptomycin (P/S, Sigma-Aldrich, Germany) in the incubator at 37 °C, 5%CO_2.

To evaluate the biocompatibility of Zr-MOF, cells were seeded at 96-well plate (growth area per well A_{well} 0.34 cm^2, Greiner bio-one, Austria) at a density of 7500 cells per well ($N_{cells/well}$: 7500 cells) in a volume V_{well} of 100 µL /well. On the next day, Zr-MOF was diluted from the stock solution ($C_{Zr\text{-}MOF}$ = 5mg/mL) with fresh medium to the desired concentrations. The exposure concentrations were given in Table 3-1. Zr-MOF with the range of concentrations $C_{Zr(add)}$ was exposed to cells with a volume of 100 µL /well for 24 and 48 hours. Keep some wells for control cells. After the specified exposure time, the supernatant was removed and cells were washed once with 100 µL/well of phosphate buffered saline (PBS, Gibco, Invitrogen, Belgium). Then, 10% resazurin solution (dilute the resazurin salt solution [2.5 mg/mL] with complete cell medium) in a volume of 100 µL/well was incubated with cells for 4 hours in the incubator[6]. The fluorescence of the cells was detected by fluorescence meter (Fluorolog-3, Horiba Jobin Yvon, Germany) with an excitation wavelength of 560 nm and an emission wavelength of 570-620 nm. The reduced environment in mitochondria of live cells can convert the non-fluorescent dye to the highly fluorescent substances. The change of fluorescent signal is proportional to the number of living cells in the sample. The data of cell viability (V) have been analyzed by Matlab. The experiment had been conducted three times (n=3). (Figure 3-3).

Table 3-1. The used concentrations of Zr-MOF for cytotoxicity study, in terms of the concentration of Zr-MOF $C_{Zr\text{-}MOF}$ [µg/ml] and the exposure concentration of Zr C_{Zr} [µg/ml]. The dilution of Zr-MOF is a two-fold serial dilution.

Samples	$C_{Zr\text{-}MOF}$ [µg/ml]	$C_{Zr(add)}$ [µg/ml]
1#-15#	3.05×10^{-2}-5.00×10^{2}	2.28×10^{-2}-3.11×10^{1}

3.4.4. Zr-MOF uptake and degradation tested by flow cytometry

For the study of cellular uptake and biodegradation of Zr-MOF by flow cytometry (BD LSRFortessa™, BD Biosciences, US)[33], cells were seeded in 24-well plate (growth area per well A_{well} 1.87 cm^2 ,Sartstedt, Germany) at the intensity of 40,000 ($N_{cells/well}$ =40,000 cells) with V_{well} of 1 mL/well. On the next day, Zr-MOF were diluted from the stock solution ($C_{Zr\text{-}MOF}$ = 5mg/mL) to the various concentrations. The concentrations showed in Table3-2. Zr-MOF at different concentrations in a volume of 0.5 mL was treated with Hela cells. For uptake study, cells were exposed to the Zr-MOF with different concentrations for specific exposure time (t_{exp}=6, 24, 48 hours). For degradation study, the supernatant was removed and cells were washed three times with 1 ml of PBS after 24h exposure time (t_{exp}=24 hours). Fresh medium with volume of 0.5 mL/well were added to keep additional incubation times for 0, 24, 48 and 72 hours (t_{inc} =0, 24, 48, 72 hours, Figure 3-1). At desired time points, the growth medium was aspirated, cells were washed three times with PBS in a volume of 1 mL (each well). 0.1 mL of 0.05 % trypsin-EDTA was added to each well to detach cells. After trypsinization, cells were neutralized with 0.5 mL of complete cell medium, collected and centrifuged at 300 × g for 5 minutes. Then, discard the supernatants and cell pellets were re-suspended in PBS with a final volume of 300 µL. The cell number of each sample has been counted by the Neubauer chamber. The fluorescence of Atto-647 originating from Hela cells was detected by flow cytometry with laser 633 nm. For a set of experiments, the uptake and degradation studies have been explored at the same time. We used flowjo to analyze the data. The mean fluorescence $I_{Atto/cell\ (intra)}$ was adopted to show the data from four independence experiments (Figure 3-4). The experiment had been conducted three times (n=3).

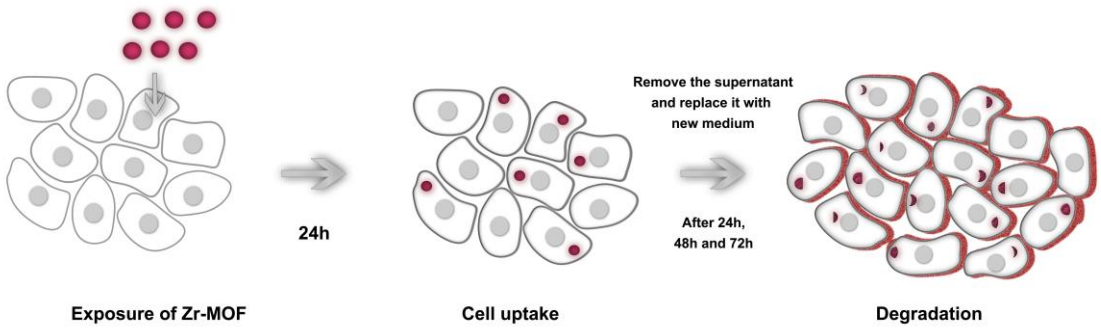

Figure3-1. *Schematic illustration of degradation study. Exposed Zr-MOF to cells for 24 hours. Aspirated the supernatant, washed and resuspended the cells with the new medium. At specific time points, the degradation behaviors have been tracked by flow cytometry and ICP-MS.*

Table 3-2. Range of Zr-MOF concentrations used in cellular uptake and biodegradation study, in terms of mass concentration of Zr-MOF $C_{Zr\text{-}MOF}$ [μg/ml] and mass concentration of Zr $C_{Zr(add)}$ [μg/ml] at exposure time.

Sample	$C_{Zr\text{-}MOF}$ [μg/ml]	$C_{Zr(add)}$ [μg/ml]
1#	1.56	0.56±0.26
2#	3.13.	0.83±0.21
3#	6.25	1.23±0.18
4#	12.50	2.15±0.29
5#	25	3.49±0.70
6#	50	6.24±0.97
7#	100	9.04±1.06

3.4.5. Zr-MOF uptake and degradation tested by ICP-MS

To detect the cellular uptake and biodegradation of Zr-MOF by ICP-MS[5], cells were seeded in 6-well plates (growth area well A_{well} 8.87 cm^2, Sarstedt, Germany) at the intensity of 207,890 cells per well ($N_{cells/well}$:207,890 cells) with V_{well} of 2 mL. Zr-MOF has been diluted from the stock solution ($C_{Zr\text{-}MOF}$ = 5mg/mL) with complete cell medium to the designed concentrations C_{Zr}. The exact concentrations are provided in Table 3-2. The medium containing Zr-MOF at different concentrations $C_{Zr(add)}$ (Table 3-2) were added to the cells in a volume of 2 mL /well. Cells were exposed to Zr-MOF for 6, 24 and 48 hours (t_{exp}: 6, 24, 48 hours) to monitor the cellular uptake. For the biodegradation study, cells were treated with Zr-MOF at different concentrations for 24 hours (t_{exp}: 24 hours). Remove the supernatant and wash cells with 2 mL/ well of PBS three times. Add the fresh medium to each well in a volume of 2 mL. Keep the cellular incubation of Zr-MOF for 24, 48 and 72 hours (t_{inc}: 24, 48, 72 hours). At the specific time points, 1 mL of supernatant was collected. The cells were then washed with 2 mL/well of PBS three times. Treated cells with 0.2 mL/well of 0.05% trypsin-EDTA (Thermofisher, USA) to get detachment and PBS in a volume of 2 mL were added to each well. Collect the samples to Eppendorf tubes (Eppendorf, Germany). Each sample was counted by Neubauer chamber (Celeromics Technologies, Spain). For the samples of supernatant, 100 μL of supernatant was digested with 100 μL of aqua regia (concentrated HNO_3 (67 wt%, Fisher Chemical, USA) and HCl (35 wt%, Fisher Chemical, USA) with a volume ratio of 1:3) overnight. The digested samples were diluted with 1.8 ml of 2% HCl to obtain the tested samples with total volume V_{tes} of 2 mL. The mass concentrations of Zr in the samples were detected by ICP-MS. For the samples of cells,

cell pellets were obtained through centrifugation at 4000 rpm for 10 min. The cell pellets were subjected to digestion with 75 µL of HNO_3 overnight. Then, 150 µL of HCl was adopted to make sure of the complete digestion. Dilute the digested samples with 2.275 mL of 2% HCl to get the tested samples with V_{tes} of 2.5 mL. For a set of experiments, the uptake and biodegradation studies have been explored at the same time. Results are from more than three independent experiments (Figure 3-5 and Figure3-6). The experiment had been conducted three times (n=3).

To compare the mass concentration of Zr in the supernatant and pellet, C_{Zr} refers to the effective final incubation concentrations in the V_{well} of each well. Since the V_{well} of supernatant is the same to V_{tes}, there is no volume dilution factor. For the cell pellet, the V_{well} is 2 mL. Whereas the V_{tes} is 2.5 mL. The mass concentrations of Zr for the cell pellet from ICP-MS should multiply with 1.25. The mass concentration of Zr in cells $C_{Zr\ (intra)}$ and supernatant $C_{Zr\ (sup)}$ against $C_{Zr\ (add)}$ was plotted to determine the uptake and biodegradation of Zr-MOF

3.5 Results and discussions

3.5.1. The synthesis and characterizations of Zr-MOF

Zr-MOF was fabricated according to Zimpel et al[99] under formic acid-mediated hydrothermal conditions. The resulting Zr-MOF was then dispersed in bistilled water and their size and surface charge were characterized by DLS (Figure3-2). The results demonstrated the uniform size distribution of Zr-MOF with 68.61±8.67 nm and the negative surface potential of -15.50±0.35 mv (Table 3-3). Furthermore, the concentrations of Zr-MOF $C_{Zr\text{-}MOF}$ and Zr C_{Zr} had been clarified by ICP-MS (Figure 3-2).

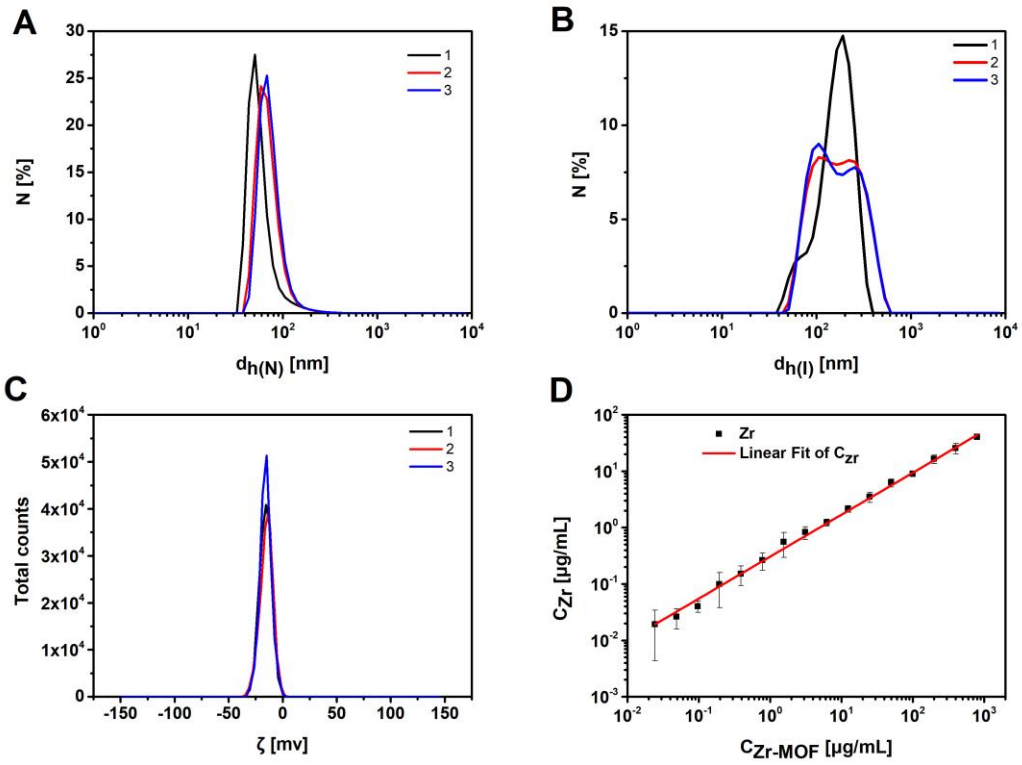

Figure 3-2. *The hydrodynamic diameter d_h of Zr-MOF as characterized by DLS in Milli-Q water. Number distribution $d_{h(N)}$ (A), Intensity distribution $d_{h(I)}$ (B)and ζ-distribution ζ(C) of Zr-MOF. The standard curve of the relationship between the concentration of Zr-MOF C_{Zr-MOF} and the amount of Zr C_{Zr}, determined by ICP-MS. For the relationship between C_{Zr-MOF} and C_{Zr}, the equation is y=0.7439x-0.515 R^2=0.9970.*

Table3-3. The hydrodynamic diameter d_h of Zr-MOF characterized by DLS in Milli-Q water. Number distribution $d_{h(N)}$, Intensity distribution $d_{h(I)}$ and ζ-distribution ζ of NHs. Results repeated three measurements are shown.

Sample	$d_{h(N)}$ [nm]	$d_{h(I)}$ [nm]	PDI	ζ [mV]
Zr-MOF	68.61±8.68	209.47±18.65	0.31±0.02	-15.50±0.35

3.5.2. Biodegradation behaviors of Zr-MOF monitored by fluorescence

Generally speaking, the biological applications of MOF are hindered by their stability and biocompatibility. The high biocompatibility of Zr-MOF had been shown in Hela cells, which lays the foundation for us to conduct the biodegradation study (Figure 3-3).

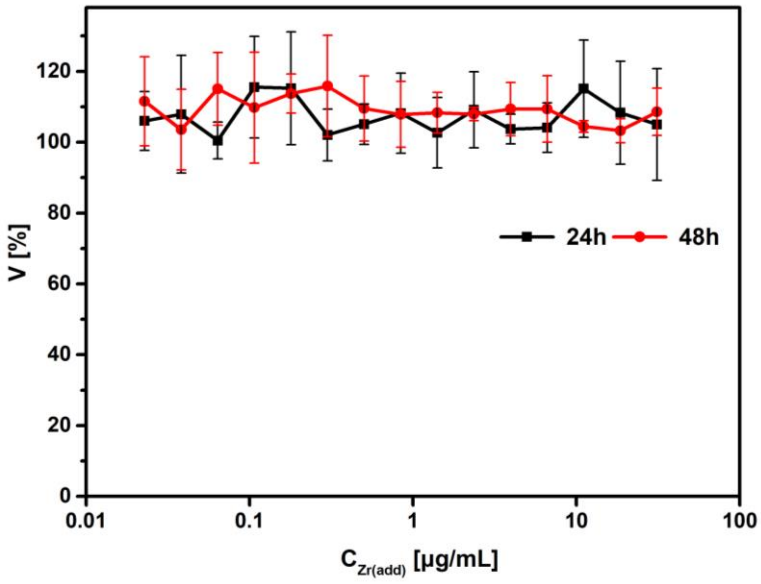

***Figure 3-3**. Cell Viability V of Hela cells incubated with Zr-MOF for 24 hours and 48 hours. Cells were exposed to Zr-MOF with serials dilution in complete cell medium. The test was determined by reasuzrin assay*

It can be inferred from the flow cytometry results, that the cellular uptake was saturated at 24 hours, and that exocytosis may decrease the concentration of Zr-MOF inside cells at 48 hours. In addition, the fluorescence per cell was drastically reduced to about 50% during the biodegradation (Figure 3-4). The significant reduction in fluorescence may come from three factors, degradation, exocytosis and cell growth. To exclude the influence of cell growth, the specific fluorescence originated from cells had been normalized by cell growth. Comparatively, the normalized signal stayed constant. The amount of MOF in one mother cell can pass to two daughter cells through cell division. Cell growth is the most powerful way to dilute Zr-MOF inside an individual cell. However, the normalized fluorescence on the surface of MOF kept invariable during the bio-dilution procedures (Figure 3-4). Hence, it is difficult to conclude the Zr-MOF didn't degrade throughout cell division. The fluorescence on the surface derives from the polymer. The detachment between the polymer and inorganic core may occur as well during their cellular journey. In summary, the fluorescence in an individual cell showed a substantial reduction associated with the cell division, while the normalized fluorescence within the whole cell was almost unchanged

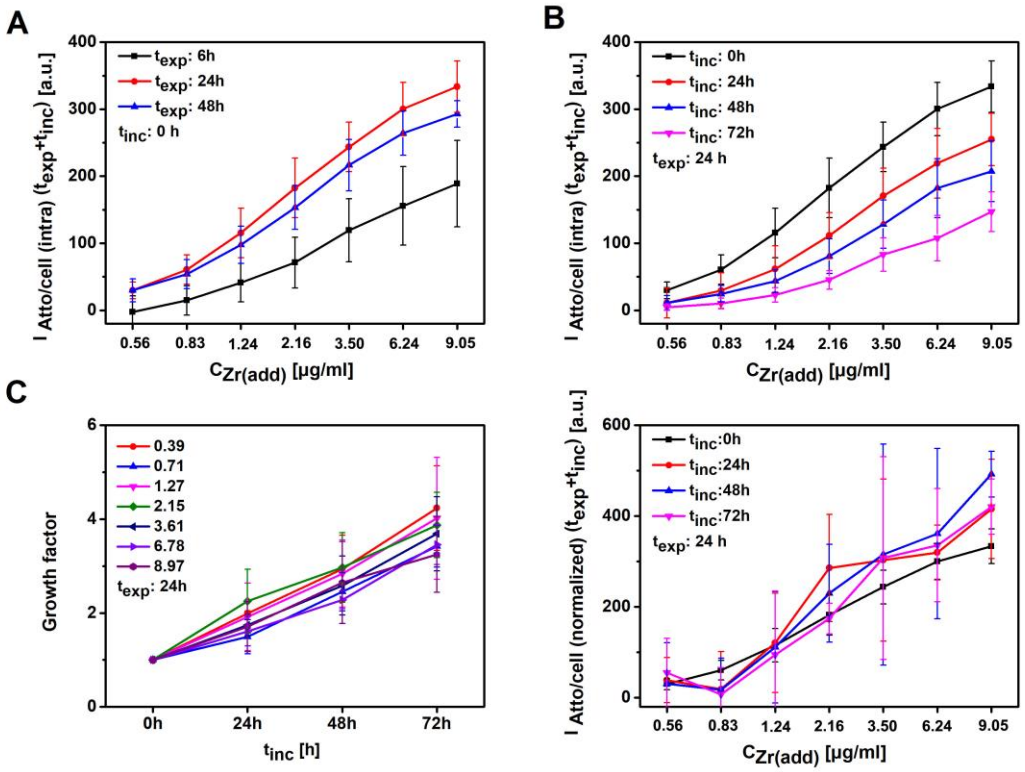

Figure 3-4. *Cellular uptake and biodegradation study carried out with Zr-MOF by flow cytometry. Mean fluorescence $I_{Atto/cell\ (intra)}$ originating from Hela cells during the uptake (A) and biodegradation study (B), is plotted for different exposure concentrations of Zr $C_{Zr(add).}$ The growth factor was termed as the cell number at different incubation time (t_{inc}) divided by the one at t_{inc}=0 hours (C). The normalized fluorescence $I_{Atto/cell\ (normalized)}$ was obtained by the $I_{Atto/cell\ (intra)}$ multiply the corresponding growth factor (D).*

3.5.3. Cellular behaviors of Zr-MOF tracked by metal concentrations

To further deepen the understanding, the concentration of Zr had been monitored by ICP-MS during the uptake and degradation process. In terms of the concentration of Zr per cell, the cellular uptake of Zr-MOF was efficient for the first 6 h, while there was no significant difference after 24h of incubation. The decrease at 48h can be explained by the exocytosis (Figure 3-5). In contrast to flow cytometry, the measurement by ICP-MS includes Zr-MOF inside cells as well as Zr-MOF attached to the cell membranes simultaneously. The concentration of Zr per cell remarkably decreased in the process of biodegradation, which could be attributed to cell division. Considering the interference of cell growth, we further explored the total concentration of Zr. The results revealed the total concentration of Zr was relatively the same during the whole process (Figure 3-6). However, the amount of Zr in the supernatant increased with time, suggesting the ion leakage of degraded Zr-MOF or exocytosis. Moreover, similar to the surface fluorescence, cells diluted inside Zr-MOF by cells division, without affecting the total amount of Zr.

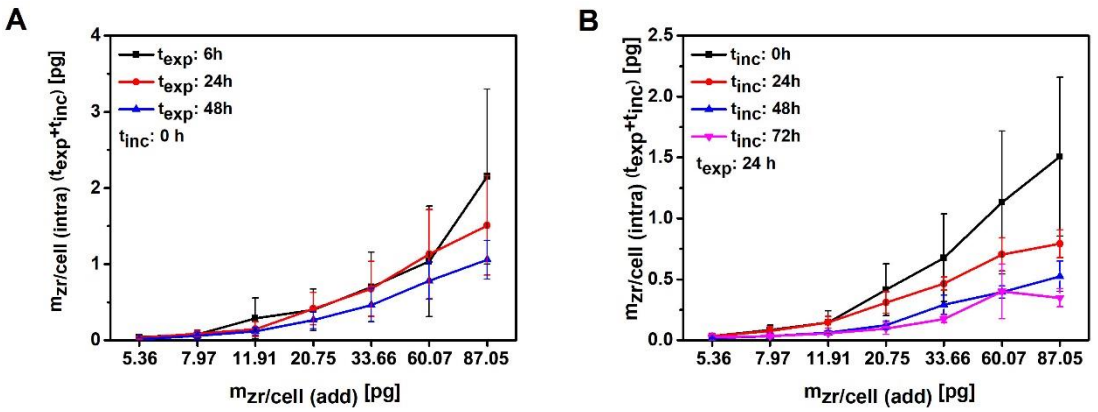

Figure 3-5. *ICP-MS analysis of Zr-MOF uptake and degradation by Hela cells. The data is shown as the mass concentration of Zr per cell $m_{Zr/cell\ (intra)}$ for different exposure time (t_{exp} 6, 24, 48 hours, A) for uptake study and incubation time (t_{inc} 0, 24, 48,72 hours, B) for biodegradation study.*

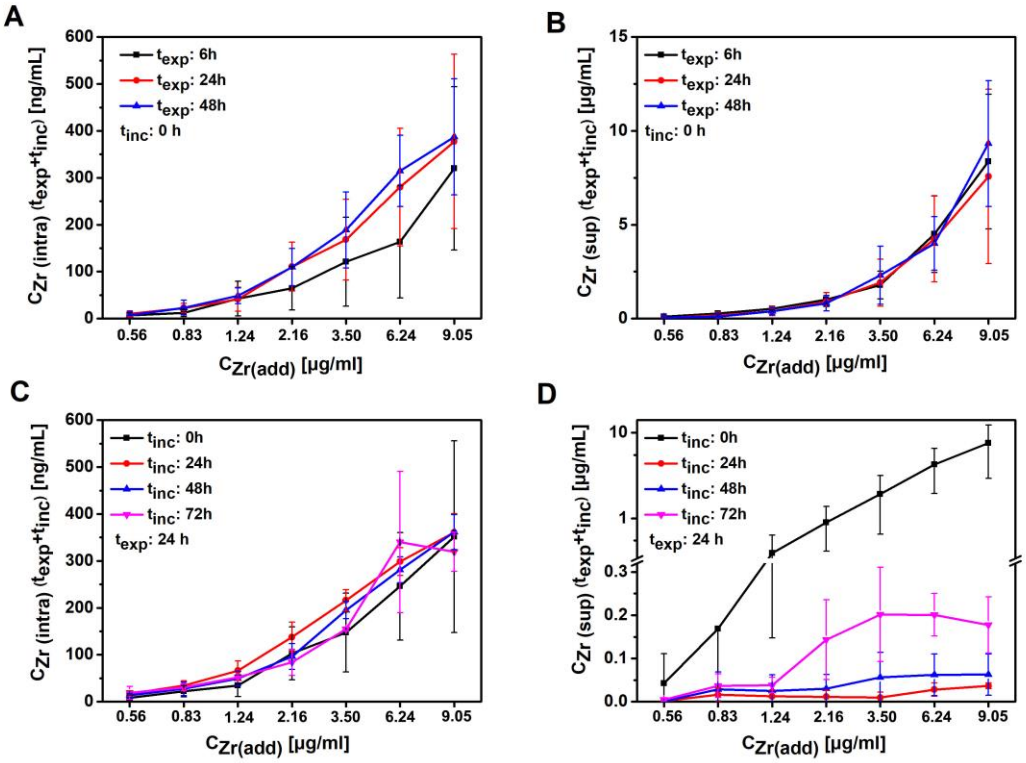

Figure 3-6. *Cellular uptake and biodegradation of Zr-MOF by Hela with the different exposure time and incubation time, as presented in the mass concentration of Zr in cell pellet $C_{Zr\ (intra)}$ (A) and supernatant $C_{Zr\ (sup)}$ (B). Biodegradation of Zr-MOF inside Hela cells, in terms of the $C_{Zr\ (intra)}$ (C) and $C_{Zr\ (sup)}$ (D).*

To compare the variation between the surface fluorescence and the inorganic part, we plotted the ratio of $I_{Atto/cell\ (intra)}$ and $m_{Zr/cell\ (intra)}$ (Figure 3-7).There was little change in the ratio during the uptake and degradation process, which suggested the Zr-MOF may keep inert in the biological environment from uptake to degradation. The cells can exocytose a part of the MOF, but the *in vitro* condition didn't change their fluorescence and amount of Zr.

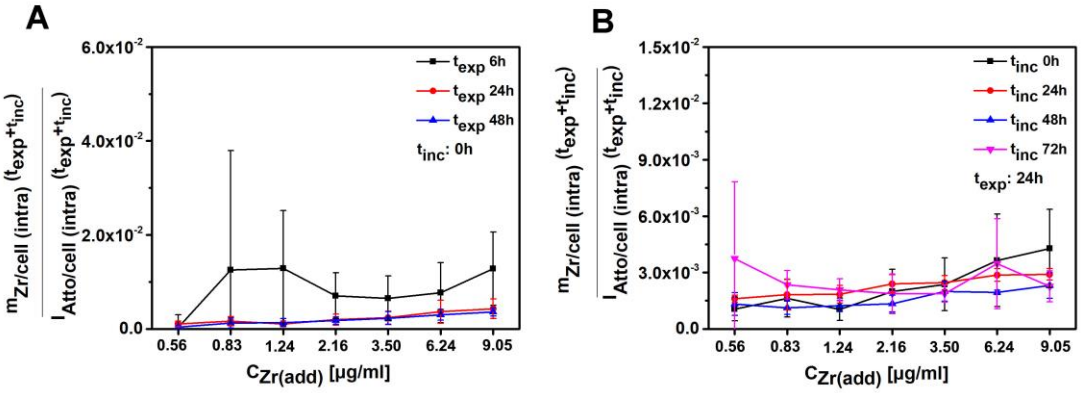

Figure 3-7. *The ratio of $m_{Zr/cell\ (intra)}$/ $I_{Atto/cell\ (intra)}$ during the time period of uptake (A) and biodegradation (B).*

3.6 Summary for Chapter 3

To begin with, the Zr-MOF labeled with Atto-647 was obtained, which was composed of the fluorescence on the surface of the organic shell and Zr inside the inorganic core. In this study, when Zr-MOF was administrated to cells, the intensity of fluorescence and the amount of Zr drastically decreased. But, the reduction was totally inhibited when growth factor was adopted revealing that the reduction results from cell division instead of degradation.

Some studies showed Zr-MOF suffered a fast degradation over time at pH3.5 buffer. However, as a matter of fact, the Zr-MOF almost remained inert under *in vitro* environment. Cells growth diluted the amount of MOF per cell, which has a slight impact on the total fluorescence and the amount of Zr. It was speculated the PC on the surface of MOF can protect them from degradation under biological conditions. Once MOF is administrated *in vitro*, it will interact with various components, proteins in particular, to reduce their huge surface energy. In this procedure, the so-called PC was formed which was reported by previous studies to slow down the degradation behaviors of NHs[49].

4. Summary and Outlook

4.1. The degradation scenarios of RE-based NHs

While RE-based NHs create multiple possibilities for MRI imaging or cancer therapy, their intracellular behaviors remain to be fully documented. Besides, it appears that RE-based NHs will dissolve in acid solution, suggesting further investigation of their response to lysosome. The degradation of RE-based NHs in pH 3.5 buffer encourages us to study their biological manners within cells. Specifically, with the help of flow cytometry and ICP-MS, we investigated their transformations upon internalization in Hela cells. After normalization with cell growth, a significant reduction in fluorescence and the amount of RE elements was observed within 72 hours. Later on, regarded as fingerprint of the degradation process, the shape evolution was tracked by TEM, which showed the defined cubic shapes transformed to irregular elongated objects. Moreover, the calculation of shape parameters, which is similarly applicable to detection of shape variation for proteins, cells and other types of NHs, had been introduced to bring the semiquantitative proof of shape change. Furthermore, our results opened a door in screening the correlation between the biodegradation and cell growth. The inseparable relationship must be carefully liberated in the development of biodegradation process. In summary, we demonstrated that the facile metrics of biodegradation process, consist of detecting multiple changes concerning fluorescence, amount of elements as well as shape change, which enriches our knowledge of nanoplatforms design, and is bound to facilitate us to design more fancy nanoplatforms in the future.

4.2. The degradation behaviors of Zr-MOF within cells

As the biological applications of Zr-MOF are essential to nanomedicine. It is considerably meaningful to evaluate the fate of Zr-MOF inside cells. Herein, the biological behaviors of Zr-MOF were explored. After internalized by Hela cells, Zr-MOF was substantially reduced in the single cell. Cell division is the most powerful way to achieve bio-dilution. Nonetheless, the surface fluorescence and amount of Zr remained relatively unchanged after normalized by cell growth for 72 hours, which unveiled the inert behavior of Zr-MOF inside cells. Thus, it was assumed that the PC on the surface of the MOF functions as a shield against the hostile environment so that activate enzymes and low pH conditions can't react with Zr-MOF directly, which has been already testified by previous study[49].

4.3. The novelties of our study

1. Numerous NHs had been applied to biological and medical applications, but very few of them were used for clinical research. In order to accelerate the translation from chemical design to clinical applications, the degradation behaviors of RE-based NHs and Zr-MOF inside cells was probed into at the very beginning.

2. Detecting effective biodegradation is a challenging task, which requires consideration of two major categories of interferences, namely, cell growth and exocytosis. In avoidance of the impacts from cell growth, the growth factor was employed to normalize the results from flow cytometry and ICP-MS. Moreover, to distinguish the exocytosis of inert NPs and degraded one, the ratiometric between different elements had been plotted and calculated. In this method, a useful fool was attained to investigate the *in vitro* biodegradation.

3. In a combination of Cell profiler and Matlab, shape parameters rendered an opportunity to semiquantitatively detect the shape evolution in the course of degradation process. We believe that this knowledge may provide with a valuable method for precise investigation of shape change for different nanomaterials or micromaterials.

4.4. Future perspectives

We successfully revealed the degradation behaviors of RE- based NHs at acid buffer and *in vitro* condition, precisely recorded the shape change and clearly distinguished the degradation from exocytosis. For the Zr-MOF study, their inert behaviors were observed *in vitro* condition. In spite of the above achievements, it is still imperative to continue this project, so we intend to carry out following works in the future,

1) Test the degradation of Zr-MOF at acid buffer to track the change in fluorescence, amount of Zr and shape.
2) We speculated that the inert behaviors of Zr-MOF are the results from the protection of PC. Therefore, we are supposed to evaluate the *in vitro* degradation behaviors of Zr-MOF without serum.

References

1. Dai, Q.; Wilhelm, S.; Ding, D.; Syed, A. M.; Sindhwani, S.; Zhang, Y.; Chen, Y. Y.; MacMillan, P.; Chan, W. C. W. *ACS Nano* **2018,** 12, (8), 8423-8435.
2. Fleischer, C. C.; Payne, C. K. *Accounts of Chemical Research* **2014,** 47, (8), 2651-2659.
3. Albanese, A.; Walkey, C. D.; Olsen, J. B.; Guo, H.; Emili, A.; Chan, W. C. W. *ACS Nano* **2014,** 8, (6), 5515-5526.
4. Ashby, J.; Pan, S.; Zhong, W. *ACS applied materials & interfaces* **2014,** 6, (17), 15412-9.
5. Xu, M.; Soliman, M. G.; Sun, X.; Pelaz, B.; Feliu, N.; Parak, W. J.; Liu, S. *ACS Nano* **2018,** 12, (10), 10104-10113.
6. Zhang, Q.; Lai, W.; Yin, T.; Zhang, C.; Yue, C.; Cheng, J.; Wang, K.; Yang, Y.; Cui, D.; Parak, W. J. *Bioconjugate chemistry* **2018,** 29, (6), 2120-2125.
7. Mahmoudi, M.; Abdelmonem, A. M.; Behzadi, S.; Clement, J. H.; Dutz, S.; Ejtehadi, M. R.; Hartmann, R.; Kantner, K.; Linne, U.; Maffre, P.; Metzler, S.; Moghadam, M. K.; Pfeiffer, C.; Rezaei, M.; Ruiz-Lozano, P.; Serpooshan, V.; Shokrgozar, M. A.; Nienhaus, G. U.; Parak, W. J. *ACS Nano* **2013,** 7, (8), 6555-6562.
8. Tenzer, S.; Docter, D.; Kuharev, J.; Musyanovych, A.; Fetz, V.; Hecht, R.; Schlenk, F.; Fischer, D.; Kiouptsi, K.; Reinhardt, C.; Landfester, K.; Schild, H.; Maskos, M.; Knauer, S. K.; Stauber, R. H. *Nat Nanotechnol* **2013,** 8, (10), 772-81.
9. Sacchetti, C.; Motamedchaboki, K.; Magrini, A.; Palmieri, G.; Mattei, M.; Bernardini, S.; Rosato, N.; Bottini, N.; Bottini, M. *Acs Nano* **2013,** 7, (3), 1974-1989.
10. Yan, Y.; Gause, K. T.; Kamphuis, M. M. J.; Ang, C.-S.; O'Brien-Simpson, N. M.; Lenzo, J. C.; Reynolds, E. C.; Nice, E. C.; Caruso, F. *ACS Nano* **2013,** 7, (12), 10960-10970.
11. Serpooshan, V.; Mahmoudi, M.; Zhao, M.; Wei, K.; Sivanesan, S.; Motamedchaboki, K.; Malkovskiy, A. V.; Goldstone, A. B.; Cohen, J. E.; Yang, P. C.; Rajadas, J.; Bernstein, D.; Woo, Y. J.; Ruiz-Lozano, P. *Advanced Functional Materials* **2015,** 25, (28), 4379-4389.
12. Cheng, X.; Tian, X.; Wu, A.; Li, J.; Tian, J.; Chong, Y.; Chai, Z.; Zhao, Y.; Chen, C.; Ge, C. *ACS applied materials & interfaces* **2015,** 7, (37), 20568-75.
13. Paula, A. J.; Araujo Junior, R. T.; Martinez, D. S.; Paredes-Gamero, E. J.; Nader, H. B.; Duran, N.; Justo, G. Z.; Alves, O. L. *ACS applied materials & interfaces* **2013,** 5, (17), 8387-93.
14. Caracciolo, G. *Nanomedicine* **2015,** 11, (3), 543-57.
15. Ritz, S.; Schottler, S.; Kotman, N.; Baier, G.; Musyanovych, A.; Kuharev, J.; Landfester, K.; Schild, H.; Jahn, O.; Tenzer, S.; Mailander, V. *Biomacromolecules* **2015,** 16, (4), 1311-21.
16. Calatayud, M. P.; Sanz, B.; Raffa, V.; Riggio, C.; Ibarra, M. R.; Goya, G. F. *Biomaterials* **2014,** 35, (24), 6389-99.
17. De Paoli, S. H.; Diduch, L. L.; Tegegn, T. Z.; Orecna, M.; Strader, M. B.; Karnaukhova, E.; Bonevich, J. E.; Holada, K.; Simak, J. *Biomaterials* **2014,** 35, (24), 6182-94.
18. Hu, W.; Peng, C.; Lv, M.; Li, X.; Zhang, Y.; Chen, N.; Fan, C.; Huang, Q. *ACS Nano* **2011,** 5, (5), 3693-3700.
19. Salvati, A.; Pitek, A. S.; Monopoli, M. P.; Prapainop, K.; Bombelli, F. B.; Hristov, D. R.; Kelly, P. M.; Aberg, C.; Mahon, E.; Dawson, K. A. *Nat Nanotechnol* **2013,** 8, (2), 137-43.
20. Kittler, S.; Greulich, C.; Diendorf, J.; Köller, M.; Epple, M. *Chemistry of Materials* **2010,** 22, (16), 4548-4554.
21. Levy, M.; Luciani, N.; Alloyeau, D.; Elgrabli, D.; Deveaux, V.; Pechoux, C.; Chat, S.; Wang, G.; Vats, N.; Gendron, F.; Factor, C.; Lotersztajn, S.; Luciani, A.; Wilhelm, C.; Gazeau, F. *Biomaterials* **2011,** 32, (16), 3988-99.

22. Mahon, E.; Hristov, D. R.; Dawson, K. A. *Chem Commun (Camb)* **2012,** 48, (64), 7970-2.
23. Li, Y.; Zhang, X.; Zhang, Z.; Wu, H.; Xu, X.; Gu, Z. *Materials Horizons* **2018,** 5, (6), 1047-1057.
24. Chanana, M.; Rivera Gil, P.; Correa-Duarte, M. A.; Liz-Marzan, L. M.; Parak, W. J. *Angew Chem Int Ed Engl* **2013,** 52, (15), 4179-83.
25. Bargheer, D.; Giemsa, A.; Freund, B.; Heine, M.; Waurisch, C.; Stachowski, G. M.; Hickey, S. G.; Eychmuller, A.; Heeren, J.; Nielsen, P. *Beilstein J Nanotechnol* **2015,** 6, 111-123.
26. Feliu, N.; Docter, D.; Heine, M.; Del Pino, P.; Ashraf, S.; Kolosnjaj-Tabi, J.; Macchiarini, P.; Nielsen, P.; Alloyeau, D.; Gazeau, F.; Stauber, R. H.; Parak, W. J. *Chem Soc Rev* **2016,** 45, (9), 2440-57.
27. Hühn, J.; Carrillo-Carrion, C.; Soliman, M. G.; Pfeiffer, C.; Valdeperez, D.; Masood, A.; Chakraborty, I.; Zhu, L.; Gallego, M.; Yue, Z.; Carril, M.; Feliu, N.; Escudero, A.; Alkilany, A. M.; Pelaz, B.; del Pino, P.; Parak, W. J. *Chemistry of Materials* **2016,** 29, (1), 399-461.
28. Sun, X.; Gamal, M.; Nold, P.; Said, A.; Chakraborty, I.; Pelaz, B.; Schmied, F.; von Pückler, K.; Figiel, J.; Zhao, Y.; Brendel, C.; Hassan, M.; Parak, W. J.; Feliu, N. *Applied Materials Today* **2019,** 15, 267-279.
29. Chakraborty, I.; Feliu, N.; Roy, S.; Dawson, K.; Parak, W. J. *Bioconjugate chemistry* **2018,** 29, (4), 1261-1265.
30. Nguyen, V. H.; Lee, B. J. *Int J Nanomedicine* **2017,** 12, 3137-3151.
31. Mahmoudi, M.; Bertrand, N.; Zope, H.; Farokhzad, O. C. *Nano Today* **2016,** 11, (6), 817-832.
32. Mortensen, N. P.; Hurst, G. B.; Wang, W.; Foster, C. M.; Nallathamby, P. D.; Retterer, S. T. *Nanoscale* **2013,** 5, (14), 6372-80.
33. Zyuzin, M. V.; Yan, Y.; Hartmann, R.; Gause, K. T.; Nazarenus, M.; Cui, J.; Caruso, F.; Parak, W. J. *Bioconjugate chemistry* **2017,** 28, (8), 2062-2068.
34. Bertrand, N.; Grenier, P.; Mahmoudi, M.; Lima, E. M.; Appel, E. A.; Dormont, F.; Lim, J. M.; Karnik, R.; Langer, R.; Farokhzad, O. C. *Nat Commun* **2017,** 8, (1), 777.
35. Aggarwal, P.; Hall, J. B.; McLeland, C. B.; Dobrovolskaia, M. A.; McNeil, S. E. *Adv Drug Deliv Rev* **2009,** 61, (6), 428-37.
36. Ma, Z.; Bai, J.; Jiang, X. *ACS Appl Mater Interfaces* **2015,** 7, (32), 17614-22.
37. de la Rica, R.; Aili, D.; Stevens, M. M. *Adv Drug Deliv Rev* **2012,** 64, (11), 967-78.
38. Mura, S.; Nicolas, J.; Couvreur, P. *Nat Mater* **2013,** 12, (11), 991-1003.
39. Aimetti, A. A.; Machen, A. J.; Anseth, K. S. *Biomaterials* **2009,** 30, (30), 6048-54.
40. Wen, J.; Anderson, S. M.; Du, J.; Yan, M.; Wang, J.; Shen, M.; Lu, Y.; Segura, T. *Adv Mater* **2011,** 23, (39), 4549-53.
41. Park, C.; Kim, H.; Kim, S.; Kim, C. *Journal of the American Chemical Society* **2009,** 131, (46), 16614-16615.
42. Sun, Y. L.; Zhou, Y.; Li, Q. L.; Yang, Y. W. *Chem Commun (Camb)* **2013,** 49, (79), 9033-5.
43. Lunov, O.; Syrovets, T.; Rocker, C.; Tron, K.; Nienhaus, G. U.; Rasche, V.; Mailander, V.; Landfester, K.; Simmet, T. *Biomaterials* **2010,** 31, (34), 9015-22.
44. Yang, G.; Phua, S. Z. F.; Bindra, A. K.; Zhao, Y. *Adv Mater* **2019,** 31, (10), e1805730.
45. Van de Walle, A.; Plan Sangnier, A.; Abou-Hassan, A.; Curcio, A.; Hémadi, M.; Menguy, N.; Lalatonne, Y.; Luciani, N.; Wilhelm, C. *Proceedings of the National Academy of Sciences* **2019,** 116, (10), 4044.
46. Kagan, V. E.; Konduru, N. V.; Feng, W.; Allen, B. L.; Conroy, J.; Volkov, Y.; Vlasova, II; Belikova, N. A.; Yanamala, N.; Kapralov, A.; Tyurina, Y. Y.; Shi, J.; Kisin, E. R.; Murray, A. R.; Franks, J.; Stolz, D.; Gou, P.; Klein-Seetharaman, J.; Fadeel, B.; Star, A.; Shvedova, A. A. *Nat Nanotechnol* **2010,** 5, (5), 354-9.
47. Kreyling, W. G.; Abdelmonem, A. M.; Ali, Z.; Alves, F.; Geiser, M.; Haberl, N.; Hartmann, R.; Hirn, S.; de Aberasturi, D. J.; Kantner, K.; Khadem-Saba, G.; Montenegro, J. M.; Rejman, J.; Rojo, T.; de Larramendi,

I. R.; Ufartes, R.; Wenk, A.; Parak, W. J. *Nat Nanotechnol* **2015,** 10, (7), 619-23.
48. Soliman, M. G.; Pelaz, B.; Parak, W. J.; del Pino, P. *Chemistry of Materials* **2015,** 27, (3), 990-997.
49. Stepien, G.; Moros, M.; Perez-Hernandez, M.; Monge, M.; Gutierrez, L.; Fratila, R. M.; Las Heras, M.; Menao Guillen, S.; Puente Lanzarote, J. J.; Solans, C.; Pardo, J.; de la Fuente, J. M. *ACS Appl Mater Interfaces* **2018,** 10, (5), 4548-4560.
50. Kolosnjaj-Tabi, J.; Javed, Y.; Lartigue, L.; Volatron, J.; Elgrabli, D.; Marangon, I.; Pugliese, G.; Caron, B.; Figuerola, A.; Luciani, N.; Pellegrino, T.; Alloyeau, D.; Gazeau, F. *ACS Nano* **2015,** 9, (8), 7925-7939.
51. Mazuel, F.; Espinosa, A.; Luciani, N.; Reffay, M.; Le Borgne, R.; Motte, L.; Desboeufs, K.; Michel, A.; Pellegrino, T.; Lalatonne, Y.; Wilhelm, C. *ACS Nano* **2016,** 10, (8), 7627-38.
52. Mazuel, F.; Espinosa, A.; Radtke, G.; Bugnet, M.; Neveu, S.; Lalatonne, Y.; Botton, G. A.; Abou-Hassan, A.; Wilhelm, C. *Advanced Functional Materials* **2017,** 27, (9), 1605997.
53. Caballero-Díaz, E.; Pfeiffer, C.; Kastl, L.; Rivera-Gil, P.; Simonet, B.; Valcárcel, M.; Jiménez-Lamana, J.; Laborda, F.; Parak, W. J. *Particle & Particle Systems Characterization* **2013,** 30, (12), 1079-1085.
54. Bouzigues, C.; Gacoin, T.; Alexandrou, A. *ACS Nano* **2011,** 5, (11), 8488-8505.
55. Shen, J.; Sun, L. D.; Yan, C. H. *Dalton Trans* **2008**, (42), 5687-97.
56. Wang, L.; Li, P.; Wang, L. *Luminescence* **2009,** 24, (1), 39-44.
57. van de Rijke, F.; Zijlmans, H.; Li, S.; Vail, T.; Raap, A. K.; Niedbala, R. S.; Tanke, H. J. *Nature Biotechnology* **2001,** 19, (3), 273-276.
58. Lommerse, P. H. M.; Blab, G. A.; Cognet, L.; Harms, G. S.; Snaar-Jagalska, B. E.; Spaink, H. P.; Schmidt, T. *Biophysical journal* **2004,** 86, (1 Pt 1), 609-616.
59. Moore, E. G.; Samuel, A. P. S.; Raymond, K. N. *Accounts of Chemical Research* **2009,** 42, (4), 542-552.
60. Casanova, D.; Bouzigues, C.; Nguyen, T. L.; Ramodiharilafy, R. O.; Bouzhir-Sima, L.; Gacoin, T.; Boilot, J. P.; Tharaux, P. L.; Alexandrou, A. *Nat Nanotechnol* **2009,** 4, (9), 581-5.
61. Bottrill, M.; Kwok, L.; Long, N. J. *Chem Soc Rev* **2006,** 35, (6), 557-71.
62. Hifumi, H.; Yamaoka, S.; Tanimoto, A.; Citterio, D.; Suzuki, K. *Journal of the American Chemical Society* **2006,** 128, (47), 15090-15091.
63. Bridot, J.-L.; Faure, A.-C.; Laurent, S.; Rivière, C.; Billotey, C.; Hiba, B.; Janier, M.; Josserand, V.; Coll, J.-L.; Vander Elst, L.; Muller, R.; Roux, S.; Perriat, P.; Tillement, O. *Journal of the American Chemical Society* **2007,** 129, (16), 5076-5084.
64. Zhou, L.; Chen, Z.; Dong, K.; Yin, M.; Ren, J.; Qu, X. *Biomaterials* **2014,** 35, (30), 8694-702.
65. Morris, R. E.; Wheatley, P. S. *Angew Chem Int Ed Engl* **2008,** 47, (27), 4966-81.
66. Falcaro, P.; Ricco, R.; Doherty, C. M.; Liang, K.; Hill, A. J.; Styles, M. J. *Chem Soc Rev* **2014,** 43, (16), 5513-60.
67. Horcajada, P.; Chalati, T.; Serre, C.; Gillet, B.; Sebrie, C.; Baati, T.; Eubank, J. F.; Heurtaux, D.; Clayette, P.; Kreuz, C.; Chang, J. S.; Hwang, Y. K.; Marsaud, V.; Bories, P. N.; Cynober, L.; Gil, S.; Ferey, G.; Couvreur, P.; Gref, R. *Nat Mater* **2010,** 9, (2), 172-8.
68. Keskin, S.; Kızılel, S. *Industrial & Engineering Chemistry Research* **2011,** 50, (4), 1799-1812.
69. McKinlay, A. C.; Morris, R. E.; Horcajada, P.; Ferey, G.; Gref, R.; Couvreur, P.; Serre, C. *Angew Chem Int Ed Engl* **2010,** 49, (36), 6260-6.
70. Zhu, X.; Zheng, H.; Wei, X.; Lin, Z.; Guo, L.; Qiu, B.; Chen, G. *Chem Commun (Camb)* **2013,** 49, (13), 1276-8.
71. Aguilera-Sigalat, J.; Bradshaw, D. *Chem Commun (Camb)* **2014,** 50, (36), 4711-3.
72. Li, H.-Y.; Wei, Y.-L.; Dong, X.-Y.; Zang, S.-Q.; Mak, T. C. W. *Chemistry of Materials* **2015,** 27, (4), 1327-

1331.

73. Wang, F.; Zhang, Y.; Liu, Z.; Du, Z.; Zhang, L.; Ren, J.; Qu, X. *Angew Chem Int Ed Engl* **2019**.

74. Cedervall, T.; Lynch, I.; Lindman, S.; Berggård, T.; Thulin, E.; Nilsson, H.; Dawson, K. A.; Linse, S. *Proceedings of the National Academy of Sciences* **2007,** 104, (7), 2050.

75. Lundqvist, M.; Stigler, J.; Elia, G.; Lynch, I.; Cedervall, T.; Dawson, K. A. *Proceedings of the National Academy of Sciences* **2008,** 105, (38), 14265.

76. Lartigue, L.; Alloyeau, D.; Kolosnjaj-Tabi, J.; Javed, Y.; Guardia, P.; Riedinger, A.; Péchoux, C.; Pellegrino, T.; Wilhelm, C.; Gazeau, F. *ACS Nano* **2013,** 7, (5), 3939-3952.

77. Balasubramanian, S. K.; Jittiwat, J.; Manikandan, J.; Ong, C. N.; Yu, L. E.; Ong, W. Y. *Biomaterials* **2010,** 31, (8), 2034-42.

78. Zhang, Y.; Zhang, Y.; Hong, G.; He, W.; Zhou, K.; Yang, K.; Li, F.; Chen, G.; Liu, Z.; Dai, H.; Wang, Q. *Biomaterials* **2013,** 34, (14), 3639-46.

79. Yang, K.; Wan, J.; Zhang, S.; Zhang, Y.; Lee, S.-T.; Liu, Z. *ACS Nano* **2011,** 5, (1), 516-522.

80. Sun, L. D.; Wang, Y. F.; Yan, C. H. *Acc Chem Res* **2014,** 47, (4), 1001-9.

81. Yuan, P.; Mao, X.; Wu, X.; Liew, S. S.; Li, L.; Yao, S. Q. *Angew Chem Int Ed Engl* **2019**.

82. Chen, F.; Wang, G.; Griffin, J. I.; Brenneman, B.; Banda, N. K.; Holers, V. M.; Backos, D. S.; Wu, L.; Moghimi, S. M.; Simberg, D. *Nat Nanotechnol* **2017,** 12, (4), 387-393.

83. Ke, P. C.; Lin, S.; Parak, W. J.; Davis, T. P.; Caruso, F. *ACS Nano* **2017,** 11, (12), 11773-11776.

84. Chen, Y.; Chen, H.; Shi, J. *Advanced Materials* **2013,** 25, (23), 3144-3176.

85. Escudero, A.; Carrillo-Carrión, C.; Zyuzin, M. V.; Ashraf, S.; Hartmann, R.; Núñez, N. O.; Ocaña, M.; Parak, W. J. *Nanoscale* **2016,** 8, 12221-12236.

86. Schmandke, A.; Schmandke, A.; Pietro, M. A.; Schwab, M. E. *PLOS ONE* **2013,** 8, (10), e78212.

87. Kim, D.-J.; Lee, G.; Kim, G.-S.; Lee, S.-K. *Nanoscale Research Letters* **2012,** 7, (1), 637.

88. Bailey, S. N.; Ali, S. M.; Carpenter, A. E.; Higgins, C. O.; Sabatini, D. M. *Nature Methods* **2006,** 3, (2), 117-122.

89. Jhala, D.; Rather, H.; Kedaria, D.; Shah, J.; Singh, S.; Vasita, R. *Bioactive Materials* **2019,** 4, (1), 79-86.

90. Wang, Z.; Tonderys, D.; Leggett, S. E.; Williams, E. K.; Kiani, M. T.; Spitz Steinberg, R.; Qiu, Y.; Wong, I. Y.; Hurt, R. H. *Carbon* **2016,** 97, 14-24.

91. Hulshof, F. F. B.; Papenburg, B.; Vasilevich, A.; Hulsman, M.; Zhao, Y.; Levers, M.; Fekete, N.; de Boer, M.; Yuan, H.; Singh, S.; Beijer, N.; Bray, M.-A.; Logan, D. J.; Reinders, M.; Carpenter, A. E.; van Blitterswijk, C.; Stamatialis, D.; de Boer, J. *Biomaterials* **2017,** 137, 49-60.

92. Criscenti, G.; Vasilevich, A.; Longoni, A.; De Maria, C.; van Blitterswijk, C. A.; Truckenmuller, R.; Vozzi, G.; De Boer, J.; Moroni, L. *Acta Biomaterialia* **2017,** 55, 310-322.

93. Ma, X.; Hartmann, R.; Jimenez de Aberasturi, D.; Yang, F.; Soenen, S. J. H.; Manshian, B. B.; Franz, J.; Valdeperez, D.; Pelaz, B.; Feliu, N.; Hampp, N.; Riethmüller, C.; Vieker, H.; Frese, N.; Gölzhäuser, A.; Simonich, M.; Tanguay, R. L.; Liang, X.-J.; Parak, W. J. *ACS Nano* **2017,** 11, (8), 7807-7820.

94. Escudero, A.; Carrillo-Carrion, C.; Zyuzin, M. V.; Ashraf, S.; Hartmann, R.; Nunez, N. O.; Ocana, M.; Parak, W. J. *Nanoscale* **2016,** 8, (24), 12221-36.

95. Bai, Y.; Dou, Y.; Xie, L. H.; Rutledge, W.; Li, J. R.; Zhou, H. C. *Chem Soc Rev* **2016,** 45, (8), 2327-67.

96. Zhang, M.; Chen, Y.-P.; Bosch, M.; Gentle Iii, T.; Wang, K.; Feng, D.; Wang, Z. U.; Zhou, H.-C. *Angewandte Chemie International Edition* **2014,** 53, (3), 815-818.

97. Morris, W.; Briley, W. E.; Auyeung, E.; Cabezas, M. D.; Mirkin, C. A. *J Am Chem Soc* **2014,** 136, (20), 7261-4.

98. Zahn, G.; Schulze, H. A.; Lippke, J.; König, S.; Sazama, U.; Fröba, M.; Behrens, P. *Microporous and Mesoporous Materials* **2015,** 203, 186-194.
99. Zimpel, A.; Al Danaf, N.; Steinborn, B.; Kuhn, J.; Höhn, M.; Bauer, T.; Hirschle, P.; Schrimpf, W.; Engelke, H.; Wagner, E.; Barz, M.; Lamb, D. C.; Lächelt, U.; Wuttke, S. *ACS Nano* **2019,** 13, (4), 3884-3895.

Publications

[1]. Dingcheng Zhu, Sathi Roy, **Ziyao Liu**, Horst Weller, Wolfgang Park, Neus Feliu, Advanced Drug Delivery Reviews, 2019,13,117-132.

Nowadays, scientists often adopt external stimuli to achieve the desired release, which allowing precise, real time control of *in vitro* and *in vivo* releases. In this review we discussed the use of stimuli-responsive controlled release systems that can respond to light and magnetic field triggers for manipulating the release of encapsulated cargo within cells. We summarized established ways and technologies and described prominent examples. The advantages and disadvantages of different manners are discussed.

The author contributed with TOC figures, the edition of figures and literature searching.

[2]. A significant part of this work is currently prepared for submission: Ziyao Liu, Alberto Escudero, Carolina Carrillo, Indranath Chakraborty, Dingcheng Zhu, Marta Gallego, Wolfgang Parak, Neus Feliu "Biodegradation of bi-labelled polymer-coated rare-earth nanoparticles in adherent cell cultures"

Acknowledgements

First of all, I would like to thank Prof. Wolfgang Parak for offering me the opportunity to work in his group during my doctoral study, it was an honor for me to study in the Biophotonics group at the University of Hamburg, and I appreciate his continuous support and kind help in all the time of my research.

Then, I want to express my thanks to my supervisor Dr. Neus Feliu for her constructive discussions and always helping me to fix problems. I am also grateful to her warm caring for all the time.

I want to thank all the members of Biophotonics group to let me work in a very pleasant and friendly atmosphere.

Besides, I want to thank Marta Gallego for measuring TEM images in CIC biomaGUNE (Spain) and Dr. Indranath Chakroborty for helping me with ICP-MS measurements. Many thanks for Dr. Dingcheng Zhu for writing Matlab code. I appreciate Dr. Alberto Escudero and Dr. Carolina Carrillo for the synthesis of nanoparticles.

Lastly, I do appreciate the fellowship support from China Scholarship Council.

Abbreviations

NHs	nanohybrids
RE	rare earth
MOF	metal–organic frameworks
PC	protein corona
SPIOs	superparamagnetic, iron oxide nanoparticles
Au	gold
DLS	dynamic light scattering
TEM	transmission electron microscopy
ICP-MS	inductively coupled plasma mass spectrometry
LDA	laser Doppler anemometry
EG	ethylene glycol
RT	room temperature
FA	fluoresceinamine
A_{NHs}	area
Ec_{NHs}	eccentricity
Ex_{NHs}	extent
F_{NHs}	F factor
S_{NHs}	solidity

Z^0_{NHs}	Z factor
C_{NHs}	compactness
α_{NHs}	angle
FBS	fetal bovine serum
PBS	phosphate buffered saline
CQ	choloroquine
NH_4Cl	ammonium chloride
PA	pepstatin A
SF	serum free

List of hazardous substances

Substance	GHS pictograms	Hazard Sentences	Precaution Sentence
$Eu(NO_3)_3 \cdot 5H_2O$	 GHS03, GHS07 Danger	H272-H315-H319-H335	P220-P261-P305 + P351 + P338
$Bi(NO_3)_3 \cdot 5H_2O$	 GHS03, GHS07 Danger	H272-H315-H319-H335	P210-P220-P221-P305 + P351 + P338-P370 + P378
$Gd(NO_3)_3 \cdot 6H_2O$	 GHS03, GHS07 Danger	H272-H315-H319-H335	P220-P261-P305 + P351 + P338
Ethylene glycol	 GHS07, GHS08 Harmful	H302,H373	P314
Na_3VO_4	 GHS07 Warning	H302	P301 + P312 + P330
Polyacrylic acid	Not hazardous substance		
Citric acid	 GHS07 Warning	H319	P264-P280-P305 + P351 + P338-P337 + P313
Sodium phospate dibasic	Not hazardous substance		
Nitric acid	 GHS03, GHS05 Danger	H272 ,H290 ,H314 ,H318	P210 ,P220 ,P221 ,P234 , P260,P264, P280, P301+P330+P331 ,P303+P361+P353 ,P304+P340 , P305+P351+P338 ,P310, P321,P363,P370+P378,P

			390 ,P405 ,P406,P501
Hydrochloric acid	 GHS05, GHS07 Danger	H290, H314, H335	P260, P280 P303+P361+P353, P305+P351+P338, P390 , P403+P233 P501
Dulbecco's modified eagle medium	Not hazardous substance		
Penicillin/streptomycin	Not hazardous substance		
Fetal bovine serum	Not hazardous substance		
Resazurin	Not hazardous substance		
Phosphate buffered saline	Not hazardous substance		
0.05% trypsin/EDTA	Not hazardous substance		
Triton X-100	Not hazardous substance		
Chloroquien disphsophate salt	 GHS07 Warning	H302	
Ammonium chloride	 GHS07 Warning	H302-H319	P301 + P312 + P330-P305 + P351 + P338
Pepstatin A	Not hazardous substance		
Glutaraldehyde	 GHS05,GHS06, GHS08,GHS09 Danger	H301 + H331-H314-H317-H334-H335-H410	P261-P273-P280-P301 + P310 + P330-P303 + P361 + P353-P304 + P340 + P310-P305 + P351 + P338 + P310-P342 + P311-P391-P403 + P233

Sodium cacodylate trihydrate	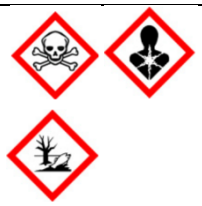 GHS06,GHS08, GHS09 Danger	H301 + H331-H351-H410	P201-P273-P280-P301 + P310 + P330-P391-P403 + P233
Zirconium (IV) chloride	 GHS05, Danger	H290-H314	P280-P305 + P351 + P338-P310
Fumaric acid	 GHS07, GHS09 Warning	H312-H315-H317-H319-H335-H411	P261-P264-P273-P280-P302 + P352 + P312-P391
Atto-647	Not hazardous substance		

Declaration on oath

I hereby declare on oath, that I have written the present dissertation by my own and have not used other than the acknowledged resources and aids.

Date

Signature